

**ASSESSMENT OF THE STABILITY AND BIOLOGICAL ACTIVITY OF FOUR
MODEL PROTEINS ENCAPSULATED IN HYDROGEL MEMBRANES**

By
Celimar Valentín Rodríguez

A thesis submitted in partial fulfillment of the requirements for the degree of

MASTER OF SCIENCE
in
CHEMICAL ENGINEERING

UNIVERSITY OF PUERTO RICO
MAYAGÜEZ CAMPUS

2007

Approved by:

Juan López Garriga, Ph.D.
Member, Graduate Committee

Date

Lorenzo Saliceti Piazza, Ph.D.
Member, Graduate Committee

Date

Madeline Torres Lugo, Ph.D.
President, Graduate Committee

Date

Gustavo López, Ph.D.
Representative of Graduate Studies

Date

David Suleiman, Ph.D.
Chairperson of the Department

Date

ABSTRACT

Proteins are biological macromolecules which have a unique spatial conformation. This spatial conformation can be affected by extremes in pH, temperature, and organic solvents. Once this 3D spatial conformation is affected the protein's biological stability and activity can be severely limited. For these reasons, this investigation focuses on the effects of pre-polymeric solution components on the behavior of proteins to be encapsulated by the entrapment technique in anionic, cationic, and neutral hydrogel membranes. Five proteins were utilized in this investigation: equine skeletal muscle myoglobin (MMb), equine heart myoglobin (HMb), bovine hemoglobin (bHb), porcine hemoglobin (pHb), and hen egg white lysozyme (HEWL). Three hydrogel morphologies were examined: methacrylic acid-poly(ethylene glycol) dimethacrylate (n=1000) (MAA:PEGDMA1000), dimethylaminoethyl methacrylate-poly(ethylene glycol) dimethacrylate (n=1000) (DMAEM:PEGDMA1000), and poly(ethylene glycol) (200) monomethyl ether-methacrylate-poly(ethylene glycol) dimethacrylate (n=1000) (PEGMA200:PEGDMA1000). The four hemeproteins were put in contact with different ratios of the pre-polymeric solution components. UV-vis spectroscopy was utilized to monitor displacements in the Soret Bands to determine any changes in biological stability. Optimized morphologies were then synthesized. The Soret bands of the proteins in the pre-polymeric solution were at the expected wavelengths ($\lambda = 408$ (Mb), 406 (Hb)). Yet, upon polymerization, the Soret bands of the encapsulated proteins in ionic morphologies suffered blue shifts. Soret bands of the metaquo, deoxy, and carboxy states were all blue-shifted. Such phenomenon may be attributed to the breakage of the histidine-iron bond. Examination of the results revealed possible coexistence of metaquo/oxy and carboxy/oxy states within the polymerized membranes. Small displacements of the Soret bands upon changes from deoxy to carboxy states possibly expose higher affinity of CO to the polymer than to the heme group. HEWL crystals were exposed to pre-polymeric solutions of MAA:PEGDMA1000. Microscopy revealed that HEWL crystals were stable in these solutions for several hours. These morphologies will be polymerized in presence of HEWL crystals to investigate if crystals endure the polymerization process.

RESUMEN

Las proteínas son macromoléculas biológicas que tienen una conformación espacial única. Esta conformación especial se ve afectada por extremos en pH, extremos en temperatura y la presencia de solventes orgánicos en el medio donde éstas se encuentran. Una vez este arreglo tridimensional cambia, la estabilidad y la actividad biológica de las proteínas se afectan severamente. Por estas razones, esta investigación se enfoca en los efectos de los componentes de la solución pre-polimérica en el comportamiento de las proteínas a ser encapsuladas en membranas de hidrogeles aniónicas, catiónicas y neutrales por la técnica de atrapamiento. Cinco proteínas se utilizaron para estos estudios: mioglobina de músculo esquelético de caballo (mMb), mioglobina de músculo cardíaco de caballo (hMb), hemoglobina bovina (bHb), hemoglobina porcina (pHb) y lisozima de clara de huevo de gallina (HEWL). Se examinaron tres morfologías de hidrogeles: ácido metacrílico-glicol de polietileno dimetacrilato (n=1000) (MAA:PEGDMA1000), dimetilamino etil metacrilato-glicol de polietileno dimetacrilato (n=1000) (DMAEM:PEGDMA1000) y glicol de polietileno (200) monometil eter metacrilato-glicol de polietileno dimetacrilato (n=1000) (PEGMA200:PEGDMA1000). Las cuatro hemo-proteínas estuvieron en contacto con diferentes razones de los componentes de las soluciones pre-poliméricas anteriores. Se utilizó la técnica de espectroscopia de luz ultra violeta visible para observar los desplazamientos de las bandas Soret y Q de las proteínas para determinar si hubo cambios en la estabilidad biológica de las proteínas. Luego, las morfologías optimizadas fueron sintetizadas. Las bandas Soret de las proteínas en las soluciones pre-poliméricas se encontraron en los largos de onda esperados (Mb - 408nm y Hb - 406nm). Aun así, luego de la polimerización, las proteínas encapsuladas en las morfologías iónicas sufrieron desplazamientos azules de sus bandas Soret. Este fenómeno puede atribuirse al rompimiento del uno de los enlaces hierro-histidina. Estas mismas bandas en los estados metaquo, deoxy y carboxy también sufrieron desplazamientos azules. Estos resultados se pueden atribuir a la coexistencia de estados metaquo/oxy y carboxy/oxy dentro de las membranas. Los desplazamientos pequeños que se observan al cambiar de estado deoxy a carboxy en las proteínas encapsuladas en las membranas de PEGMA200 pueden ser causados por una posible afinidad más alta del PEG al CO que del grupo hemo al CO. Cristales de HEWL fueron expuestos a soluciones pre-poliméricas de MAA:PEGDMA1000. Se observó, utilizando la técnica de espectroscopia de luz, que estos cristales fueron estables en estas soluciones por varias horas. Estas morfologías se sintetizarán en presencia de cristales de HEWL para investigar si los cristales sobreviven al proceso de polimerización.

*We are all inventors, each sailing
out on a voyage of discovery,
guided each by a private chart,
of which there is no duplicate.
The world is all gates, all
opportunities.*
Ralph Waldo Emerson

To my parents, who have shown me
the true meaning of *passion*,
perseverance, *dedication*, and
determination.

ACKNOWLEDGEMENTS

I would first and foremost like to thank the Chemical Engineering Department at the University of Puerto Rico, Mayagüez, for accepting me into this remarkable graduate program. I would also like to acknowledge Dr. Madeline Torres-Lugo for giving me the opportunity of working in such a remarkable laboratory with so many wonderful human beings and for taking chances on a student with no chemical engineering background. Thank you for believing in me and for always pushing me forward. I would also like to thank Dr. Juan López-Garriga and Dr. Lorenzo Saliceti-Piazza for their help during this grueling investigation process. Thank you is in order for Dr. López-Garriga's investigation group: Waleska, Ruth, Elddie, and all the other students who trained me and always extended a helping hand. I would like to recognize Dr. Carlos Rinaldi for giving me the opportunity of working in his laboratory as an undergraduate and who provided me with a first taste of chemical engineering at UPRM. I would like to acknowledge NIH-INBRE Grant P20-RR016470, for the financial support during these past two years.

I would like to thank all those special people who work and have worked at the Biomaterials and Biomedical Engineering Laboratory, BBEA. Lorena, you always treated me as an equal, even when I was a freshman in this program. Thank you for all those scientific talks we used to have. I only wish the best for you and your family. You are a true inspiration. Thanks to Janet, Nilmarie, and all the undergraduate students who have worked hand-in-hand on this project with me: Cinthya, Alexandra, and Luis.

Hector Luis, you have been a true friend since I took my first steps in this laboratory. Never would have I imagined that I would have been blessed with such a wonderful friendship as the one you and I share. I could have never asked for a better

laboratory partner and friend. We have cried and laughed, yelled and whispered together. This is a friendship that will last throughout the ages. You will always be like the older brother I never had. There will never be a duet like you and I. Aside from this title and diploma I will receive; you are the best thing that I will take with me when I leave this laboratory. I love you and I will always be proud of being your friend. You are a warrior and you will win all the battles you choose to win, no matter what obstacles you are faced with. Always remember that.

I would also like to thank Sindia, Natacha, and Milton who befriended me since my first days here UPRM. Thank you for always lending me a hand and a shoulder on which to cry on. I will always treasure your friendships dearly. You have also been true friends through thick and thin. I only wish that one day I will see you all as successful doctors and I hope we always keep in touch.

Finally, I would like to thank my parents, Caroline and Francisco. Thank you for teaching me the value of education, of responsibility, and of independence. It has been through you that I have learned that we are never too late to follow our dreams. I will never meet two individuals who have more passion for what they do every single day. Thank you for being true teachers. Thank you for never giving up, for enjoying what you do, and for being the best parents in the world. You have given me everything I have ever needed and more. Whenever I have failed, whenever I have fallen, you have always been there to get me up and pushing me forward. God could not have given me better parents. I will love you always. I hope I have made you proud.

To my siblings, Francisco, Clarisabeth, and Eddalys, thank you. You have always shared your undivided love with me. You have never judged me, but have always loved

me. I hope I am an example for you, as you have been a true example for me. Francisco, you have shown me that raw talent is not enough, that dedication and perseverance are more important. Always remember that you are gifted in many ways. You are an intelligent and wonderful human being. Do not let any gift go to waste, as God has blessed you with them because He knows you are capable of amazing things. Clarisabeth, you have always taught me that love is the answer. Follow your dreams; do not pay attention to comparisons, for you are a unique human being with amazing possibilities. Thank you for always showing me that following the crowd never pays off.

To all those other people who have been there throughout these past two and a half years, thank you. To all my friends, you all have given me a bit of yourselves. Therefore, this work includes bits and pieces of you all. Never has a person been blessed with such a wonderful group of friends. You know who you are. You will always be in my heart.

TABLE of CONTENTS

List of Tables.....	xi
List of Figures.....	xii
List of Equations.....	xiv
List of Appendixes.....	xv
Chapter One	
Introduction.....	1
1.1 Motivation.....	1
1.2 Project Description.....	2
1.3 References.....	5
Chapter Two	
Background.....	6
2.1 Hydrogel Membranes.....	6
2.2 Model Proteins.....	12
2.2.1 Horse Skeletal Muscle Myoglobin and Horse Heart Myoglobin	14
2.2.2 Bovine and Porcine Hemoglobins.....	16
2.2.3 Hen Egg White Lysozyme.....	22
2.3 Protein Crystallization.....	25
2.3.1 Vapor diffusion and Hanging-drop Method	29
2.3.2 Protein Crystallization by Counter-diffusion in GCBs.....	31
2.4 References.....	35

Chapter Three

Literature Review.....	38
3.1 Protein Stability in Aqueous/Non-aqueous Environments	38
3.1.1 Aqueous Environments.....	38
3.1.2 Non-aqueous Environments.....	41
3.2 Protein Encapsulation.....	45
3.2.1 Protein Encapsulation in Hydrogel Membranes	46
3.2.2. Heme-protein Encapsulation in Sol-Gel Glasses	47
3.3 References	51

Chapter Four

Objectives.....	54
-----------------	----

Chapter Five

Materials and Methods.....	55
5.1 Polymerization of Hydrogel Membranes.....	55
5.2 Proteins.....	56
5.3 Stability and Biological Activity Studies.....	56
5.4 Correlation Length Measurements.....	59
5.5 Protein Crystallization.....	60

Chapter Six

Results and Discussion.....	62
-----------------------------	----

6.1 Stability of Heme-Proteins After Exposure to UV Light.....	62
6.2 Stability of Heme-Proteins in Pre-Polymeric Solutions.....	64
6.3 Biological Activity of Heme-Proteins in Hydrogel Membranes.....	73
6.4 Correlation Length Measurements.....	83
6.5 Lysozyme Crystal Stability in Pre-Polymeric Solutions.....	86
6.6 References.....	93
Chapter Seven	
Conclusions.....	95
Appendices.....	98

LIST of TABLES

Table 2.1	Primary Structure of Horse Heart Myoglobin and Skeletal Muscle Myoglobin	18
Table 2.2	Spectral Properties of Ferrous and Ferric Horse Myoglobin	19
Table 2.3	Primary Structures of α and β Chains of Porcine Hemoglobin and Bovine Hemoglobin	20,21
Table 2.4	Primary Structure of Hen Egg White Lysozyme	24
Table 2.5	Crystallization Methods	27
Table 6.1	Comparison of Optimized Hydrogel Morphologies	66
Table 6.2	Soret and Q band Positions of All Proteins Exposed to Pre-Polymeric Solution Components of the Anionic Morphology (Position in nm, NV = band not visible)	66
Table 6.3	Soret and Q band Positions of All Proteins Exposed to Pre-Polymeric Solution Components of the Cationic Morphology (Position in nm, NV = band not visible)	70
Table 6.4	Soret and Q band Positions of All Proteins Exposed to Pre-Polymeric Solution Components the Neutral Morphology (Position in nm, NV – band not visible)	72
Table 6.5	Absorbance parameters of Met, Deoxy, and Carboxy Proteins Encapsulated in the Anionic Morphology (Position in nm, NV – band not visible)	74
Table 6.6	Absorbance parameters of Met, Deoxy, and Carboxy Proteins Encapsulated in the Cationic Morphology (Position in nm, NV – band not visible)	76
Table 6.7	Absorbance parameters of Met, Deoxy, and Carboxy Proteins Encapsulated in the Neutral Morphology (Position in nm, NV – band not visible)	78
Table 6.8	Duration of HEWL Tetragonal Crystals in Pre-Polymeric Solution Components	88
Table 6.9	Duration of HEWL Tetragonal Crystals Exposed to Various MAA:PEGDMA1000 Morphologies	91

LIST of FIGURES

Figure 2.1	Representation of ξ , Correlation Length	9
Figure 2.2	Porphin ring and heme pocket representation	15
Figure 2.3	Structures of (left) horse skeletal muscle myoglobin and (right) horse heart myoglobin	17
Figure 2.4	Structure of (left) Hen Egg White Lysozyme structure and (right) HEWL tetragonal crystal	24
Figure 2.5	Schematic of Hanging Drop Method for Protein Crystallization	30
Figure 2.6	Granada Crystallization Box Setup	33
Figure 6.1	Comparison of the UV-vis spectra of (left) mMb and (right) hMb after exposure to UV light source. ■ Native protein ($\lambda_{\max} = 406\text{nm}$); ■ after 300s ($\lambda_{\max} = 406\text{nm}$); ■ after 1200s ($\lambda_{\max} = 406\text{nm}$).	63
Figure 6.2	Effect of MAA:PEGDMA1000 Pre-Polymeric Solution Components on the UV-vis Spectrum of mMb. ■ MAA+NaOH ($\lambda_{\max} = 410$); ■ MAA+PEGDMA1000 ($\lambda_{\max} = 401$); ■ Pre-Polymeric Solution ($\lambda_{\max} = 407$); ■ EtOH (30%) ($\lambda_{\max} = 410$)	68
Figure 6.3	Effects of HCl Normality on UV-vis Spectrum of mMb. ■ Native mMb ($\lambda_{\max} = 410$); ■ HCl 6N ($\lambda_{\max} = 407$); ■ HCl 3N ($\lambda_{\max} = 401$); ■ HCl 5N ($\lambda_{\max} = 407$); ■ HCl 0.5N ($\lambda_{\max} = 404$); ■ HCl 1N ($\lambda_{\max} = 404$); ■ HCl 2N ($\lambda_{\max} = 404$)	70
Figure 6.4	Comparison of activity of mMb in (left) PEGMA200:PEGDMA1000 hydrogel membranes and (right) MAA:PEGDMA1000 hydrogel membranes. ■ Metaquo state ($\lambda_{\max} = 413, 395$); ■ Deoxy state ($\lambda_{\max} = 424, 422$); ■ Carboxy state ($\lambda_{\max} = 421, 406$)	76
Figure 6.5	Comparison of correlation length (nm) measurements of optimized morphologies. ■ PEGMA200:PEGDMA1000; ■ DMAEM:PEGDMA1000; ■ MAA:PEGDMA1000	85
Figure 6.6	Comparison of HEWL Crystal (left) Before and (right) After Exposure to 30% EtOH Solution. Time of Exposure: 2h 46min	88
Figure 6.7	Comparison of HEWL crystals before and after exposure 100% MAA Time of exposure: MAA – 165min	92

Figure 6.8 Comparison of HEWL crystal (left) before and (right) after exposure to MAA:PEGDMA1000 pre-polymeric solution. Time of exposure: 92 155min

LIST of EQUATIONS

Equation 2.1	Peppas-Merrill Model for $1/M_c$	8
Equation 2.2	M_n , number average molecular weight between crosslinks	10
Equation 2.3	n , number of crosslinks along the polymer chain	10
Equation 2.4	$\left(\overline{r^2}\right)^{1/2}$, root mean squared end-to-end distance of the polymer chain in the freely jointed state	11
Equation 2.5	$\left(\overline{r_o^2}\right)^{1/2}$, root mean squared end-to-end distance of the polymer chain in the unperturbed state	11
Equation 2.6	Correlation Length, ξ	11

APPENDIX 1

Appendix 1.1	Soret Band of hMb in MAA:PEGDMA1000 Pre-Polymeric Solution Components. ■ hMb+MAA+NaOH 5M ($\lambda_{\max} = 410\text{nm}$); ■ hMb+PEGDMA1000+EtOH ($\lambda_{\max} = 413\text{nm}$); ■ hMb+Pre-Polymeric Solution ($\lambda_{\max} = 407\text{nm}$)	94
Appendix 1.2	Soret and Q Bands of bHb in MAA:PEGDMA1000 Pre-Polymeric Solution Components. ■ bHb+MAA+NaOH 5M (Soret $\lambda_{\max} = 406\text{nm}$; Q $\lambda_{\max} = 628\text{nm}$); ■ bHb+PEGDMA1000+EtOH (Soret $\lambda_{\max} = 414\text{nm}$; Q $\lambda_{\max} = 524\text{nm}$); ■ bHb+Pre-Polymeric Solution (Soret $\lambda_{\max} = 406\text{nm}$; Q $\lambda_{\max} = \text{NV}$). NV = not visible	95
Appendix 1.3	Soret and Q Bands of pHb in MAA:PEGDMA1000 Pre-Polymeric Solution Components. ■ pHb+MAA+NaOH 5M (Soret $\lambda_{\max} = 416\text{nm}$; Q $\lambda_{\max} = \text{NV}$); ■ pHb+PEGDMA1000+EtOH (Soret $\lambda_{\max} = 408\text{nm}$; Q $\lambda_{\max} = \text{NV}$); ■ pHb+Pre-Polymeric Solution (Soret $\lambda_{\max} = 410\text{nm}$; Q $\lambda_{\max} = \text{NV}$)	96
Appendix 1.4	Soret Band of mMb in DMAEM:PEGDMA1000 Pre-Polymeric Solution. ■ mMb+DMAEM+HCl 6N ($\lambda_{\max} = 410\text{nm}$); ■ mMb+PEGDMA1000+EtOH ($\lambda_{\max} = 410\text{nm}$); ■ mMb+Pre-Polymeric Solution ($\lambda_{\max} = 410\text{nm}$)	97
Appendix 1.5	Soret band of hMb in DMAEM:PEGDMA1000 Pre-polymeric Solution Components. ■ hMb+DMAEM+HCl 6N ($\lambda_{\max} = 401\text{nm}$); ■ hMb+PEGDMA1000+EtOH ($\lambda_{\max} = 413\text{nm}$); ■ hMb+Pre-Polymeric Solution ($\lambda_{\max} = 404\text{nm}$)	98
Appendix 1.6	Soret and Q Bands of bHb in DMAEM:PEGDMA1000 Pre-Polymeric Solution Components. ■ bHb+DMAEM+HCl 6N (Soret $\lambda_{\max} = 406\text{nm}$; Q $\lambda_{\max} = 538\text{nm}$); ■ bHb+PEGDMA1000+EtOH (Soret $\lambda_{\max} = 406\text{nm}$; Q $\lambda_{\max} = 630\text{nm}$); ■ bHb+Pre-Polymeric Solution (Soret $\lambda_{\max} = 406\text{nm}$; Q $\lambda_{\max} = \text{NV}$). NV = not visible	99
Appendix 1.7	Soret and Q bands of pHb in DMAEM:PEGDMA1000 Pre-polymeric Solution Components. ■ pHb+DMAEM+HCl 6N (Soret $\lambda_{\max} = 412\text{nm}$; Q $\lambda_{\max} = 521\text{nm}$); ■ pHb+PEGDMA1000+EtOH (Soret $\lambda_{\max} = 410\text{nm}$; Q $\lambda_{\max} = 573\text{nm}, 630\text{nm}$); ■ pHb+Pre-Polymeric Solution (Soret $\lambda_{\max} = 412\text{nm}$; Q $\lambda_{\max} = 531\text{nm}$)	100

Appendix 1.8	Soret Bands of mMb in PEGMA200:PEGDMA1000 Pre-polymeric Solution Components. ■ mMb+PEGDMA1000+EtOH ($\lambda_{\max} = 413\text{nm}$); ■ mMb+PEGMA200+EtOH ($\lambda_{\max} = 401\text{nm}$); ■ mMb+Pre-Polymeric Solution ($\lambda_{\max} = 410\text{nm}$)	101
Appendix 1.9	Soret Band of hMb in PEGMA200:PEGDMA1000 Pre-polymeric Solution Components. ■ hMb+PEGMA200 ($\lambda_{\max} = 401\text{nm}$); ■ hMb+PEGDMA1000+EtOH ($\lambda_{\max} = 410\text{nm}$); ■ hMb+Pre-Polymeric Solution ($\lambda_{\max} = 413\text{nm}$)	102
Appendix 1.10	Soret and Q bands of bHb in PEGMA200:PEGDMA1000 Pre-polymeric Solution Components. ■ bHb+PEGMA200+EtOH (Soret $\lambda_{\max} = 406\text{nm}$; Q $\lambda_{\max} = 630\text{nm}$); ■ bHb+PEGDMA1000+EtOH (Soret $\lambda_{\max} = 406\text{nm}$; Q $\lambda_{\max} = 626\text{nm}$); ■ bHb+Pre-Polymeric Solution (Soret $\lambda_{\max} = 406\text{nm}$; Q $\lambda_{\max} = 628\text{nm}$)	103
Appendix 1.11	Soret and Q bands of pHb in PEGMA200:PEGDMA1000 Pre-polymeric Solution Components. ■ pHb+PEGMA200+EtOH (Soret $\lambda_{\max} = 408$; Q $\lambda_{\max} = 630\text{nm}$); ■ pHb+PEGDMA1000+EtOH (Soret $\lambda_{\max} = 404$; Q $\lambda_{\max} = 636\text{nm}$); ■ pHb+Pre-Polymeric Solution (Soret $\lambda_{\max} = 406$; Q $\lambda_{\max} = 628\text{nm}$)	104
Appendix 1.12	Soret and Q bands of mMb After Exposure to UV light. ■ native mMb (Soret $\lambda_{\max} = 406\text{nm}$; Q $\lambda_{\max} = 634\text{nm}$); ■ mMb after 300s (Soret $\lambda_{\max} = 410\text{nm}$; Q $\lambda_{\max} = 580\text{nm}$); ■ mMb after 1200s (Soret $\lambda_{\max} = 410\text{nm}$; Q $\lambda_{\max} = \text{NV}$). NV = not visible	105
Appendix 1.13	Soret and Q bands of hMb After Exposure to UV light. ■ native hMb (Soret $\lambda_{\max} = 410\text{nm}$; Q $\lambda_{\max} = \text{NV}$); ■ hMb after 300s (Soret $\lambda_{\max} = 410\text{nm}$; Q $\lambda_{\max} = \text{NV}$); ■ hMb after 1200s (Soret $\lambda_{\max} = 410\text{nm}$; Q $\lambda_{\max} = \text{NV}$). NV = not visible	106
Appendix 1.14	Soret and Q bands of bHb After Exposure to UV light. ■ native bHb (Soret $\lambda_{\max} = 406\text{nm}$; Q $\lambda_{\max} = 536\text{nm}, 578\text{nm}, 626\text{nm}$); ■ bHb after 300s (Soret $\lambda_{\max} = 406\text{nm}$; Q $\lambda_{\max} = 536\text{nm}, 578\text{nm}, 626\text{nm}$); ■ bHb after 1200s (Soret $\lambda_{\max} = 406\text{nm}$; Q $\lambda_{\max} = \text{NV}$). NV = not visible	107
Appendix 1.15	Soret and Q bands of pHb After Exposure to UV light. ■ native pHb (Soret $\lambda_{\max} = 406\text{nm}$; Q $\lambda_{\max} = 536\text{nm}, 630\text{nm}$); ■ pHb after 300s (Soret $\lambda_{\max} = 406\text{nm}$; Q $\lambda_{\max} = 536\text{nm}, 630\text{nm}$); ■ pHb after 1200s (Soret $\lambda_{\max} = 406\text{nm}$; Q $\lambda_{\max} = 536\text{nm}, 630\text{nm}$)	108

Appendix 1.16	Biological Activity of mMb in MAA:PEGDMA1000 Membranes. ■ metaquo ($\lambda_{\max} = 395\text{nm}$); ■ deoxy ($\lambda_{\max} = 422\text{nm}$); ■ carboxy ($\lambda_{\max} = 406\text{nm}$)	109
Appendix 1.17	Biological Activity of hMb in MAA:PEGDMA1000 Membranes. ■ metaquo ($\lambda_{\max} = 396\text{nm}$); ■ deoxy ($\lambda_{\max} = 421\text{nm}$); ■ carboxy ($\lambda_{\max} = 405\text{nm}$)	110
Appendix 1.18	Biological Activity of bHb in MAA:PEGDMA1000 Membranes. ■ metaquo (Soret $\lambda_{\max} = 396\text{nm}$; Q $\lambda_{\max} = 629\text{nm}$); ■ deoxy (Soret $\lambda_{\max} = 416\text{nm}$; Q $\lambda_{\max} = 628\text{nm}$); ■ carboxy (Soret $\lambda_{\max} = 405\text{nm}$; Q $\lambda_{\max} = 522\text{nm}, 628\text{nm}$)	111
Appendix 1.19	Biological Activity of bHb in MAA:PEGDMA1000 Membranes. ■ metaquo (Soret $\lambda_{\max} = 396\text{nm}$; Q $\lambda_{\max} = \text{NV}$); ■ deoxy (Soret $\lambda_{\max} = 419\text{nm}$; Q $\lambda_{\max} = \text{NV}$); ■ carboxy (Soret $\lambda_{\max} = 406\text{nm}$; Q $\lambda_{\max} = 525\text{nm}, 560\text{nm}$). NV = not visible	112
Appendix 1.20	Biological Activity of mMb in DMAEM:PEGDMA1000 Membranes. ■ metaquo ($\lambda_{\max} = 398\text{nm}$); ■ deoxy ($\lambda_{\max} = 421\text{nm}$); ■ carboxy ($\lambda_{\max} = 421\text{nm}$)	113
Appendix 1.21	Biological Activity of hMb in DMAEM:PEGDMA1000 Membranes. ■ metaquo ($\lambda_{\max} = 397\text{nm}$); ■ deoxy ($\lambda_{\max} = 418\text{nm}$); ■ carboxy ($\lambda_{\max} = 409\text{nm}$)	114
Appendix 1.22	Biological Activity of bHb in DMAEM:PEGDMA1000 Membranes. ■ metaquo (Soret $\lambda_{\max} = 393\text{nm}$; Q $\lambda_{\max} = 628\text{nm}$); ■ deoxy (Soret $\lambda_{\max} = 416\text{nm}$; Q $\lambda_{\max} = 628\text{nm}$); ■ carboxy (Soret $\lambda_{\max} = 409\text{nm}$; Q $\lambda_{\max} = 628\text{nm}$)	115
Appendix 1.23	Biological Activity of pHb in DMAEM:PEGDMA1000 Membranes. ■ metaquo (Soret $\lambda_{\max} = 397\text{nm}$; Q $\lambda_{\max} = 577\text{nm}, 628\text{nm}$); ■ deoxy (Soret $\lambda_{\max} = 417\text{nm}$; Q $\lambda_{\max} = 553\text{nm}$); ■ carboxy (Soret $\lambda_{\max} = 409\text{nm}$; Q $\lambda_{\max} = 548\text{nm}, 560\text{nm}, 628\text{nm}$)	116
Appendix 1.24	Biological Activity of mMb in PEGMA200:PEGDMA1000 Membranes. ■ metaquo ($\lambda_{\max} = 413\text{nm}$); ■ deoxy ($\lambda_{\max} = 424\text{nm}$); ■ carboxy ($\lambda_{\max} = 421\text{nm}$)	117
Appendix 1.25	Biological Activity of hMb in PEGMA200:PEGDMA1000 Membranes. ■ metaquo ($\lambda_{\max} = 411\text{nm}$); ■ deoxy ($\lambda_{\max} = 422\text{nm}$); ■ carboxy ($\lambda_{\max} = 418\text{nm}$)	118

Appendix 1.26 Biological Activity of bHb in PEGMA200:PEGDMA1000 Membranes. ■ metaquo (Soret λ_{\max} = 403nm); Q λ_{\max} = 628nm); ■ deoxy (Soret λ_{\max} = 406nm, 419nm); Q λ_{\max} = 533nm, 560nm, 628nm); ■ carboxy (Soret λ_{\max} = 421nm; Q λ_{\max} = 534nm, 560nm, 630nm) 119

Appendix 1.27 Biological Activity of pHb in PEGMA200:PEGDMA1000 Membranes. ■ metaquo (Soret λ_{\max} = 408nm; Q λ_{\max} = 635nm); ■ deoxy (Soret λ_{\max} = 424nm; Q λ_{\max} = 532nm, 558nm, 630nm); ■ carboxy (Soret λ_{\max} = 420nm; Q λ_{\max} = 535nm, 569nm, 633nm) 120

1 INTRODUCTION

1.1 Motivation

Protein stability is a major concern in the areas of drug delivery and biosensors. The encapsulation and immobilization of proteins and enzymes as biocatalysts and recognition elements for sensors has great limitations. One of the major challenges is that the environments to which these biomolecules will be exposed do not resemble the physiological milieu from which they come from. Some of these limitations are pH, organic solvents, and extreme temperatures.

In most cases, such proteins and enzymes will be encapsulated inside hydrophilic polymer networks, or hydrogel membranes, as these are highly biocompatible. However, immobilization by entrapment of biomolecules in hydrogel membranes requires the exposure of these to organic solvents which may be detrimental to the molecule's stability. Research has shown that certain protein residues are more susceptible than others to interactions with organic solvents such as alcohols [1]. Therefore, the understanding of the effects of pre-polymeric solution components such as monomers, cross-linkers and organic solvents, such as ethanol, is of uttermost importance due to the intrinsic differences between proteins. Characteristics such as isoelectric points and secondary and tertiary structures are essential to the comprehension of the behavior of proteins in different organic environments.

Even though research has focused on the effect of organic media on proteins and enzymes for biocatalysis, very little attention has been paid to the stability of proteins

prior to their incorporation into hydrogel membranes. Various incorporation methods exist and each affects proteins in its own manner. This investigation focuses on the examination of the effects of pre-polymeric solution components on proteins before and after hydrogel polymerization. The results obtained will provide insight into the underlying causes of complete protein degradation, protein conformational changes, and changes in protein activity upon exposure to these environments. This information will then allow for adequate and rational design of polymeric systems that do not adversely affect proteins and enzymes.

1.2 Project Description

This project aimed to study the behavior of hemeproteins prior to and after encapsulation in cationic, anionic, and neutral hydrophilic polymer networks, from here on forth named hydrogel membranes. Four proteins were employed: (1) horse skeletal muscle myoglobin (mMb), (2) horse heart myoglobin (hMb), (3) bovine hemoglobin (bHb), and (4) porcine hemoglobin (pHb). One last protein, lysozyme from hen egg white (HEWL), was utilized for crystallization studies. The choice of proteins for this investigation was not random. Equine skeletal muscle myoglobin (mMb), equine heart myoglobin (hMb), bovine hemoglobin (bHb), porcine hemoglobin (pHb), and hen egg-white lysozyme (HEWL) share certain characteristics that make them attractive. All five proteins are globular proteins. mMb, hMb, bHb, and pHb share isoelectric points: mMb and hMb have near “neutral” pIs in the range of 7.1 to 7.4, while bHb and pHb have a pI

of 6.8. HEWL has a basic pI of 9.2. They also hold promise in fields of interest such as medical diagnostics and environmental or biological sensors.

These proteins were encapsulated in pH-sensitive hydrogel membranes which are explored as an alternate encapsulation media. These are ideal for this type of application as hydrogels resemble natural living tissue due to their high water content which contributes to their biocompatibility [2-4].

Three monomers and one cross-linker were investigated: methacrylic acid (anionic, MAA), dimethylaminoethyl methacrylate (cationic, DMAEM) and poly(ethylene glycol) monomethyl ether methacrylate n=200 (neutral, PEGMA200), and poly(ethylene glycol) dimethacrylate n=1000 (cross-linker, PEGDMA1000). Experiments focused on the optimization of the three morphologies for the encapsulation of all five proteins as the pre-polymeric solution contains organic solvents with extreme pH, such as the monomers and ethanol. The proteins were exposed to ratios of these components until no significant displacements in the Soret bands of the hemeproteins were observed. These morphologies were then polymerized and the activity of the proteins was assessed by UV-vis spectroscopy. Activity of the proteins was evaluated as the ability of these to change oxidation states: metaquo to deoxy and deoxy to carboxy. The location and intensity of the Soret and Q bands were also evaluated.

The swelling behavior of the hydrogel membranes was investigated by measuring the mesh size of the networks, ξ , with the Peppas-Merill model. This parameter was obtained by measuring the post-polymerization, dry, and equilibrium swollen volumes of the empty membranes. All three monomers utilized in this investigation presented distinct swelling characteristics as dictated by the presence and absence of ionic moieties. The

characterization of this parameter provided an estimate of the space available for protein encapsulation at different pH conditions, as well as the hydrogel response to varying conditions. It is important to mention that highly cross-linked morphologies were utilized to impede protein release.

It has been demonstrated that crystallized proteins maintain their biological activity, and are even more active and more efficient than their solubilized counterparts. Therefore, this investigation also focused on the employment of hydrogel membranes as media for protein crystallization through the method of counterdiffusion, specifically utilizing the Granada Crystallization Box (GCB). This device utilizes gels – commonly silica and agarose gels- to minimize the effects of convection during the crystallization process. Numerous experiments have shown superior crystalline qualities, as well as larger crystal sizes, ideal for X-ray diffraction studies and applications such as those pursued in this investigation. Due to the sensitive nature of the material utilized for the construction of the GCB, the neutral morphologies PEGMA200-PEGDMA1000 and HEMA-PEGDMA1000 were synthesized within the GCB to test whether crystals could be successfully grown in the capillaries. This morphology was optimized to enhance diffusion of the buffer/precipitant solution as well as entrance of the capillary, as this polymer tends to be brittle.

In line with the stability experiments performed with solubilized heme-proteins, these were also attempted with tetragonal lysozyme crystals grown by the hanging-drop method. These crystals were exposed to different proportions of pre-polymeric solution components and the crystal stability was visually assessed by microscopy. The

morphology chosen was one where crystals lasted the longest without considerable dissolution and could be successfully encapsulated within hydrogel membranes.

1.3 References

- [1] C. L. Stevenson, "Characterization of protein and peptide stability and solubility in non-aqueous solvents," *Current Pharmaceutical Biotechnology*, vol. 1, pp. 165-82, Sep 2000.
- [2] N. Peppas, J. Hilt, A. Khademhosseini, and R. Langer, "Hydrogels in biology and medicine: From molecular principles to bionanotechnology," *Advanced Materials*, vol. 18, pp. 1345-1360, JUN 6 2006.
- [3] N. Peppas, P. Bures, W. Leobandung, and H. Ichikawa, "Hydrogels in pharmaceutical formulations," *European Journal of Pharmaceutics and Biopharmaceutics*, vol. 50, pp. 27-46, JUL 2000.
- [4] N. Peppas, Y. Huang, M. Torres-Lugo, J. Ward, and J. Zhang, "Physicochemical, foundations and structural design of hydrogels in medicine and biology," *Annual Review of Biomedical Engineering*, vol. 2, pp. 9-29, 2000.

2 BACKGROUND

2.1 Hydrogel Membranes

Hydrophilic polymer networks have become, in the last twenty years, important tools in the substitution of live tissue and the controlled administration of pharmaceuticals or “drug delivery.” Hydrogel membranes are enticing for their biocompatibility and the ability to mold their properties to the user’s advantage. Drug delivery applications include, but are not limited to peroral delivery, transdermal delivery, drug delivery in the GI tract, and rectal delivery [1, 2]. Hormonal and nicotine patches, improvement in the bioadhesiveness of rectal suppositories, direct delivery of antibiotics for the treatment of stomach ulcers caused by the organism *Helicobacter pylori*, and oral administration of insulin for the treatment of diabetes are some of the areas where hydrogels are making surprising contributions.

Other areas within medicine where hydrogels have become essential tools are the areas of tissue engineering, diagnostic devices, and medical sensors [1, 3]. In tissue engineering, hydrogel membranes serve as scaffolds that mimic the extracellular matrix, providing cells the necessary rigidity, support, and adhesion to promote cell migration and formation of tissue. Fibroblasts, chondrocytes, and osteoblasts have been successfully immobilized in hydrogel membranes and have demonstrated superior attachment to hydrogels than to other types of supports [4]. Due to their response to diverse stimuli, hydrogels have been incorporated in diagnostic devices to control the

location of cells and proteins. Hydrogels synthesized with gradients of particular molecules have been used to promote cell adhesion and migration [1].

The aforementioned capability of hydrogels to respond to pH, temperature, or concentration of a molecule has been taken advantage for sensor design. Chromate (CrO_4^{2-}) [5] and lead II (Pb^{2+}) [6] sensors are some examples. Glucose oxidase, lactate oxidase, and alcohol oxidase have been immobilized in hydrogels and used as biosensors for diverse analytes [7-11].

Hydrogels are three-dimensional, hydrophilic, polymeric networks that can absorb and retain vast amounts of water and/or biological fluids [12, 13]. These can be composed of a single polymer (homopolymers) or a mixture of polymers (copolymers). The insolubility of these networks is provided by chemical or physical crosslinks (tie-points, entanglements, etc.) [13]. Hydrogels' water content, consistency, and biocompatibility make them unique candidates for studies involving live tissue, cells, and biomolecules [14].

Hydrogel membranes can be classified as ionic or neutral. This is due to the pendant groups of the polymeric chains. Ionic membranes can be reclassified as anionic or cationic. Anionic membranes swell at high pH and collapse at low pH. Cationic membranes have the opposite behavior [12, 13]. Examples of ionic pendant groups may be carboxylic or sulfonic acid. Examples of these monomers are methacrylic acid (MAA – anionic), dimethylaminoethyl methacrylate (DMAEM – cationic), and poly(ethylene glycol monomethyl ether methacrylate) (PEGMA200 – neutral).

The characterization of these membranes has been achieved by several experimentally determined parameters, one of the most important being the correlation

length or average pore size, ξ , illustrated in Figure 2.1. The polymers utilized in this investigation are pH-sensitive and their swelling behavior is dependent on the pH of the solution. It is also important to understand ξ , as this parameter provides a measure of the space available for diffusion within the membrane. Membranes which have a ξ not proportional to the radius of the protein to be encapsulated may cause size exclusion effects or precipitation of the protein from solution. Membranes which have a ξ much larger than the protein's radius may cause the proteins to be released prematurely. Two other important parameters include the polymer volume fraction in the swollen state ($v_{2,s}$), and the average molecular weight between crosslinks (M_c) [1, 13, 15, 16]. The first is a measure of the amount of fluid absorbed by the membrane and the second is a measure of the degree of crosslinking of the membrane. The determination of the network pore size provides an estimate of the space available within the hydrogel membranes for the encapsulated proteins, since the main objective of this investigation is encapsulation and retention, not release.

The parameters ξ and M_c , correlation length and number average molecular weight between crosslinks, respectively, are determined by the Peppas-Merrill model [17],

$$\frac{1}{M_c} = \frac{2}{M_n} - \frac{\left(\frac{\bar{v}}{V_1}\right) \left[\ln(1 - v_{2,s}) + v_{2,s} + \chi_1 v_{2,s}^2 \right]}{v_{2,r} \left[\left(\frac{v_{2,s}}{v_{2,r}}\right)^{1/3} - \frac{1}{2} \left(\frac{v_{2,s}}{v_{2,r}}\right) \right]} \quad (2.1)$$

where \bar{v} is the specific volume of the polymer, and V_1 is the molar volume of the swelling agent, in this case, water. The polymer volume fraction immediately

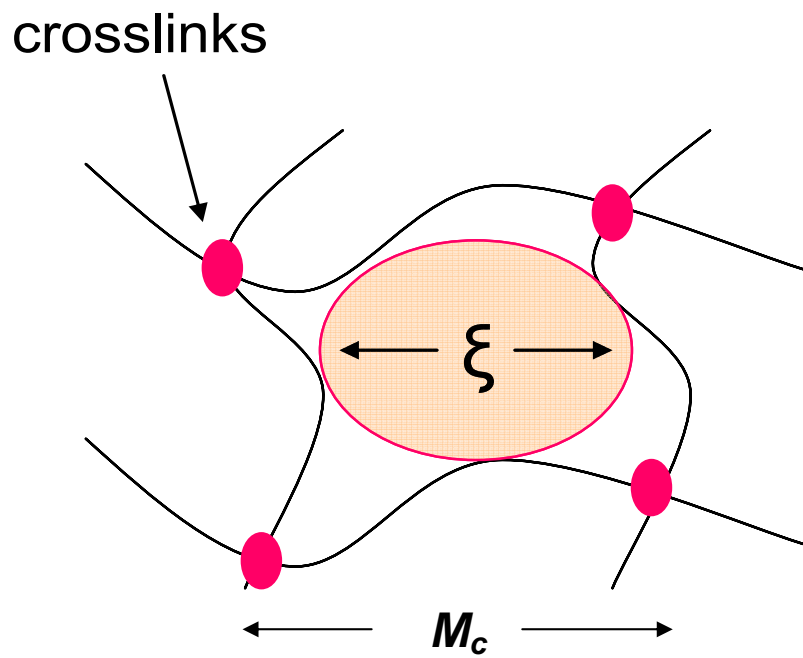


Figure 2.1. Representation of ξ , correlation length.

after polymerization is represented by $v_{2,r}$ and it is determined by dividing the polymer volume after polymerization by the polymer volume after drying. The next parameter is $v_{2,s}$, the swollen polymer volume fraction, and it is a ratio of the dry polymer volume to the equilibrium swollen polymer volume. The Flory polymer-solvent interaction parameter is given by χ_1 and M_n is the number average molecular weight between crosslinks given by equation 2.2,

$$\bar{M}_n = M_o \frac{k_p [M]}{(fk_d k_t [I])^{1/2}} \quad (2.2)$$

where M_o is the molecular weight of the monomer unit, $[M]$ is the monomer concentration, and $[I]$ is the initiator concentration. The following are initiator parameters: k_d is the initiator's kinetic constant of decay, k_t is the initiator's kinetic constant of termination, and k_p is the initiator's kinetic constant of propagation. Finally, f is the initiator's efficiency. The number of crosslinks along the polymer chain, n , can be calculated from the average molecular weight between crosslinks, M_c , as follows,

$$n = \frac{2\bar{M}_c}{M_r} \quad (2.3)$$

where M_r is the molecular weight of the repeating unit (monomer). The root mean squared end-to-end distance of the polymer chain in the freely jointed state, $\left(\bar{r}^2\right)^{1/2}$, is given by the following equation,

$$\left(\bar{r}^2\right)^{1/2} = l\sqrt{n} \quad (2.4)$$

where l is the bond length (0.154 nm) and n was defined in equation 2.3. The root mean squared end-to-end distance of the polymer chain in the unperturbed state, $\left(\bar{r}_o^2\right)^{1/2}$, is calculated with the following expression,

$$\left(\bar{r}_o^2\right)^{1/2} = \sqrt{C_n}\left(\bar{r}^2\right)^{1/2} \quad (2.5)$$

where C_n is the characteristic ratio of the polymer and $\left(\bar{r}^2\right)^{1/2}$ was defined in equation

2.4. The mesh size or correlation length is given by equation 2.6. The parameters $\nu_{2,s}$ and

$\left(\bar{r}_o^2\right)^{1/2}$ were defined in equations 2.1 and 2.5, respectively.

$$\xi = \nu_{2,s}^{-1/3}\left(\bar{r}_o^2\right)^{1/2} \quad (2.6)$$

Characterization of these parameters is important as these can provide indications towards the behavior of the membrane once proteins are encapsulated in their interior. It is important to consider that proteins that are larger than the available pore size will probably aggregate and precipitate from solution even before the membrane is polymerized.

2.2 Model Proteins

Immobilization of proteins within hydrogel membranes is vital for the improvement of certain applications such as drug administration and recognition elements for biosensors, because of their ability to become powerful drugs and to replace sensors due to their high specificity and selectivity. The proteins employed in this investigation are globular proteins which occur in aqueous, intracellular environments or in the plasma. These are approximately spherical and consist of several domains. Globular proteins are highly soluble in aqueous solutions and upon solubilization form colloidal solutions. Globins are often modeled as consisting of a hydrophobic core surrounded by a hydrophilic external surface which interacts with water. More to the point, residues with apolar side chains are buried within the center of the molecule while polar residues remain exposed to the aqueous environments. This is known as the “hydrophobic effect,” aggregation and burial of hydrophobic residues reduce the number of unfavorable interactions of these residues with water.

Even though globular proteins consist of hydrophobic cores, almost 50% of hydrophobic residues lie on the external surface of the proteins. These apolar patches are

of utmost significance as interactions with other hydrophobic domains on other molecules are possible due to this phenomenon. Globular proteins have a dynamic role in metabolism, in contrast with fibrous proteins which only serve a structural purpose. Globular proteins include all enzymes (lysozyme), protein hormones (calcitonin), albumins, antibodies (immunoglobulins), and lastly heme proteins (hemoglobin and myoglobin).

Hemoglobin and myoglobin are responsible for oxygen transport and sequestration in blood and tissues. This gas transport and storing ability is due to the presence of a non-protein group: heme prosthetic group, see Figure 2.2. Hemoglobin is found in the blood and its main function is oxygen transport to oxygen-depleted tissues, although it also transports carbon dioxide from tissue to the lungs where it is expelled from the body.

Hemoglobins are tetramers, consisting of four chains of two types, α and β . The α -chains are structurally homologous to a myoglobin molecule. Each chain contains a heme group that can bind ligands such as O_2 , CO_2 , CO , and CN , among others. Oxygen binding by hemoglobin is reversible and this facilitates oxygen transport to tissues.

Myoglobin is found in tissues, specifically in muscles, and due to its higher binding affinity to oxygen than hemoglobin, acts as a reserve supply for oxygen (oxymyoglobin). Myoglobins are usually single chains (monomeric) and 75% of the secondary structure of myoglobin is α -helical in nature, which is unusual for globular proteins. Myoglobins are comprised of eight right-handed α -helices connected by short non-helical regions and contain only one heme group per molecule.

The heme prosthetic group is made up of a proto-porphyrin IX ring and an iron Fe^{2+} ion as depicted in Figure 2.2. The porphyrin ring is based on porphin, a tetrapyrrole ring, and each pyrrole contains four carbon atoms and one nitrogen atom. The ferrous iron binds four nitrogen atoms within the porphyrin ring and forms two additional bonds on either side of the heme plane. One of these is to a nitrogen atom on the proximal histidine residue and the sixth remaining bond is protected by the distal histidine residue. This protection is crucial to heme's function as it prevents neighboring heme groups from coming in contact with each other and oxidizing Fe^{2+} to Fe^{3+} , thus preventing the binding of O_2 . Secondly, CO is prevented from irreversibly binding to the Fe^{2+} ion, which impedes the binding of O_2 to the heme group.

Four oxidizing states exist for heme, depending on the sixth coordinate position of Fe: deoxy, with an empty position; oxy, with the position occupied by O_2 ; met or ferri, with the position occupied by H_2O ; and carboxy, with the position occupied by CO. All these states have unique UV absorption spectra.

The heme proteins employed in this investigation are two myoglobins – horse skeletal muscle myoglobin and horse heart myoglobin, - and two hemoglobins – porcine and bovine. These were chosen for their similar structural characteristics as well as for their commercial availability.

2.2.1 Horse Skeletal Muscle Myoglobin and Horse Heart Myoglobin

The main function of mMb and hMb is the rapid transport and diffusion of oxygen to the mitochondria in rapidly contracting muscle tissue; mMb within skeletal

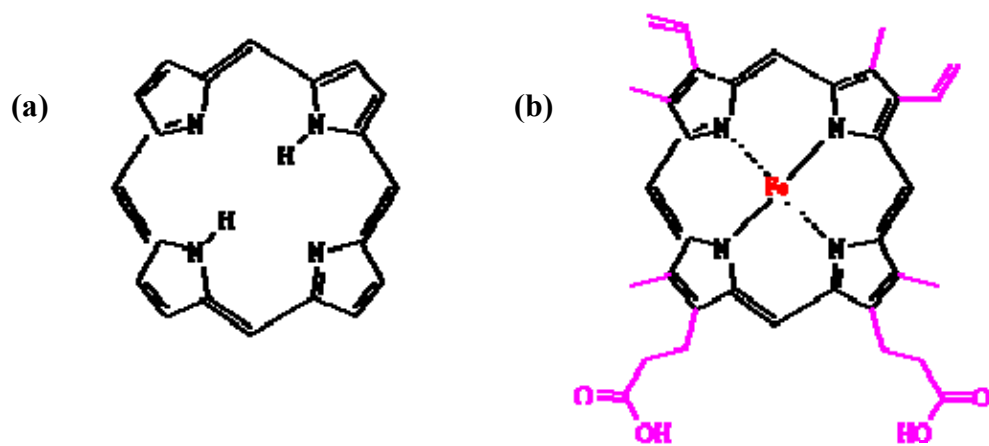


Figure 2.2. (a) Porphyrin ring and (b) heme pocket representation.

muscle, and hMb within cardiac muscle. mMb and hMb are both a single polypeptide chain of 153 amino acid residues with no disulfide bridges, and with a molecular weight of 16.9kDa [18]. The major component of mMb has an isoelectric point of 7.3 and its minor component's pI is 6.8. The pI of hMb's major component is 7.2, while its minor component's pI is the same as mMb's. There is an 88% homology between the primary structures of both proteins. The only difference are the positions 2, 11, 29, 32, 40, 49, 69, 76, 86, 89, 104, 115, 137, and 149, where hMb has a lysine residue while mMb has leucine. Structurally, however, these two myoglobins are identical. Figure 2.3 illustrates the structure of hMb and mMb and Table 2.1 shows a comparison between the primary structures of both proteins.

mMb and hMb are also commercially available proteins. These were chosen on account of similar spectroscopic and functional characteristics to HbI. Encapsulated mMb and hMb in hydrogel membranes could find potential uses as oxygen carriers to regenerating tissue. They could also stand alone as environmental sensors for CO, NO and CN, since it is widely known that heme has greater affinity for CO and other ligands. Table 2.2 shows spectral properties of ferric and ferrous Mb.

2.2.2 Bovine and Porcine Hemoglobins

BHb and pHb have two sets of α and β chains as discussed earlier. The α and β chains of bHb have molecular weights of 15.1kDa and 15.9kDa, respectively. The α chain is 141 residues in length and the β chain is 145 residues long. The α and β chains of pHb have molecular weights of 15.1kDa and 16.1kDa, respectively. Its α chain is also

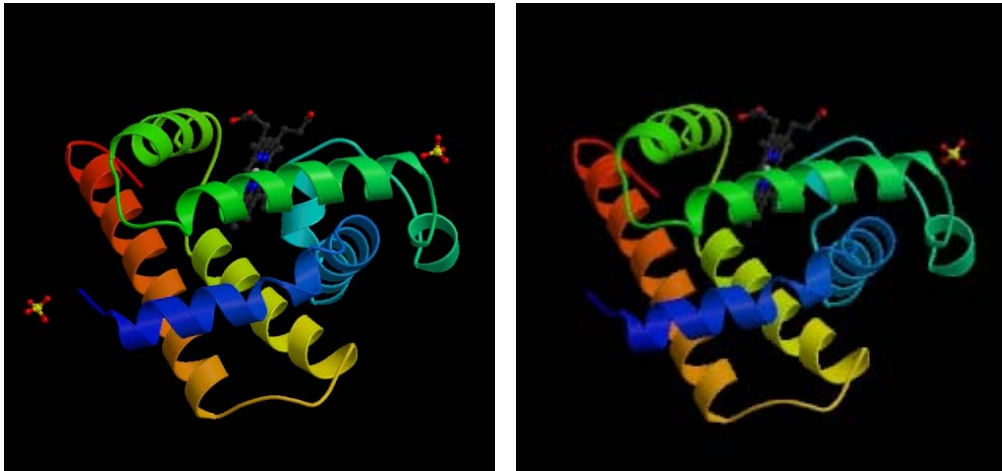


Figure 2.3. Structures of (left) horse skeletal muscle myoglobin and (right) horse heart myoglobin (Courtesy of RCSB Protein Data Bank)

Table 2.1. Primary structure of horse heart myoglobin and skeletal muscle myoglobin.

Residue	hMb	mMb									
1	Gly	Gly	41	Glu	Glu	81	His	His	121	Gly	Gly
2	Lys	Leu	42	Lys	Lys	82	His	His	122	Asp	Asp
3	Ser	Ser	43	Phe	Phe	83	Glu	Glu	123	Phe	Phe
4	Asp	Asp	44	Asp	Asp	84	Ala	Ala	124	Gly	Gly
5	Gly	Gly	45	Lys	Lys	85	Glu	Glu	125	Ala	Ala
6	Glu	Glu	46	Phe	Phe	86	Lys	Leu	126	Asp	Asp
7	Trp	Trp	47	Lys	Lys	87	Lys	Lys	127	Ala	Ala
8	Gln	Gln	48	His	His	88	Pro	Pro	128	Gln	Gln
9	Gln	Gln	49	Lys	Leu	89	Lys	Leu	129	Gly	Gly
10	Val	Val	50	Lys	Lys	90	Ala	Ala	130	Ala	Ala
11	Lys	Leu	51	Thr	Thr	91	Gln	Gln	131	Met	Met
12	Asn	Asn	52	Glu	Glu	92	Ser	Ser	132	Thr	Thr
13	Val	Val	53	Ala	Ala	93	His	His	133	Lys	Lys
14	Trp	Trp	54	Glu	Glu	94	Ala	Ala	134	Ala	Ala
15	Gly	Gly	55	Met	Met	95	Thr	Thr	135	Lys	Leu
16	Lys	Lys	56	Lys	Lys	96	Lys	Lys	136	Glu	Glu
17	Val	Val	57	Ala	Ala	97	His	His	137	Lys	Leu
18	Glu	Glu	58	Ser	Ser	98	Lys	Lys	138	Phe	Phe
19	Ala	Ala	59	Glu	Glu	99	Ile	Ile	139	Arg	Arg
20	Asp	Asp	60	Asp	Asp	100	Pro	Pro	140	Asn	Asn
21	Ile	Ile	61	Lys	Leu	101	Ile	Ile	141	Asp	Asp
22	Ala	Ala	62	Lys	Lys	102	Lys	Lys	142	Ile	Ile
23	Gly	Gly	63	Lys	Lys	103	Tyr	Tyr	143	Ala	Ala
24	His	His	64	His	His	104	Lys	Leu	144	Ala	Ala
25	Gly	Gly	65	Gly	Gly	105	Glu	Glu	145	Lys	Lys
26	Gln	Gln	66	Thr	Thr	106	Phe	Phe	146	Tyr	Tyr
27	Glu	Glu	67	Val	Val	107	Ile	Ile	147	Lys	Lys
28	Val	Val	68	Val	Val	108	Ser	Ser	148	Glu	Glu
29	Lys	Leu	69	Lys	Leu	109	Asp	Asp	149	Lys	Leu
30	Ile	Ile	70	Thr	Thr	110	Ala	Ala	150	Gly	Gly
31	Arg	Arg	71	Ala	Ala	111	Ile	Ile	151	Phe	Phe
32	Lys	Leu	72	Lys	Leu	112	Ile	Ile	152	Gln	Gln
33	Phe	Phe	73	Gly	Gly	113	His	His	153	Gly	Gly
34	Thr	Thr	74	Gly	Gly	114	Val	Val			
35	Gly	Gly	75	Ile	Ile	115	Lys	Leu			
36	His	His	76	Lys	Leu	116	His	His			
37	Pro	Pro	77	Lys	Lys	117	Ser	Ser			
38	Glu	Glu	78	Lys	Lys	118	Lys	Lys			
39	Thr	Thr	79	Lys	Lys	119	His	His			
40	Lys	Leu	80	Gly	Gly	120	Pro	Pro			

Table 2.2. Spectral properties of ferrous and ferric horse myoglobin.

Derivate	Ferrous Mb	
	λ_{\max} (nm)	ϵ (mM ⁻¹ cm ⁻¹)
Mb (deoxy)	435	121
	560	13.8
MbO ₂ (oxy)	542	13.9
	580	14.4
MbCO (carboxy)	424	207
	540	15.4
	579	13.9
Derivate	Ferric Mb	
	λ_{\max} (nm)	ϵ (mM ⁻¹ cm ⁻¹)
Mb ⁺ (H ₂ O) (metaquo) pH 6.4	408	188
	502	10.2
	630	3.9
Mb ⁺ (NO) (nitric oxide)	422	116
	540	11.3

Table 2.3. Primary structures of α and β chains of porcine hemoglobin and bovine hemoglobin.

Residue	α -pHb	α -bHb	β -pHb	β -bHb
1	Val	Val	Val	
2	Lys	Lys	His	Met
3	Ser	Ser	Lys	Lys
4	Ala	Ala	Ser	THR
5	Ala	Ala	Ala	Ala
6	Asp	Asp	Glu	Glu
7	Lys	Lys	Glu	Glu
8	Ala	Gly	Lys	Lys
9	Asn	Asn	Glu	Ala
10	Val	Val	Ala	Ala
11	Lys	Lys	Val	Val
12	Ala	Ala	Lys	Thr
13	Ala	Ala	Gly	Ala
14	Trp	Trp	Lys	Phe
15	Gly	Gly	Trp	Trp
16	Lys	Lys	Gly	Gly
17	Val	Val	Lys	Lys
18	Gly	Gly	Val	Val
19	Gly	Gly	Asn	Lys
20	Gln	His	Val	Val
21	Ala	Ala	Asp	Asp
22	Gly	Ala	Glu	Glu
23	Ala	Glu	Val	Val
24	His	Tyr	Gly	Gly
25	Gly	Gly	Gly	Gly
26	Ala	Ala	Glu	Glu
27	Glu	Glu	Ala	Ala
28	Ala	Ala	Lys	Lys
29	Lys	Lys	Gly	Gly
30	Glu	Glu	Arg	Arg
31	Arg	Arg	Lys	Lys
32	Met	Met	Lys	Lys
33	Phe	Phe	Val	Val
34	Lys	Lys	Val	Val
35	Gly	Ser	Tyr	Tyr
36	Phe	Phe	Pro	Pro
37	Pro	Pro	Trp	Trp
38	Thr	Thr	Thr	Thr
39	Thr	Thr	Gln	Gln
40	Lys	Lys	Arg	Arg
41	Thr	Thr	Phe	Phe
42	Tyr	Tyr	Phe	Phe
43	Phe	Phe	Glu	Glu
44	Pro	Pro	Ser	Ser
45	His	His	Phe	Phe
46	Phe	Phe	Gly	Gly
47	Asn	Asp	Asp	Asp
48	Lys	Lys	Lys	Leu
49	Ser	Ser	Ser	Ser
50	His	His	Asn	Thr
51	Gly	Gly	Ala	Ala
52	Ser	Ser	Asp	Asp

Table 2.3 (Cont.) Primary structures of α and β chains of porcine hemoglobin and bovine hemoglobin.

Residue	α -pHb	α -bHb	β -pHb	β -bHb
53	Asp	Ala	Ala	Ala
54	Gln	Gln	Val	Val
55	Val	Val	Met	Met
56	Lys	Lys	Gly	Asn
57	Ala	Gly	Asn	Asn
58	His	His	Pro	Pro
59	Gly	Gly	Lys	Lys
60	Gln	Ala	Val	Val
61	Lys	Lys	Lys	Lys
62	Val	Val	Ala	Ala
63	Ala	Ala	His	His
64	Asp	Ala	Gly	Gly
65	Ala	Ala	Lys	Lys
66	Lys	Lys	Lys	Lys
67	Thr	Thr	Val	Val
68	Lys	Lys	Leu	Lys
69	Ala	Ala	Gln	Asp
70	Val	Val	Ser	Ser
71	Gly	Glu	Phe	Phe
72	His	His	Ser	Ser
73	Lys	Lys	Asp	Asn
74	Asp	Asp	Gly	Gly
75	Asp	Asp	Lys	Met
76	Lys	Lys	Lys	Lys
77	Pro	Pro	His	His
78	Gly	Gly	Lys	Lys
79	Ala	Ala	Asp	Asp
80	Lys	Lys	Asn	Asp
81	Ser	Ser	Lys	Lys
82	Ala	Glu	Lys	Lys
83	Lys	Lys	Gly	Gly
84	Ser	Ser	Thr	Thr
85	Asp	Asp	Phe	Phe
86	Lys	Lys	Ala	Ala
87	His	His	Lys	Ala
88	Ala	Ala	Lys	Lys
89	His	His	Ser	Ser
90	Lys	Lys	Glu	Glu
91	Lys	Lys	Lys	Lys
92	Arg	Arg	His	His
93	Val	Val	Cys	Cys
94	Asp	Asp	Asp	Asp
95	Pro	Pro	Gln	Lys
96	Val	Val	Lys	Lys
97	Asn	Asn	His	His
98	Phe	Phe	Val	Val
99	Lys	Lys	Asp	Asp

Residue	α -pHb	α -bHb	β -pHb	β -bHb
100	Lys	Lys	Pro	Pro
101	Lys	Lys	Glu	Glu
102	Ser	Ser	Asn	Asn
103	His	His	Phe	Phe
104	Cys	Ser	Arg	Lys
105	Lys	Lys	Lys	Lys
106	Lys	Lys	Lys	Lys
107	Val	Val	Gly	Gly
108	Thr	Thr	Asn	Asn
109	Lys	Lys	Val	Val
110	Ala	Ala	Ile	Lys
111	Ala	Ser	Val	Val
112	His	His	Val	Val
113	His	Lys	Val	Val
114	Pro	Pro	Lys	Lys
115	Asp	Ser	Ala	Ala
116	Asp	Asp	Arg	Arg
117	Phe	Phe	Arg	Asn
118	Asn	Thr	Lys	Phe
119	Pro	Pro	Gly	Gly
120	Ser	Ala	His	Lys
121	Val	Val	Asp	Glu
122	His	His	Phe	Phe
123	Ala	Ala	Asn	Thr
124	Ser	Ser	Pro	Pro
125	Lys	Lys	Asp	Val
126	Asp	Asp	Val	Lys
127	Lys	Lys	Gln	Gln
128	Phe	Phe	Ala	Ala
129	Leu	Leu	Ala	Asp
130	Ala	Ala	Phe	Phe
131	Asn	Asn	Gln	Gln
132	Val	Val	Lys	Lys
133	Ser	Ser	Val	Val
134	Thr	Thr	Val	Val
135	Val	Val	Ala	Ala
136	Leu	Leu	Gly	Gly
137	Thr	Thr	Val	Val
138	Ser	Ser	Ala	Ala
139	Lys	Lys	Asn	Asn
140	Tyr	Tyr	Ala	Ala
141	Arg	Arg	Leu	Leu
142			Ala	Ala
143			His	
144			Lys	
145			Tyr	
146			His	

141 residues in length and the β chain is 146 residues long. Both hemoglobins have a pI of 6.8. The homology between the α chains of both proteins is 87% and that of the β chains is 84% [19]. One important discrepancy in the structure of bHb's β chain is the deletion of a histidine residue in position 2. This deletion provides the protein with the ability to function without the aid of 2,3-diphosphoglycerate (DPG), the principal allosteric effector of human adult hemoglobin and it translates into a lower oxygen affinity compared to other hemoglobins [19]. Figure 2.4 shows the structure of pHb and bHb.

2.2.3 Hen Egg White Lysozyme

HEWL or muramidase is a highly compact globular protein composed of 129 amino acids and with an average molecular weight of 14.4 kDa. This enzyme has an $\alpha+\beta$ fold consisting of five to seven α helices and a three-stranded antiparallel β sheet. HEWL has an ellipsoidal shape with a large cleft on one side where the active site is located. This protein is a natural antibiotic and is found in high concentrations in mammalian mucus, tears, saliva, kidneys, milk, and in blood. HEWL's antibacterial action lies on its preferential hydrolysis of the β -1,4 glucosidic linkages between N-acetylmuramic acid and N-acetylglucosamine which occur in the mucopeptide cell wall structure of certain microorganisms [20, 21]. Table 2.7 shows the primary structure of HEWL.

Lysozyme's crystal structure was solved with 2Å resolution in 1965 by David Chilton Phillips [22]. Lysozyme crystals may be tetragonal, orthorhombic, triclinic, and monoclinic, depending on the crystallization conditions. Tetragonal crystals are the most

common and easiest to attain, while orthorhombic crystals grow at temperatures greater than 298K. The tetragonal lattice has two three dimensions. Of these, two are equal. In the case of HEWL, $a = b = 39\text{\AA}$, and $c = 78\text{\AA}$. Figure 2.5 shows the molecular structure of HEWL and a tetragonal crystal grown in our laboratory. HEWL crystals are some of the simplest crystals to grow and solubility diagrams are available for different systems.

As mentioned previously, crystallized proteins often retain their native functions due to the hydration layer that remains upon crystallization. Therefore, it is highly desirable to study if the encapsulation of such crystals is possible in the hydrogel systems studied in this investigation. The HEWL tetragonal crystal is used as a model, due to the ease with which the crystal can be grown.

2.3 Protein Crystallization

A protein crystal is a viable form of the protein which has been shown to retain its native activity. Therefore, it is important to regard these as potential substitutes for soluble protein solutions. For many years, protein crystallization and crystallography were regarded more of an art than a science. Only in recent years, with the advent of proteomics and genomics, has protein crystallization become vital in such fields such as cosmetics, nano-structured materials (electronics), the wine industry, and medicine, to mention just a few.

There is no standard buffer or solvent that can maintain a protein in solution stable without any significant loss of structure and biological activity. Protein

Table 2.4. Primary structure of hen egg white lysozyme

Residue	HEWL								
1	Lys	27	Asn	53	Tyr	79	Pro	105	Met
2	Val	28	Trp	54	Gly	80	Cys	106	Asn
3	Phe	29	Val	55	Ile	81	Ser	107	Ala
4	Gly	30	Cys	56	Lys	82	Ala	108	Trp
5	Arg	31	Ala	57	Gln	83	Lys	109	Val
6	Cys	32	Ala	58	Ile	84	Lys	110	Ala
7	Glu	33	Lys	59	Asn	85	Ser	111	Trp
8	Lys	34	Phe	60	Ser	86	Ser	112	Arg
9	Ala	35	Glu	61	Arg	87	Asp	113	Asn
10	Ala	36	Ser	62	Trp	88	Ile	114	Arg
11	Ala	37	Asn	63	Trp	89	Thr	115	Cys
12	Met	38	Phe	64	Cys	90	Ala	116	Lys
13	Lys	39	Asn	65	Asn	91	Ser	117	Gly
14	Arg	40	Thr	66	Asp	92	Val	118	Thr
15	His	41	Gln	67	Gly	93	Asn	119	Asp
16	Gly	42	Ala	68	Arg	94	Cys	120	Val
17	Lys	43	Thr	69	Thr	95	Ala	121	Gln
18	Asp	44	Asn	70	Pro	96	Lys	122	Ala
19	Asn	45	Arg	71	Gly	97	Lys	123	Trp
20	Tyr	46	Asn	72	Ser	98	Ile	124	Ile
21	Arg	47	Thr	73	Arg	99	Val	125	Arg
22	Gly	48	Asp	74	Asn	100	Ser	126	Gly
23	Tyr	49	GLy	75	Lys	101	Asp	127	Cys
24	Ser	50	Ser	76	Cys	102	Gly	128	Arg
25	Lys	51	Thr	77	Asn	103	Asn	129	Lys
26	Gly	52	Asp	78	Ile	104	Gly		

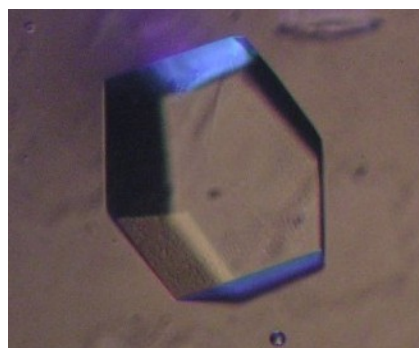
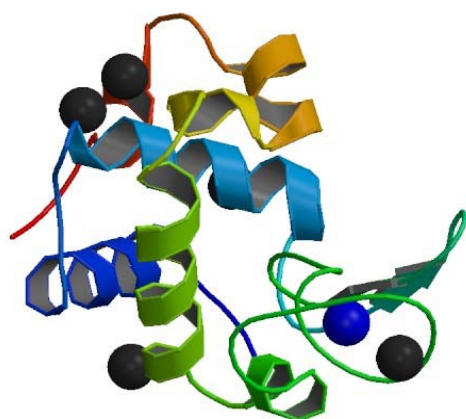


Figure 2.4. Structure of (left) Hen Egg White Lysozyme structure (Courtesy of RCSB Protein Data Bank) and (right) HEWL tetragonal crystal

crystallization may be the answer to some of the riddles that encompass protein encapsulation since this process does not damage the protein but merely “freezes it,” conserving its structural integrity as well as biological function. Therefore, protein crystallization is of interest to this investigation as it could resolve the primary concern of protein stability within hydrogel membranes.

Protein crystallization has three major fields of application: (1) structural biology and drug design; (2) bioseparations; and (3) controlled drug delivery. The first application involves the determination of the three dimensional structure of proteins to determine the primary structure and therefore aid in the characterization of the macromolecule. This, in turn, allows the design of molecules that can exactly fit into binding sites of macromolecules and block their function in a disease pathway. Protein crystallization is a benign procedure which facilitates the downstream processing of products of fermentation, such as insulin or other proteins. Finally, the administration of crystallized active ingredients renders in more potent and long-lasting doses with less concentration of the drug [23].

Crystallization methods are diverse [24] and some are mentioned in Table 2.8. Of these, the most popular are batch methods, evaporation, dialysis methods, free interface diffusion, vapor diffusion methods, and temperature-induced crystallization. Batch methods entail the mixing of the sample with the precipitant and appropriate additives to create homogeneous crystallization requiring no equilibration with a reservoir. This is a popular method for crystallization of small molecules. Advantages of this method are its speed and simplicity. However, only a narrow space of precipitant/sample concentration

can be sampled with a single experiment. To achieve crystallization, the experiment must be close to crystal-promoting conditions.

Evaporation works by reducing the volume of the saturated solution by heating. This causes the sample excess to be discarded as crystals because the reduced volume cannot hold the same amount of sample. This method is not always practicable as impurities present in the solution will also crystallize along with the desired crystals. Therefore, to obtain pure crystals, evaporation of the solvent must be stopped before the impurities begin to separate out.

The dialysis method necessitates that the protein concentration be constant (if it is assumed that the membrane stretching is negligible and the initial solution fills the crystallization chamber completely). This method has the advantage that the precipitant concentration can be altered during the course of the experiment. Microdialysis is one of the most popular variations of this method. The sample is separated from the precipitant solution by a semi-permeable membrane which allows small molecules such as ions, buffers, and salts to pass, but prevent biological macromolecules from crossing the membrane. Equilibration kinetics depends on the molecular weight cut-off of the dialysis membrane, the precipitant, the ratio of volume, the concentration of the components inside and outside of the microdialysis cell and the geometry of the cell.

Free interface diffusion is a popular method used by NASA in microgravity experiments [24]. The protein sample comes in liquid contact with the precipitant solution in an attempt to create a clearly defined interface between the sample and the precipitant. Over time, the sample and precipitant diffuse into one another and crystallization occurs at the interface, on the side of high sample/low precipitant or

Table 2.5. Crystallization Methods

1	Bulk Crystallization	<ul style="list-style-type: none">○ Fast○ Simple○ Good for small molecules
2	Evaporation	<ul style="list-style-type: none">○ Sample must be free of impurities○ Impurity crystallization
3	Dialysis	<ul style="list-style-type: none">○ Protein concentration constant○ Protein concentration may be altered
4	Free interface diffusion	<ul style="list-style-type: none">○ Allows for screening of crystallization conditions○ Used in microgravity experiments
5	Vapor diffusion on plates (sitting drop)	<ul style="list-style-type: none">○ Easy○ Fast○ Requires small amount of sample
6	Vapor diffusion in hanging drops	
7	Temperature-induced crystallization	<ul style="list-style-type: none">○ Reversible control of supersaturation○ Screen crystallization conditions for samples with temperature-dependent solubility

vice versa. This technique allows for screening a gradient of sample/precipitant concentration combinations.

Vapor diffusion by sitting drop is an easy method, requires a small amount of sample and allows a large amount of flexibility during screening and optimization. This method also allows for speed and simplicity. However, crystals can adhere to the surface where the drop sits on, making removal difficult. This can also be an advantage to the method, as this surface can assist in nucleation.

Temperature influences nucleation and crystal growth by manipulating solubility and supersaturation of the sample. An advantage of tweaking crystallization by manipulation of temperature is the precise, quick, and reversible control of relative supersaturation. Temperature fluctuations can be useful in obtaining high quality crystals by screening a larger range of crystallization conditions since for a sample with temperature-dependent solubility, changes in temperature can equate to changes in crystallization reagent conditions.

2.3.1 Vapor diffusion and Hanging-drop Method

The crystallization methods relevant to this investigation are the hanging drop method and counter-diffusion, which were utilized for crystal growth (hanging drop) and experimentation (counterdiffusion). The principle of vapor diffusion is to equilibrate a drop of a protein solution, buffer, and precipitant with a reservoir of buffer and precipitant in a sealed environment [24]. The amount of precipitant in the drop is initially

insufficient to induce nucleation and crystallization. Equilibration of the system commences and water is incorporated into the reservoir. The drop volume decreases yet the protein and precipitant concentrations increase, bringing the protein past the metastable point to nucleation. Equilibration is rapid at first, yet decreases as the difference in concentration of the precipitant between the drop and the reservoir approach each other. The equilibration rate is a function of the precipitants used and their concentrations, the distance between the reservoir and drop, temperature, and droplet to reservoir volume ratio. This process is essentially complete when the osmolarities of both solutions are equal. Vapor diffusion provides two mechanisms to drive the system to supersaturation: increase in precipitant concentration and increase in protein concentration.

The hanging-drop method uses the aforementioned vapor diffusion principles. Figure 2.6 illustrates the setup. Essentially, the drop is placed on a siliconized cover glass which is placed upside down. It is important to mention that the rim of the well is covered with a thin film of high vacuum grease or silicon to seal the environment and prevent drop desiccation. Although this method is essentially a micro-scale experiment it can be scaled up once adequate crystallization conditions are found. Any type of protein can be grown utilizing this method. Crystals of canavalin and concanavalin B have even been grown by the hanging-drop method in experiments conducted in space shuttles [24].

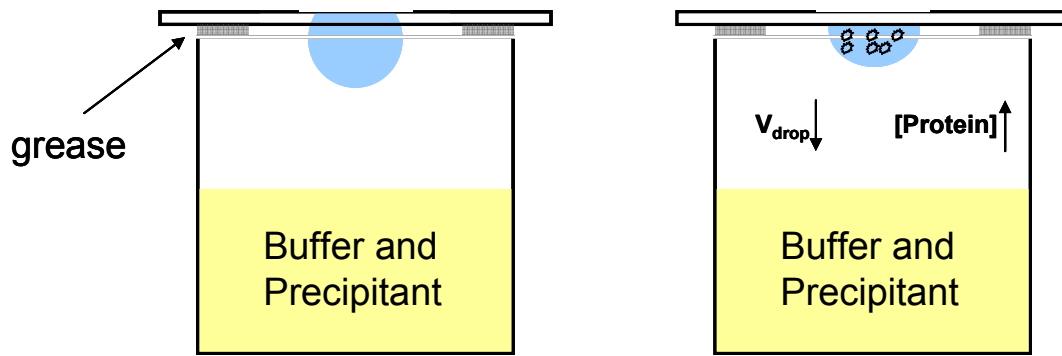


Figure 2.5. Schematic of hanging drop method for protein crystallization.

2.3.2 Protein Crystallization by Counter-diffusion in Granada

Crystallization Boxes

Crystallization in gels was developed to solve several problems of batch crystallization methods. The main limitation of these crystallization techniques is the lack of control over the development of supersaturation, as a supersaturation value is instantaneously achieved; the supersaturation rate is then fixed and controlled solely by the growth process [25]. This is a severe restriction for biomolecules which nucleate at high supersaturation. Therefore, these methods rely on mechanisms such as temperature changes and solvent evaporation, amongst others, to reach the necessary supersaturation level. However, three difficulties arise: first, the rate of change of supersaturation must be adjusted to ensure that it is not too slow or too fast; second, the rate of increase of supersaturation is dependent on the solubility of the molecule to be crystallized; and third, nucleation and growth kinetics may be governed by more than one parameter. These last two problems present the need for screening for optimum crystallization conditions and increase the time and work necessary to obtain high quality crystals.

Crystallization by counterdiffusion, also known as the gel-acupuncture method was designed to decrease convective flux by confining the mother solution into growth cells with small characteristic dimensions (capillaries) and by this taking advantage of a geometry allowing a long diffusional path (capillary length) with a narrow area of diffusion front (capillary cross-section) [26, 27]. The main result is the existence of two large gradients of two or more quantities that control supersaturation. This in turn, ensures that crystals grow at different points of the capillary under different

supersaturation values and supersaturation rates of change, essentially screening and optimizing crystallization conditions at once [25].

This method establishes diffusion as the primary mechanism of mass transport by the utilization of gels. Gels, in turn, eliminate the dependence of the process on viscosity. Thus, convection is removed and crystal sedimentation is avoided. This method essentially mimics microgravity. Gels used for this method have been polyacrylamide, agarose, and silica [24].

The method of counter diffusion was developed by Garcia-Ruiz et al. [24, 28] and it utilizes the principles of crystallization in gels. It consists of a small rectangular polystyrene box called the Granada Crystallization Box (GCB). The box is filled with gel by two ways: agarose gel with buffer and precipitant is allowed to solidify inside the box or a thin cap of agarose gel is solidified on top of the buffer and precipitant solution. The buffer/precipitant solution can also be allowed to diffuse into the solidified agarose gel. A capillary is filled with the protein solution and then it is capped with wax to avoid evaporation of the protein solution. The capillary is then introduced into the gel and the cap is placed on the crystallization box. Figure 2.6 depicts a schematic.

The process by which protein crystals grow inside this capillary is known as counterdiffusion. The precipitant diffuses into the capillary and as it goes deeper and deeper, it produces a continuous supersaturation gradient. That is, three areas of

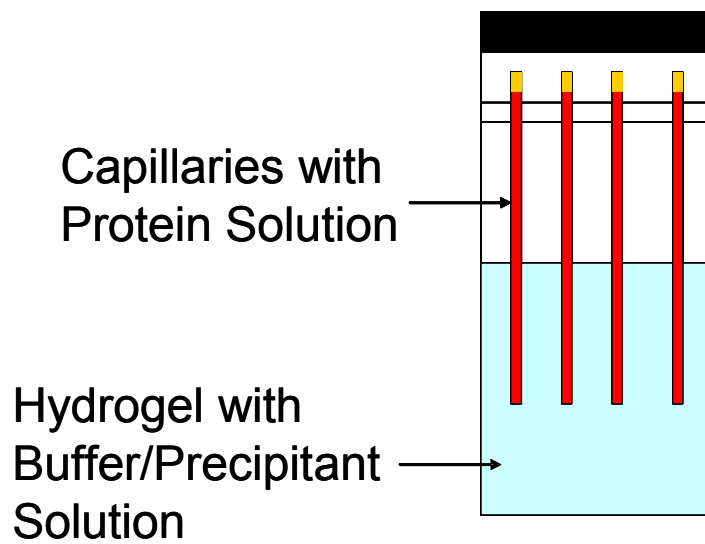


Figure 2.6. Granada Crystallization Box Setup

saturation exist: a subsaturated region where no crystallization or nucleation events occur, a labile region where a supersaturation state is attained, and a metastable region where crystals can grow in a continuous range. Therefore, crystallization is caused by the evolution of a nucleation front in the absence of convective fluid motion. Crystals produced at the beginning of this front or in the supersaturated region may be small and even amorphous. Deeper into the capillary or deeper into the metastable region crystals grow larger and also fewer, since small crystals tend to redissolve. In the end, high quality crystals are obtained.

The utilization of hydrogels as convection-eliminating agents for protein crystallization allows for the possibility of growing protein crystals in membranes where the proteins have already been encapsulated. It has been suggested that protein crystals, since they are crystallized with their hydration layer intact, are active and stable for longer periods of time than proteins in solution [23]. Therefore, this could provide an alternate protein encapsulation for use in therapeutic or biosensorial applications [14]. As an example, insulin is the only drug that is administered in a crystalline form [29] and cross-linked enzymes and proteins have been tested and investigated for possible use as vaccines and are already marketed for the treatment of specific digestive tract diseases [30, 31]. These experiments would provide valuable insight into the possible utilization, stability and activity of protein crystals as substitutes for proteins in solution.

2.4 References

- [1] N. Peppas, J. Hilt, A. Khademhosseini, and R. Langer, "Hydrogels in biology and medicine: From molecular principles to bionanotechnology," *Advanced Materials*, vol. 18, pp. 1345-1360, JUN 6 2006.
- [2] N. Peppas, P. Bures, W. Leobandung, and H. Ichikawa, "Hydrogels in pharmaceutical formulations," *European Journal of Pharmaceutics and Biopharmaceutics*, vol. 50, pp. 27-46, JUL 2000.
- [3] F. Cavalieri, F. Miano, P. D'Antona, and G. Paradossi, "Study of gelling behavior of poly(vinyl alcohol)-methacrylate for potential utilizations in tissue replacement and drug delivery," *Biomacromolecules*, vol. 5, pp. 2439-2446, NOV-DEC 2004.
- [4] S. Sershen, G. Mensing, M. Ng, N. Halas, D. Beebe, and J. West, "Independent optical control of microfluidic valves formed from optomechanically responsive nanocomposite hydrogels," *Advanced Materials*, vol. 17, pp. 1366+, JUN 6 2005.
- [5] Y. Zhang, F. Ji, G. M. Brown, and T. Thundat, *Anal. Chem.*, vol. 75, 2003.
- [6] K. Liu and H. F. Ji, *Anal Sci*, vol. 20, 2004.
- [7] K. Sirkark, M. Revzin, and V. Pishko, *Anal Chem*, 2000.
- [8] G. Jobst, I. Moser, M. Varahram, P. Svasek, E. Aschauer, Z. Trajanoski, P. Wach, P. Kotanko, F. Skrabal, and G. Urban, *Anal Chem*, vol. 68, 1996.
- [9] C. Jimenez, J. Bartrol, N. Derooij, and M. Koudelkahep, *Anal Chim Acta*, vol. 351, 1997.
- [10] M. V. Pishko, A. C. Michael, and A. Heller, *Anal Chem*, vol. 63, 1991.
- [11] D. W. Schmidtke and A. Heller, *Anal Chem*, vol. 70, 1998.
- [12] N. A. Peppas and A. R. Khare, "Preparation, Structure and Diffusional Behavior of Hydrogels in Controlled-Release," *Advanced Drug Delivery Reviews*, vol. 11, pp. 1-35, JUL-AUG 1993.
- [13] N. Peppas, Y. Huang, M. Torres-Lugo, J. Ward, and J. Zhang, "Physicochemical, foundations and structural design of hydrogels in medicine and biology," *Annual Review of Biomedical Engineering*, vol. 2, pp. 9-29, 2000.

- [14] C. K. Simi and T. E. Abraham, "Encapsulation of crosslinked subtilisin microcrystals in hydrogel beads for controlled release applications," *European Journal of Pharmaceutical Sciences*, vol. 32, pp. 17-23, 2007.
- [15] C. Hassan, F. Doyle, and N. Peppas, "Dynamic behavior of glucose-responsive poly(methacrylic acid-g-ethylene glycol) hydrogels," *Macromolecules*, vol. 30, pp. 6166-6173, OCT 6 1997.
- [16] C. Bell and N. Peppas, "Water, solute and protein diffusion in physiologically responsive hydrogels of poly(methacrylic acid-g-ethylene glycol)," *Biomaterials*, vol. 17, pp. 1203-1218, JUN 1996.
- [17] N. A. Peppas and E. W. Merrill, "Crosslinked PVA Hydrogels as Swollen Elastic Networks," *Journal of Applied Polymer Science*, vol. 21, pp. 1763-1770, 1977.
- [18] S. Dewilde, E. Angelini, L. Kiger, M. Marden, M. Beltramini, B. Salvato, and L. Moens, "Structure and function of the globin and globin gene from the Antarctic mollusc *Yoldia eightsi*," *Biochemical Journal*, vol. 370, pp. 245-253, FEB 15 2003.
- [19] M. K. Safo and D. J. Abraham, "The X-ray structure determination of bovine carbonmonoxy hemoglobin at 2.1 Å resolution and its relationship to the quaternary structures of other hemoglobin crystal forms," *Protein Science*, vol. 10, pp. 1091-1099, 2001.
- [20] E. Holler, J. Rupley, and G. Hess, "Productive and Unproductive Lysozyme-Chitosaccharide Complexes. Equilibrium Measurements," *Biochemistry*, vol. 14, p. 1088, 1975.
- [21] E. Holler, J. Rupley, and G. Hess, "Productive and Unproductive Lysozyme-Chitosaccharide Complexes. Kinetic Investigations," *Biochemistry*, vol. 14, p. 2377, 1975.
- [22] D. Phillips, "The Hen Egg-White Lysozyme Molecule," *Proc Natl Acad Sci U S A*, vol. 57, p. 484, 1967.
- [23] S. Pechenov, B. Shenoy, M. X. Yang, S. K. Basu, and A. L. Margolin, "Injectable controlled release formulations incorporating protein crystals," *Journal of Controlled Release*, vol. 96, pp. 149-158, 2004.
- [24] A. McPherson, *Crystallization of Biological Macromolecules* Woodbury: Cold Spring Harbor Laboratory Press, 1999.

- [25] J. M. García-Ruiz, L. A. González-Ramírez, J. A. Gavira, and F. Otálora, "Granada Crystallisation Box: a new device for protein crystallisation by counter-diffusion techniques," *Acta Crystallographica Section D Biological Crystallography*, vol. D58, pp. 1638-1642, 2002.
- [26] J. M. García-Ruiz and A. Moreno, "Investigations on Protein Crystal Growth by the Gel Acupuncture Method," *Acta Crystallographica Section D Biological Crystallography*, vol. D50, pp. 484-490, 1994.
- [27] C. Biertümpfel, J. Basquin, D. Suck, and C. Sauter, "Crystallisation of biological macromolecules using agarose gel," *Acta Crystallographica Section D Biological Crystallography*, vol. D58, pp. 1657-1659, 2002.
- [28] J. Ng, J. Gavira, and J. Garcia-Ruiz, "Protein crystallization by capillary counterdiffusion for applied crystallographic structure determination," *Journal of Structural Biology*, vol. 142, pp. 218-231, APR 2003.
- [29] S. K. Basu, C. P. Ghovardan, C. W. Jung, and A. L. Margolin, "Protein crystals for the delivery of biopharmaceuticals," *Expert opinion on biological therapy*, vol. 4, p. 17, 2004.
- [30] N. Clair, B. Shenoy, L. Jacob, and A. Margolin, "Cross-linked protein crystals for vaccine delivery," *Proceedings of the National Academy of the Sciences of the United States of America*, vol. 96, pp. 9469-9474, AUG 17 1999.
- [31] A. A. Elkordy, R. T. Forbes, and B. W. Barry, "Stability of crystallised and spray-dried lysozyme," *International Journal of Pharmaceutics*, vol. 278, pp. 209-219, 2004.

3 LITERATURE REVIEW

A fundamental objective of this investigation is the understanding of protein stability and activity in pre-polymeric solution components and in the synthesized hydrogel membranes. For this reason, it is important to understand the behavior of proteins in aqueous and non-aqueous solvents. As more interest grows for bioengineering and biotechnology, the usage of non-aqueous or organic solvents has become more frequent for several reasons: increased solubility of lipid substrates, altered substrate specificity, simpler product recovery, and reduced microbial contamination, among others [1]. It has become evident that proteins are not exclusively soluble in water or aqueous environments. Proteins, such as insulin, have higher solubility and stability in organic solvents such as SDS and ethanol [2].

3.1 Protein Stability in Aqueous/Non-aqueous Environments

3.1.1 Aqueous Environments

It is known that proteins and enzymes exist at physiological conditions: aqueous environments of specific acidity and specific components such as the cell cytosol and extracellular fluids, and specific temperatures. These aforementioned conditions are highly restricted, meaning that once out of a live organism, these conditions cease to exist. It would be easy to assume that, in any other conditions these biomolecules would degrade and denature. However, research has eradicated this thought and it is widely

known that proteins and enzymes exhibit higher catalytic activities and stability in non-aqueous environments, mainly, in organic solvents [2]. However, it is of great importance to understand the interactions of proteins in aqueous media since this gives insight into invaluable information such as their structures and interactions with the hydration layer.

Herskovits and colleagues were pioneers in this field of study as they investigated the denaturation of sperm whale myoglobin, horse heart cytochrome c, and bovine α -chymotrypsinogen by alcohols and glycols, amides, and urea in aqueous media [3-5]. The unfolding, aggregation and exposure of the heme-binding pocket of metalloproteins such as myoglobin and hemoglobin by alcohols were evident by the shifts of the maxima in the Soret band region of 405 to 410nm and their loss of intensity or absorbance. The authors also observed, using a difference spectrum that red shifts (shifts to longer wavelengths) were indicative of surface tryptophyl and tyrosyl side chains coming into contact with the surrounding solvent. Blue shifts (maxima shifts to shorter wavelengths) were indicative of denaturation or the exposure of hydrophobic residues in the core to the surrounding solvent. It was ultimately concluded that the denaturing effect of alcohols increased with an increase of their chain length or hydrocarbon content.

α -Chymotrypsin's behavior was investigated in water-organic solvent mixtures of ethanol (EtOH) and N,N-dimethyl formamide (DMF) by circular dichroism and kinetic studies [6]. Upon complexation of the enzyme with three different oligoamines: putrescine, spermidine, and spermine, the enzyme complex was exposed to different solutions of EtOH and DMF. Two major effects were observed on the catalytic activity: in presence of moderate concentrations (10-30%) of the co-solvents, the enzyme activity was 1.5 to 3 times higher than in aqueous solution, and the range of co-solvent

concentrations (20-40%) at which the enzyme complex retained its activity broadened. In this case, presence of the co-solvents did not have a destabilizing effect on the enzyme and enhanced its biological activity due to enhanced nucleophilicity of functional groups in the enzyme active site.

The stability of halophilic malate dehydrogenase from *Haloarcula marismortui* (*HmMalDH*) and bovine serum albumin (BSA) was studied by another technique, neutron scattering. Water, heavy water (D_2O), and NaCl and KCl were used as solvents. Tehei et al. observed that denaturation of *HmMalDH* NaCl solvents occurred at a higher temperature in H_2O than in D_2O [7]. They conjectured this could be due to stronger ion-water-protein bonds in the hydration shell. The same stabilizing behavior of D_2O was observed for BSA. Molar NaCl solvents had a mild stabilizing effect on BSA. However, this could be attributed to a “salting out”, rather than an actual binding of salt to the protein.

Even though, it seems counter-intuitive to think that proteins have higher stability and activity in aqueous media, the aforementioned investigations show that this is not necessarily the truth. Interactions between the proteins' hydration layer and organic solvents present in aqueous media may increase the activity of enzymes in these harsh environments. Small additions to the peptide chain can also have this same effect. Therefore, it is important to study the behavior of proteins in varying organic environments.

3.1.2 Non-aqueous Environments

It is common knowledge that a folded globular protein has its hydrophobic residues at its core and its hydrophilic residues on its surface. Contact of a protein with some type of non-aqueous, less polar solvent could cause unfolding of the protein, since the hydrophobic residues of the core would come to the surface to protect the hydrophilic residues. This, in turn, would cause a reduction in the free energy of the unfolded state of the protein, since the exposed residues are solvated.

Although this unfolding is usually irreversible, some solvents have shown this process to be reversible with the return of up to 100% biological activity [2, 6, 8-10]. Rariy and Klibanov studied the stability and activity of hen egg white lysozyme in solutions of water and glycerol [9]. After denaturing the protein in urea and dithiothreitol (DTT), they observed a refolding yield in a 90% glycerol solution similar to the refolding yield in pure aqueous media. Even in 99% glycerol, the refolding yield was one-third of that in pure aqueous solvent [9]. They also observed that the longer the reincubation time in the glycerol solutions, the higher the refolding yield. However, denatured lysozyme did not refold at all in 70-80% DMSO solutions. It was ultimately noted that the refolded lysozyme also maintained its biological activity.

UV-Vis spectroscopy and FTIR were utilized by Al-Azzam to test whether spectral changes upon protein dehydration of horse PEG-modified horse radish peroxidase (HRP-PEG) were caused by structural changes or by water removal from the protein [11]. HRP and HRP-PEG were dissolved in a PBS buffer containing toluene at pH 7.0 and containing benzene at pH 12.0. Upon protein dissolution in these solvents, a

red shift (402.5nm to 404nm) was observed in the Soret adsorption band of lyophilized HRP-PEG reconstituted in toluene and benzene. The authors suggested that this shift could be due the electronic interactions caused by binding of toluene and benzene to the heme-binding pocket of the protein. Another reason could be a slight change in the heme-binding pocket environment. A broadening in the maxima of the Q adsorption band was observed for HRP-PEG in benzene and toluene. The same occurred when the pH of the solution was changed to 12. This is explained by the binding of the strong ligand OH⁻ to the heme binding pocket. They also observed that resonant Raman spectra of HRP-PEG were no different than those for HRP alone. This demonstrated that complexation with PEG did not distort the heme-binding pocket of the protein.

The inactivation of yeast inorganic pyrophosphatase was investigated by Grazinoli-Garrido and Sola-Penna [1]. Several organic solvents were utilized, most of them alcohols: methanol (MeOH, 0M to 5M), ethanol (EtOH, 0M to 3M), 1-propanol (0M to 2.5M), 2-propanol (0M to 3M), 3-propanol (0M to 3M) and acetone (0M to 3M). It was observed that MeOH, EtOH and 1-propanol inactivated the enzyme and that the degree of inactivation increased with the hydrophobicity of the solvent at all studied dilutions. Therefore, MeOH provoked the weakest inactivation and 1-propanol the highest. The same observations were made when the inactivation of the enzyme was tested with 1-propanol, 2-propanol, and acetone. The inactivation was least with 1-propanol and greatest in acetone. They proposed that this behavior was caused by the stabilization of an unfolded protein by the hydrophobic solvents due to its interaction with the hydrophobic core residues. The exposure of these residues leads to the inactivation of the catalytic site of the enzyme.

Other investigators such as Lopes [12], and Zaks [13] made similar observations using pure organic solvents. Grazinoli-Garrido also noticed that the inactivation effectiveness of these hydrophobic solvents decreased at higher temperatures. Therefore, proteins were more stable at higher temperatures.

Santos et al. modified the enzyme subtilisin carlsberg with crown ethers and investigated their effect on stability and activity in tetrahydrofuran (THF), acetonitrile, and 1,4-dioxane, organic solvents that theoretically would not cause protein unfolding [14]. Upon verification of catalytic activity of the protein in THF and acetonitrile, increased rate enhancements were observed for the initial rates of reaction catalyzed by the enzyme lyophilized with three crown ethers: 18-c-6, 15-c-5, and 12-c-4. It was also observed that the enzyme colyophilized with 18-c-6 and 15-c-5 were less native in acetonitrile than in THF. After exposure to 1,4-dioxane, no significant spectral changes occurred and the α -helix and β -sheet contents remained almost identical for the enzyme in aqueous buffer. An unexpected result was that the enzyme complex (12-c-4) with the least native structure had the highest catalytic activity. The investigators speculated that the abnormal activation of these enzyme complexes were due to the preservation of the active sites by the crown ethers during dehydration. Upon reconstitution in organic solvents, the ethers were released but active site remained intact.

The interactions between dimethyl sulfoxide (DMSO) and proteins have been extensively studied since it is known to enhance the penetration of cosmetic preparations across the epidermis and its topical application has been shown to alleviate certain types of chronic pain [15]. DMSO is a dipolar and non-protogenic solvent. Its capacity as a hydrogen-bond acceptor disrupts the native structure of proteins because it tends to form

bonds with water and affects hydrogen bonding strength and the structure of water molecules around the protein or its hydration layer [2].

Investigators have observed that DMSO has the ability to stabilize partially unfolded configurations of diverse proteins such as insulin, lysozyme, and trypsin [2]. These proteins, recovered their native structure and some of their biological activity after reconstitution in aqueous media. Klibanov observed that lysozyme deviated very little from its conformation in aqueous media, after dissolution in 10% DMSO [9]. Cytochrome c was not really affected by the presence of DMSO, glycerol, and ethylene glycol [16]. Myoglobin, in co-solvent ratios above 30% DMSO, exhibited an increase in β -sheet content which is a sign of protein aggregation [15]. This behavior was also observed with salmon calcitonin in 70% DMSO [17]. At 100% DMSO, loose α -helices were observed, possibly due to the lack of water and non-protogenic nature of DMSO.

Studies have also been conducted by Bonner and colleagues on the structural stability of synthetic and natural DNA in glycerol, ethylene glycol, formamide, methanol, and DMSO [8]. 21-mer synthetic DNA formed and maintained a duplex structure in water and 99% glycerol. Calf thymus and salmon testes also retained their structure in 99% ethylene glycol. However, no DNA –synthetic or natural- was detected in 99% formamide, methanol, and DMSO. This degradation was explained by the hydrophobic interactions between the solvents and the DNA. Glycerol did not cause damage to the double-helical structure because it was the nonaqueous solvent closest to water, followed distantly by ethylene glycol.

All these studies coincide in that organic solvents when used at high concentrations tend to rob proteins of their hydration layers, therefore disrupting their

natural environments. These interact with hydrophobic residues to unfold the protein and cause disruption of their secondary and tertiary structures. Also, the extent of unfolding is dependent on the hydrophobicity of the solvent. More hydrophobic solvents tend to be more disruptive. It was also observed that solvents may even interact with the active sites of enzymes and change their spectral properties. However, low concentrations of these solvents, in many cases, are better stabilizers and tend to increase the initial rates of reaction of enzymes. On the other hand, no studies were found that investigate the effect of combination of solvents on proteins.

3.2 Protein Encapsulation

Numerous protein immobilization techniques exist, such as physical adsorption, covalent attachment, and encapsulation in polymer and inorganic matrices [18]. There is currently no standard method or material, since each application requires distinctive characteristics. Therefore, research focuses on optimizing each method towards specific applications such as drug delivery, tissue engineering or biosensor technology. Physical adsorption entails the contact of an unloaded matrix with a solution of the biomolecule of interest. In this method pore size is extremely important, as a small pore sizes may present size exclusion problems and a large pore sizes may cause indiscriminate release of the molecule of interest. Covalent attachment of a biomolecule to a matrix is achieved by first encapsulating the biomolecule and then forming a covalent attachment between the network and the protein by means of a chemical reaction.

Protein entrapment is advantageous over other methods aforementioned for several reasons. In this case, release from the matrix is not relevant and entrapment has been shown to limit the amount of protein that is released because the network is formed around the protein. Thus, leaching and size exclusion are no concerns. Another benefit of this technique is that the amount of organic solvents can be reduced. Entrapment of proteins and enzymes also protects the biomolecules from sudden changes in their surrounding environment, which could result detrimental to its activity and stability.

3.2.1 Protein Encapsulation in Hydrogel Membranes

Of interest to this investigation is protein encapsulation in hydrogel matrices. Protein encapsulation in hydrogel matrices or entrapment entails synthesis of the hydrogel membrane in presence of the protein or enzyme. This method has intrinsic disadvantages. Organic solvents, such as ethanol, are used to inhibit reaction of the monomers with oxygen. These, as explained in detail in section 2.1, can have adverse effects on the proteins' tertiary and quaternary structures. Monomers and cross-linkers often have extreme pH values, and as is known, proteins and enzymes function within very limited pH ranges in physiological environments. Other shortcomings of this process include protein aggregation, and radiation-induced cross-linking or chain scission of the loaded proteins [19].

Delgado et al. described the encapsulation of lysozyme, bovine serum albumin (BSA), rabbit immunoglobulin G (IgG), and α -chymotrypsin in Poly(*N,N*-

dimethylacrylamide-*cross*-(ethylenedioxy)bis[2,2'-(*N*-acryloylamino)ethane]) matrices [20]. The pre-polymeric solutions were neutralized with 2N HCl solutions to protect the proteins from harsh pH, just as will be done in this investigation. The polymerization was carried out at 0°C as a contingency. After a sodium dodecyl sulfate polyacrylamide gel electrophoresis (SDS-PAGE) analysis to the liberated lysozyme and BSA, they observed no protein fragmentation or covalent dimerization which confirms that the proteins were not damaged during the encapsulation process. Enzymatic activity studies with released α -chymotrypsin showed that the enzyme retained 90% activity compared to the free enzyme. The same studies with aldolase catalytic antibody 38C2 yielded 70% activity compared to the free enzyme. These results suggest that minimal protein perturbation and denaturation occurred during the entrapment process.

Hemoglobin (Hb) has been encapsulated primarily for use as an artificial oxygen carrier. Patton [21, 22] and Arifin [23] have entrapped bovine Hb in poly(*N*-isopropylacrylamide) hydrogel nanoparticles and in polymersomes, self-assembled amphiphilic diblock copolymers from poly(butadiene)-poly(ethylene glycol) (PBD-PEO), respectively. Both groups observed that no Hb oxidation was present and reported minimization of resistance to oxygen transport through the particles due to expansion of the hydrogel matrix caused by temperature fluctuations.

3.2.2 Heme-protein Encapsulation in Sol-Gel Glasses

Sol-gels are a popular system for protein encapsulation because proteins are physically trapped within the network without any chemical modification [24]. These gel

matrices are chemically stable and can store high loads of samples due to their porous nature. These pores are negatively charged at neutral pH, commonly used to encapsulate proteins in these glassy systems. However, encapsulation in these networks may lead to alterations of the conformational structure of the proteins due to regularly spaced oxygen atoms that can act as hydrogen-bond acceptors or to the functional groups of organically-modified networks.

Edmiston et al. encapsulated hMb in sol-gel glass bulks composed of acrylodan and TMOS and described the protein's behavior after equilibrating the glass bulks in acidic pH values [25]. UV-vis absorption spectra of entrapped hMb titrated from pH 5.5 to pH 4.0 showed that the Soret band ($\lambda = 408\text{nm}$) was blue-shifted and demonstrated an intensity reduction, aside from also being broadened. This result also correlated with the behavior of dissolved hMb [25]. An interesting observation was that the response of entrapped Mb to changes in pH was substantially less than that of the dissolved hMb. It was also observed that a major reduction in the Soret band intensity did not occur as a result of equilibration of the sol-gel in acidic values, but upon encapsulation of the protein in the glass. Two important conclusions were made: (1) upon lowering of the pH from 5.5 to 4.0, the heme binding cavity unfolds and the α -helical content of the protein reduces by approximately 50% and that (2) entrapment may generate a variety of protein structures ranging from a native state to a substantially altered one, each with a differing degree of response to pH changes.

Ellerby et al. described similar behavior of hMb in TMOS sol-gels [26]. hMb was entrapped in the silicate glasses and the protein underwent redox reactions to assess hMb's biological activity with UV-vis spectroscopy. The behavior of entrapped protein

was similar to that of the protein in solution and as with the previous studies, the Soret band of the encapsulated protein were less intense and broadened, though not as drastic as with the other investigations. However, no explanation was given as to the occurrence of this behavior.

Friedman's group has observed a different behavior of Mb encapsulated in TMOS sol-gel glasses [27, 28]. Raman resonance spectroscopy studies have revealed that different states of Mb (deoxy, carboxy) retain their spectral properties after entrapment in monoliths at neutral pH (7.0). However, intensity reduction of the peaks was reported. Upon equilibration of the monoliths at pH 2.6, spectral properties were still preserved, and the rupture of the Fe-His bond occurred more slowly than for the protein in solution [28]. The investigators attributed this phenomenon to the limitation of conformational fluctuations of the protein caused by the encapsulation [27]. In other words, entrapment of the protein in the porous structure does not allow the protein to make the necessary movements to unfold or rupture bonds, in this case, the Fe-His bond.

Bottini et al. studied the effect of the initial stages of the sol-gel process in addition to the effect of the encapsulation of mMb in inorganic-doped TMOS sol-gels by UV-vis and fluorescence spectroscopy [24]. The Soret band ($\lambda=408\text{nm}$) of mMb dissolved in the solutions prior to sol-gel formation was located at its expected wavelength but were reduced in intensity and broadened. The blue shift was reversible after the equilibration of the monoliths in pH 6.0. However, the reduced intensity and broadened peak were maintained. The investigators attributed this anomalous behavior to the presence of the protein in an altered heme environment due to a partial loss of mMb's native structure.

A controversy exists whether mMb suffers any conformational changes in these sol-gel environments. A key point is that those groups which observe blue shifts of the Soret bands of Mb, do not detail any RR temporal studies. It may be a possibility that the rupture of this important Fe-His proximal bond is gradual and immediate RR spectra could not have encountered this. It may be that the proportions of the sol-gel precursors may be different in all cases, thus, having different effects on the protein's conformation. Even though hydrogel systems are unlike sol-gels in their components, similar behavior from these proteins could be expected for certain morphologies, specifically those that are of neutral charge, such as sol-gels.

The behavior of heme-proteins in sol-gel glasses and the cause of it has not been clearly explained and it is not understandable if the changes in the UV spectra of these proteins are caused by the encapsulation itself or by the organic and polar solvents that compose the sol-gel solutions. As hydrogels are a popular system for protein encapsulation this project will focus on the observation and documentation of the behavior of heme-proteins in this system to understand if these present similar conduct as in sol-gel systems. The UV spectra of these proteins will be studied before and after encapsulation to observe the changes, if any, that are produced after each encapsulation stage and if it is possible to find a combination of pre-polymeric solution components that does not affect their behavior before the synthesis process.

3.3 References

- [1] R. Grazinolli-Garrido and M. Sola-Penna, "Inactivation of yeast inorganic pyrophosphatase by organic solvents," *Annals of the Brazilian Academy of Sciences*, vol. 76, pp. 699-705, 2004.
- [2] C. L. Stevenson, "Characterization of protein and peptide stability and solubility in non-aqueous solvents," *Current Pharmaceutical Biotechnology*, vol. 1, pp. 165-82, Sep 2000.
- [3] T. T. Herskovits, B. Gadegbeku, and H. Jaillet, "On the structural stability and solvent denaturation of proteins. I. Denaturation by the alcohols and glycols," *The Journal of Biological Chemistry*, vol. 245, pp. 2588-98, May 25 1970.
- [4] T. T. Herskovits, H. Jaillet, and B. Gadegbeku, "On the structural stability and solvent denaturation of proteins. II. Denaturation by the ureas," *The Journal of Biological Chemistry*, vol. 245, pp. 4544-50, Sep 10 1970.
- [5] T. T. Herskovits, H. Jaillet, and T. DeSena, "On the structural stability and solvent denaturation of proteins. III. Denaturation by the amides," *The Journal of Biological Chemistry*, vol. 245, pp. 6511-7, Dec 25 1970.
- [6] E. V. Kudryashova, T. M. Artemova, A. A. Vinogradov, A. K. Gladilin, V. V. Mozhaev, and A. V. Levashov, "Stabilization and activation of alpha-chymotrypsin in water-organic solvent systems by complex formation with oligoamines," *Protein Engineering*, vol. 16, pp. 303-9, Apr 2003.
- [7] M. Tehei, D. Madern, C. Pfister, and G. Zaccai, "Fast dynamics of halophilic malate dehydrogenase and BSA measured by neutron scattering under various solvent conditions influencing protein stability," *Proceedings of the National Academy of the Sciences of the United States of America*, vol. 98, pp. 14356-61, Dec 4 2001.
- [8] G. Bonner and A. M. Klibanov, "Structural stability of DNA in nonaqueous solvents," *Biotechnology and Bioengineering*, vol. 68, pp. 339-44, May 5 2000.
- [9] R. V. Rariy and A. M. Klibanov, "Correct protein folding in glycerol," *Proceedings of the National Academy of the Sciences of the United States of America*, vol. 94, pp. 13520-3, Dec 9 1997.
- [10] A. A. Vinogradov, E. V. Kudryashova, V. Y. Grinberg, N. V. Grinberg, T. V. Burova, and A. V. Levashov, "The chemical modification of alpha-chymotrypsin with both hydrophobic and hydrophilic compounds stabilizes the enzyme against denaturation in water-organic media," *Protein Engineering*, vol. 14, pp. 683-9, Sep 2001.

- [11] W. Al-Azzam, E. A. Pastrana, Y. Ferrer, Q. Huang, R. Schweitzer-Stenner, and K. Griebenow, "Structure of poly(ethylene glycol)-modified horseradish peroxidase in organic solvents: infrared amide I spectral changes upon protein dehydration are largely caused by protein structural changes and not by water removal per se," *Biophysics Journal*, vol. 83, pp. 3637-51, Dec 2002.
- [12] D. Lopes, J. Meyer-Fernandes, and M. Sola-Penna, "Effects of trehalose and ethanol on yeast cytosolic pyrophosphatase," *Z Naturforsch*, vol. 54, pp. 186-190, 1999.
- [13] A. Zaks and A. M. Klibanov, "The effect of water on enzyme action in organic media," *The Journal of Biological Chemistry*, vol. 263, pp. 8017-21, Jun 15 1988.
- [14] A. M. Santos, M. Vidal, Y. Pachecho, J. Frontera, C. Báez, O. Ornellas, G. Barletta, and K. Griebenow, "Effect of Crown Ethers on Structure, Stability, Activity, and Enantioselectivity of Subtilisin Carlsberg in Organic Solvents," *Biotechnology and Bioengineering*, vol. 74, pp. 295-308, August 20, 2001 2001.
- [15] M. Jackson and H. H. Mantsch, "Beware of proteins in DMSO," *Biochimica Biophysica Acta*, vol. 1078, pp. 231-5, Jun 24 1991.
- [16] P. Huang, A. C. Dong, and W. S. Caughey, "Effects of Dimethyl-Sulfoxide, Glycerol, and Ethylene-Glycol on Secondary Structures of Cytochrome-c and Lysozyme as Observed by Infrared-Spectroscopy," *Journal of Pharmaceutical Sciences*, vol. 84, pp. 387-392, APR 1995.
- [17] C. Stevenson and M. Tan, "Solution stability of salmon calcitonin at high concentration for delivery in an implantable system," *Journal of Peptide Research*, vol. 55, pp. 129-139, FEB 2000.
- [18] R. Bhatia, C. Brinker, A. Gupta, and A. Singh, "Aqueous sol-gel process for protein encapsulation," *Chemistry of Materials*, vol. 12, pp. 2434-2441, AUG 2000.
- [19] S. L. Bourke, M. Al-Khalili, T. Briggs, B. B. Michniak, J. Kohn, and L. A. Poole-Warren, "A Photo-Crosslinked Poly(vinyl Alcohol) Hydrogel Growth Factor Release Vehicle for Wound Healing Applications," *AAPS PharmSciTech*, vol. 5, pp. 1-44, 2003.
- [20] M. Delgado, C. Spanka, L. Kerwin, P. Wentworth, and K. Janda, "Tunable hydrogel for encapsulation and controlled release of bioactive proteins," *Biomacromolecules*, vol. 3, pp. 262-271, MAR-APR 2002.

- [21] J. Patton and A. Palmer, "Photopolymerization of bovine hemoglobin entrapped nanoscale hydrogel particles within liposomal reactors for use as an artificial blood substitute," *BIOMACROMOLECULES*, vol. 6, pp. 414-424, JAN-FEB 2005.
- [22] J. N. Patton and A. F. Palmer, "Engineering temperature-sensitive hydrogel nanoparticles entrapping hemoglobin as a novel type of oxygen carrier," *Biomacromolecules*, vol. 6, pp. 2204-12, Jul-Aug 2005.
- [23] D. R. Arifin and A. F. Palmer, "Polymersome encapsulated hemoglobin: a novel type of oxygen carrier," *Biomacromolecules*, vol. 6, pp. 2172-81, Jul-Aug 2005.
- [24] M. Bottini, A. Di Venere, and P. R. Lugli, N., "Conformation and stability of myoglobin in dilute and crowded organically modified media," *Journal of Non-Crystalline Solids*, vol. 343, pp. 101-108, 2004.
- [25] P. L. Edmiston, C. L. Wambolt, M. K. Smith, and S. S. Saavedra, "Spectroscopic Characterization of Albumin and Myoglobin Entrapped in Bulk Sol-Gel Glasses," *Journal of Colloid and Interface Science*, vol. 163, pp. 395-406, 1994.
- [26] L. M. Ellerby, C. R. Nishida, F. Nishida, S. A. Yamanaka, B. Dunn, J. Selverstone-Valentine, and J. I. Zink, "Encapsulation of Proteins in Transparent Porous Silicate Glasses Prepared by the Sol-Gel Method," *Science*, vol. 255, pp. 1113-1115, 1992.
- [27] T. K. Das, I. Khan, D. L. Rousseau, and J. M. Friedman, "Preservation of the Native Structure in Myoglobin at Low pH by Sol-Gel Encapsulation," *J. Am. Chem. Soc.*, vol. 19987, pp. 10268-10269, 1998.
- [28] L. J. Juszczak and J. M. Friedman, "UV Resonance Raman Spectra of Ligand Binding Intermediates of Sol-Gel Encapsulated Hemoglobin," *The Journal of Biological Chemistry*, vol. 274, pp. 30357-30360, 1999.

4 OBJECTIVES

The purpose of this investigation is to study the biological stability of various proteins encapsulated in cationic, anionic, and neutral hydrogel membranes. Our specific goals are to:

- investigate the morphological characteristics of MAA-PEGDMA1000, DMAEM-PEGDMA1000, and PEGMA200-PEGDMA1000;
 - by performing mesh size experiments with glutaric acid at acidic pH values near 3 and basic pH values near 8;
- examine the stability and activity of horse skeletal muscle myoglobin, horse skeletal muscle myoglobin, bovine hemoglobin, and porcine hemoglobin entrapped in the aforementioned hydrogel membranes by:
 - analysis of UV-Vis spectra of proteins in pre-polymeric solution;
 - analysis of UV-Vis spectra of proteins encapsulated in the aforementioned polymer morphologies;
 - analysis of UV-Vis spectra of proteins during oxidation-reduction reactions; and to
- explore the stability of HEWL crystals in pre-polymeric solutions and within hydrogel membranes.

5 MATERIALS AND METHODS

5.1 Polymerization of Hydrogel Membranes

Three monomers were utilized: methacrylic acid (MAA), dimethylaminoethyl methacrylate (DMAEM) and poly(ethylene glycol) monomethyl ether n=200 (PEGMA200). All were obtained from PolySciences Inc. (Warrington, PA). PEGMA200 and DMAEM were utilized as received, and MAA was purified before utilization to remove inhibitor. Poly(ethylene glycol) dimethacrylate (PEGDMA1000) (n=1000), also obtained from PolySciences Inc., was used as crosslinker and used as received. The cationic monomer DMAEM was neutralized with hydrochloric acid (HCl, Polysciences Inc.) and sodium hydroxide (NaOH, Fisher Scientific (Pittsburgh, PA)) was used to neutralize MAA. 2-hydroxycyclohexyl phenyl ketone, from Sigma-Aldrich (St. Louis, MO), was utilized as the initiator for the hydrogel synthesis, and ethanol (Fisher Scientific) was utilized as solvent.

Hydrogel membranes were synthesized in an inert glove box from Cole-Parmer Instrument Co. (Vernon Hills IL) and a mercury lamp from EXFOS Lite (Mississauga, Ontario) was utilized as the ultraviolet light source. The polymerization environment was kept inert by purging with nitrogen (N₂) gas.

Hydrogel membranes were synthesized by free-radical polymerization. Pre-polymeric solution components were weighed and mixed by sonication. Amber bottles with septum screw caps were used to prevent polymerization inside the bottle.

Microscope slides were cleaned with deionized water and soap and dried in the oven before polymerization.

The glove box compartment was purged overnight with nitrogen gas. Once the pre-polymeric solution components were completely dissolved, the gauge needle was connected to the nitrogen line and introduced, along with the smaller needle, through the cap's septum. The solution was purged for 20 minutes. After purging, the solution was left to rest for 5 minutes. Next, the pre-polymeric solution was introduced between the two microscope slides by capillarity. Any bubbles were carefully removed to ensure homogeneous polymerization. Finally, the slides were placed under the light guide, assuring that the light guide was directly over the middle of the slides. The glove compartment was covered with black felt and the UV source was turned on for the time required. After complete polymerization, the clips and Teflon spacers were removed and the two slides were carefully separated with a spatula.

5.2 Proteins

MMb, hMb, pHb, bHb, and HEWL were all purchased from Sigma-Aldrich and used as received.

5.3 Stability and Biological Activity Studies

A PowerwaveX-I UV-Vis Spectrophotometer from Bio-Tek Instruments Inc. (Winooski, VT) was utilized to obtain the proteins' spectra in the pre-polymeric solution

and immediately after polymerization. The membranes were placed in quartz screw cap cells from Starna Cells Inc. (Atascadero, CA) and activity studies were performed in a UV-Vis spectrophotometer. Chemicals used for the reduction and oxidations of the heme-proteins were sodium phosphate buffer (pH 7.4) –to keep membranes swollen-, sodium dithionite (Sigma Aldrich), carbon dioxide gas, and dilutions of sulfuric acid (Sigma Aldrich).

Protein stability in pre-polymeric MAA, DMAEM, and PEGMA200 solutions were studied by means of UV-Vis spectroscopy. Stability of the protein in the pre-polymeric solutions was determined by shifts, if any, of the characteristic peaks (Soret and Q bands) of the proteins studied and also by the intensity of these peaks.

The appropriate morphology for the hydrogel used was determined utilizing 1 gram as a base. This allowed the addition of pre-polymeric components such as ethanol, monomer, cross-linker, acid or base, in proportions identical to the conditions of polymerization. Proteins were exposed to four different environments: (1) monomer + acid/base (for ionic morphologies) + protein aliquot, (2) cross-linker + ethanol/water solution + protein aliquot, (3) ethanol/water solution + protein aliquot, and (4) monomer + cross-linker + acid/base + ethanol/water solution + protein aliquot.

Pre-polymeric components were weighed in an amber bottle. The solution was sonicated until the cross-linker was completely dissolved. For this particular experiment, the PowerWave X spectrophotometer was utilized with a step of 2 nm. Two different spectra were taken, one from 350 to 500nm (Soret band) and from 500 to 700nm (Q bands). Each well was filled with 200 μ l of liquid and three consecutive wells were used for the same liquid, i.e. three for deionized water, three for protein aliquot, three for

experimental solution, etc.). The experimental solution aliquot ranged from 100 μ l to 150 μ l, depending on the concentration of the protein used. The measured OD correlation data was used to obtain the spectra. These experiments were also performed to determine the concentration of HCl to be used, as well as the amount of ethanol in the pre-polymeric solution.

Hydrogel membranes were synthesized in presence of all heme-proteins and the CO binding capacity of these proteins was studied by simple spectra and kinetic studies. Membranes were cut, having special care to make them fill the entire volume of the Starna Cell, and placed with a PBS buffer at pH 7.4. The contents of the cells were bubbled with nitrogen for 20 minutes to remove oxygen. The cells were then loaded onto the UV-Vis Scanning Spectrophotometer and their UV spectrum was taken. After an initial spectrum, the buffer was removed with a syringe and replaced with fresh PBS buffer containing a small amount of sodium dithionite (mixture previously bubbled with nitrogen). UV spectra were taken continuously for 1 minute and then until no more spectroscopic changes were observed. A separate vial with fresh PBS buffer was bubbled with CO gas for 10 minutes. This buffer was then placed in the Starna Cells. UV spectra were taken continuously for 1 minute and then until no spectroscopic changes were detected. Some hydrogel membranes were saved and dried in a vacuum oven for a period of two to three months, then afterwards the membranes were re-swollen and the aforementioned experiments were conducted.

5.4 Correlation Length Measurements

The hydrogel membranes were synthesized in our laboratory. Glutaric acid buffer was prepared at acidic and basic pHs. 3-3'Dimethylglutaric acid (Sigma Aldrich), NaCl (Fisher Scientific) and NaOH were utilized in the preparation of the buffer. A heptane density kit was used to weigh the membranes on a Voyager Balance from Ohaus Corporation (Pine Brook, NJ).

Hydrogel membranes were synthesized as described in section 4.1, and then cut into circles with diameters of 9/16". All experiments were conducted with, at least, ten membranes per monomer. After synthesis, a heptane density kit was utilized to calculate the weight of the membrane in air, in heptane, the density and its volume. Next, each circular membrane was individually placed in an amber bottle with 15ml of deionized water. The bottles were placed in a water bath at 30°C for four days. The deionized water was changed two times a day during these four days. After the first water replacement on the fourth day, the membranes were taken out of the bottles and placed in the vacuum oven for 2 days. On the sixth day, the membranes were removed from the oven and the weight in air and heptane, the density and the volume were re-measured utilizing the heptane density kit. The circular membranes were then placed in 15ml of buffer solution at the designated pH for one more day. On the last day of the experiment, the swollen membranes were removed from the buffer and the same measurements were taken. Correlation length measurements were calculated using the Peppas-Merrill Model.

5.5 Protein Crystallization

Two crystallization methods were utilized: the hanging drop method and the counterdiffusion method. 24-well plates and borosilicate cover glasses were purchased from Hampton Research (Aliso Viejo, CA), as well as the Granada Crystallization Boxes (GCBs). Lysozyme (Sigma Aldrich) was used as a model protein. Buffer and precipitating agents included sodium chloride (Fisher Scientific) and sodium phosphate buffer (Fisher Scientific).

Stability of protein crystals, specifically, HEWL, was tested by exposing the crystals to drops of pre-polymeric solution components such as EtOH, MeOH, and MAA. HEWL crystals were grown by the hanging-drop technique. An HEWL aqueous solution was prepared by dissolving 20g of the protein in 1ml of deionized water. VDX plates were filled with 2ml of a 3.5M NaCl/100mM buffer/precipitant solution at pH 4.0. High vacuum grease was carefully applied to the edge of the wells. One μ l of the lysozyme solution was placed on a siliconized circular cover glass with a micropipette. One μ l of buffer/precipitant solution was then added to the drop, carefully mixing the contents of the drop by successively suctioning and emptying the pipette tip. The cover glass was overturned and placed on top of the high vacuum grease, carefully pushing it down to be sure that there were no air pockets between the grease seal and the cover glass.

Once crystals were observed by light microscopy, the cover glasses were carefully removed from the wells and overturned. A small volume of crystallizing solution was added to the drop and this volume was subsequently suctioned onto the bottom of a well on a black 96-well plate with a clear bottom. A whole crystal was then located within the

well and observed with a light microscope and an Olympus camera. A drop of the solution to be studied was added onto the well and the crystal was monitored by microscopy and photography until the crystal started to degrade.

6 RESULTS and DISCUSSION

6.1 Stability of Heme-Proteins After Exposure to UV Light

A factor that was studied prior to the hydrogel membrane synthesis was the proteins' exposure to the UV light utilized to synthesize the hydrogel membranes. Solubilized protein was exposed to the UV light source for 1200s in total. Samples were taken at 300s (polymerization time for neutral membranes) and 1200s (polymerization time for ionic membranes). Temperature readings were also taken at these time intervals. In all cases, except for pHb, some reduction of absorbance was evident after 300s of exposure. All four proteins showed broadened Soret bands after 1200s exposure. Figure 6.1 illustrates such behavior. A significant temperature increase from 20°C was evident after 1200s. Most proteins solutions had a temperature near 35°C. This temperature does not seem extreme, as physiological temperature where proteins operate is 37°C. However, an increase of 15°C in less than 20 minutes could be harmful to the proteins function as it is known that temperature affects the function and stability of enzymes.

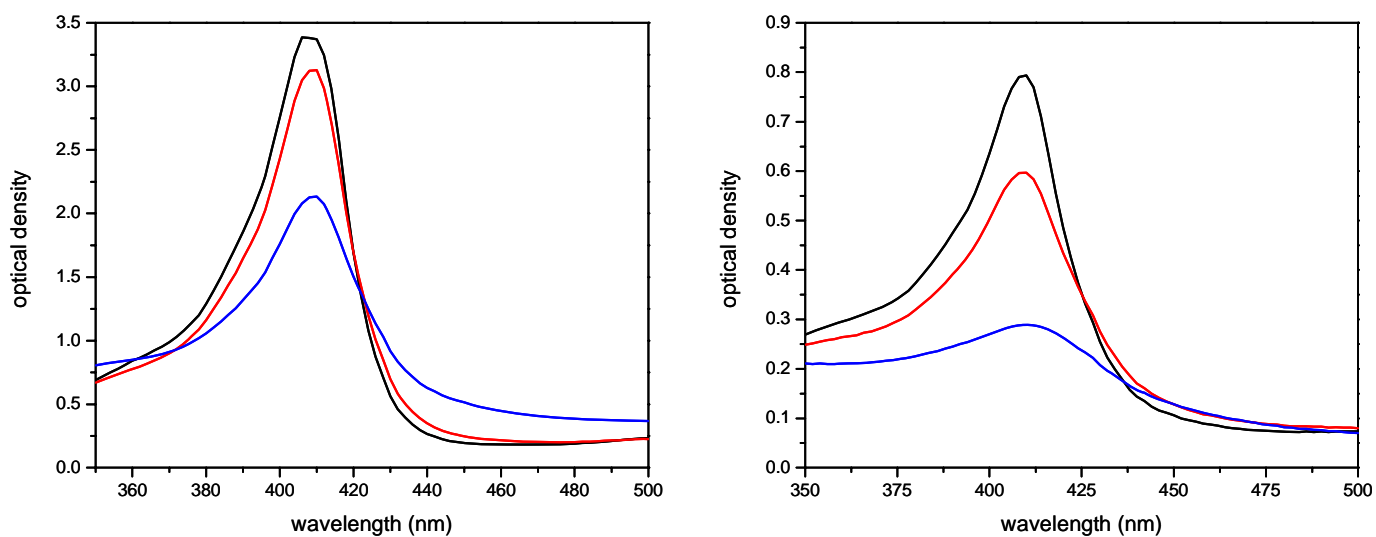


Figure 6.1. Comparison of the UV-vis spectra of (left) mMb and (right) hMb after exposure to UV light source. ■ Native protein ($\lambda_{\text{max}} = 406\text{nm}$); ■ after 300s ($\lambda_{\text{max}} = 406\text{nm}$); ■ after 1200s ($\lambda_{\text{max}} = 406\text{nm}$).

6.2 Stability of Heme-Proteins in Pre-Polymeric Solutions

Due to the polar nature of the hydrogel membrane components, it is imperative to study the effects of these chemicals on the stability and behavior of proteins before their encapsulation in these membranes. Another motivation for this study is the nature of the entrapment technique, as proteins are exposed to these components before and during the polymerization process. Even though the components utilized may be harmful to the proteins' structure and function, it is thought that a combination of these components that does not cause any premature unfolding of the proteins before encapsulation in the hydrogel membranes can be obtained.

Each protein in its metaquo state was exposed to different ratios of the pre-polymeric solution components of the three morphologies under investigation: MAA:PEGDMA1000, DMAEM:PEGDMA1000, and PEGMA200:PEGDMA1000. These included monomers (MAA, DMAEM, and PEGMA200), EtOH dilutions, crosslinker (PEGDMA1000), NaOH (in the case of the anionic morphology), and HCl (in the case of the cationic morphology). These last two were used to neutralize the monomers. The proteins were exposed to different combinations of the pre-polymeric solution components. Subsequently, the Soret and Q bands of the proteins were monitored until a component combination did not cause significant displacement of the bands. These solutions were then combined into a pre-polymeric solution and then polymerized.

Table 6.1 presents the optimized anionic, cationic, and neutral morphologies. The Soret and Q bands of all four proteins exposed to the different ratios of the anionic

morphology are shown in Table 6.2. It must be mentioned that the UV-vis spectrophotometer employed in these experiments has a sensitivity of $\pm 2\text{nm}$. Therefore, a peak that is located normally at 408nm may be located at 406nm or 410nm. It can be observed that a combination of MAA and NaOH (5M) could be obtained that did not displace the Soret band of the proteins. The crosslinker + EtOH combination causes the most displacement of the Soret band. This could be due to the destabilizing effect that EtOH has on proteins or to the interaction between the proteins and the long chains of crosslinker. Finally, the behavior of the proteins in the pre-polymeric solution is similar to that of the proteins in the MAA + NaOH solution. PHb shows a slight blue red shift from its usual metaquo peak at 406nm to 410nm. A slight reduction in absorbance of the Soret peak is visible for all proteins in all the component solutions compared to the native protein. This absorbance reduction and broadening of the Soret band is most evident for the proteins in the pre-polymeric solutions.

Figure 6.2 illustrates the UV-vis spectra for mMb exposed to the MAA:PEGDMA1000 morphology. It should be made clear that obtaining a morphology for which all the combinations tested for the various components caused no displacement of the Soret bands was cumbersome. Thus, an optimized morphology was chosen when a majority of the components caused no significant displacement of these peaks. Most importantly, for the morphology to be optimized, the pre-polymeric solution must not have caused any shifts in the spectrum maxima. The experimental spectra for all the proteins are found in the appendix.

Table 6.1 Comparison of Optimized Hydrogel Morphologies

MAA-PEGDMA1000		
MAA: PEGDMA	88:12	%Molar
Dilution	60%	%Molar
DMAEM-PEGDMA1000		
DMAEM: PEGDMA	83.2:16.8	%Molar
Dilution	40%	%Molar
PEGMA200:PEGDMA1000		
PEGMA200:PEGDMA1000	60:40	%Molar
Dilution	30%	%Molar

Table 6.2 Soret and Q band Positions of All Proteins Exposed to Pre-Polymeric Solution Components of the Anionic Morphology (Position in nm, NV = band not visible)

Proteins	MAA+NaOH		PEGDMA1000+EtOH		Pre-Polymeric Solution	
	Soret	Q	Soret	Q	Soret	Q
mMb	410	NV	401	NV	407	NV
hMb	410	NV	410	NV	410	NV
bHb	406	628	414	524	406	NV
pHb	406	NV	408	NV	410	NV

Before the stability of the proteins was tested in the cationic morphology, the proteins were exposed to different concentrations of HCl, as it has been documented that acids are denaturing agents [1]. Figure 6.3 demonstrates the spectra of mMb exposed to HCl normalities ranging from 0.5N to 6N. It can be observed that all normalities cause reduction in absorbance as well as peak broadenings. This figure evidences that a lower acid concentration is not necessarily less detrimental to the protein, as the lowest acid concentrations produced the greatest blue shifts of the Soret bands (3 and 7nm), as well as peaks with 83% reduction in absorbance compared to the native protein. The HCl concentration chosen was 6N as it produced an insignificant shift of the Soret band and the reduction in absorbance was the lowest, 50%.

Sage and coworkers studied the heme structure and behavior in low pH media [1]. Low pH affects the interaction between the distal and proximal histidine residues with the heme group. These interactions are vital to the stability of the heme group as their loss may affect protein conformation by causing more “open” protein structures, which behave differently to native protein. At pH values lower than 4, the investigators observed blue shifts (from 409nm to 370nm) of the metaquo Soret band. Edmiston and coworkers described a similar behavior when myoglobin solutions were changed from pH 5.5 to 4.0 [2]. Resonance Raman spectroscopy of such solutions revealed that the iron-histidine bond was broken at low pH. The shifts shown in Figure 6.3 are not as drastic, depicting blue shifts of at most 7nm, not comparable to the 39nm shifts mentioned above. It can be hypothesized that the acidic solutions utilized for the

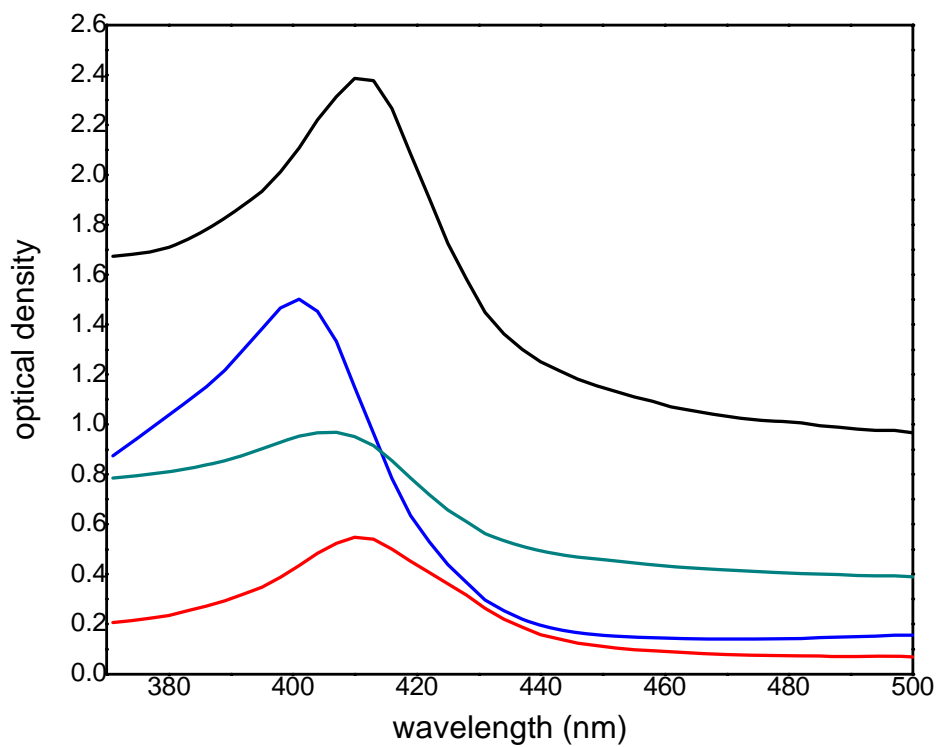


Figure 6.2. Effect of MAA:PEGDMA1000 Pre-Polymeric Solution Components on the UV-vis Spectrum of mMb.

■ MAA+NaOH ($\lambda_{\max} = 410$); ■ MAA+PEGDMA1000 ($\lambda_{\max} = 401$);
 ■ Pre-Polymeric Solution ($\lambda_{\max} = 407$); ■ EtOH (30%) ($\lambda_{\max} = 410$)

DMAEM:PEGDMA1000 morphology did not cause any significant effect on the structure and conformation of the proteins.

Table 6.3 displays the results for the proteins exposed to the DMAEM:PEGDMA1000 pre-polymeric solution components. HMb seems to be most affected by the pre-polymeric solution components of this morphology. A 9nm blue shift of the Soret band can be observed after exposure to the monomer + acid solution and a 3nm red shift after contact with the crosslinker + EtOH solution. BHb is the other protein that suffers some shifts in its Soret bands. However, these shifts are insignificant due to the equipment's sensitivity, as explained previously. Absorbance reduction of up to 70% is observed for proteins in contact with the cationic pre-polymeric solution. These results are shown in Appendix 1.

Finally, the proteins were exposed to the neutral PEGMA200:PEGDMA1000 morphology components, which are observed in Table 6.4. MMb and hMb are the most affected by the monomer + EtOH solution, as the Soret bands displace 7nm from their original location. The four proteins seem stable in the remaining two solutions, with only a slight displacement of 3nm for hMb in the pre-polymeric solution.

The Q bands of Mb and Hb in the metaquo state are localized at 502 and 630nm, as previously mentioned in Table 2.5. These, especially the 630nm Q band can be observed for some of the systems. However, due to the sensitivity of the equipment utilized for these experiments, the Q bands were not sharp enough or visible enough to provide conclusive observations on their appearance in the spectra.

Of the four proteins, bHb and pHb are the most stable in all of the solutions tested as their Soret bands in all solutions do not deviate highly from the native values. hMb

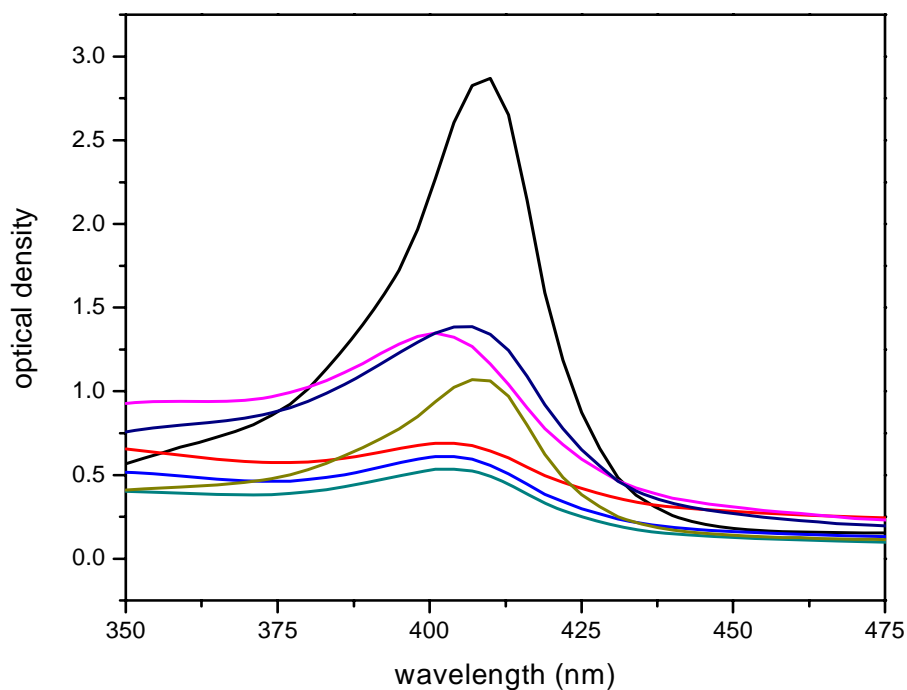


Figure 6.3. Effects of HCl Normality on UV-vis Spectrum of mMb.
 ■ Native mMb ($\lambda_{\max} = 410$); ■ HCl 6N ($\lambda_{\max} = 407$); ■ HCl 3N ($\lambda_{\max} = 401$);
 ■ HCl 5N ($\lambda_{\max} = 407$); ■ HCl 0.5N ($\lambda_{\max} = 404$); ■ HCl 1N ($\lambda_{\max} = 404$);
 ■ HCl 2N ($\lambda_{\max} = 404$)

Table 6.3 Soret and Q band Positions of All Proteins Exposed to Pre-Polymeric Solution Components of the Cationic Morphology (Position in nm, NV = band not visible)

Proteins	DMAEM + HCl (6N)		PEGDMA1000+EtOH		Pre-Polymeric Solution	
	Soret	Q	Soret	Q	Soret	Q
mMb	410	NV	410	NV	410	520 630
hMb	401	NV	413	NV	404	NV
bHb	406	538	406	630	406	NV
pHb	408	521	406	630	404	575 630

exposed to the neutral pre-polymeric solutions demonstrated a peculiar behavior, as its Soret band was red-shifted to 413nm. This red shift can be attributed to a coexistence of metaquo and deoxy states of the proteins, as the Soret band moves from its usual position at 408 nm to the region between 411 and 413nm. Spectra of the native protein taken prior to every experiment discarded the hypothesis that some of the protein used was already in a reduced state. An interaction between the pre-polymeric solution and the heme group could be causing this reduction of the heme group. However, further experimentation is necessary to verify this hypothesis.

Changes in intensity and shape also accompanied the displacements of the Soret bands observed. Experimental Soret bands lost intensity and had a wider shape than those from native proteins. Pre-polymeric solutions from the three morphologies had the greatest effect on the bands, as these were the less intense and the widest. Bottini et al. observed similar behavior of myoglobin in the initial stages of the preparation of TMOS sol-gel glasses [3]. The group observed no displacement of the metaquo Soret band with a small reduction in intensity in all of the inorganic solutions tested.

The results discussed above demonstrate in a qualitative fashion that organic solvents produce mild changes in the conformation of heme-proteins. The drastic reductions in absorbance suffered by all proteins studied and the slight displacements in the Soret bands of the proteins in the systems provide sufficient evidence to support this observation. However, it is hoped a significant variable – the drastic effect of organic solvents on the structure of the proteins - is eliminated by utilizing optimized morphologies that do not cause shifts of the Soret band, therefore, maintaining some sort of stable environment for the protein, before polymerization.

Table 6.4 Soret and Q band Positions of All Proteins Exposed to Pre-Polymeric Solution Components the Neutral Morphology
(Position in nm, NV – band not visible)

Proteins	PEGMA200+EtOH		PEGDMA1000+EtOH		Pre-Polymeric Solution	
	Soret	Q	Soret	Q	Soret	Q
mMb	401	NV	410	NV	410	527
hMb	401	NV	410	NV	413	525
bHb	406	630	406	636	406	628
pHb	406	630	406	636	406	628

6.3 Biological Activity of Heme-proteins in Hydrogel Membranes

Once hydrogel morphologies were optimized, proteins were encapsulated within the three morphologies and their activity was monitored once again by UV-vis spectroscopy. Sodium dithionate was utilized to reduce the heme group to the deoxy state (Fe^{2+}) and a buffer solution saturated with CO gas was added to place the heme groups in a carboxy state. UV-vis spectra of the hydrogel membranes were taken after each step.

Table 6.5 presents a comparison of the Soret and Q band locations of the four proteins in the MAA:PEGDMA1000 hydrogel membranes. Encapsulation of all proteins in this morphology caused a shift of the Soret band, usually located at 408nm to the 395nm and 396nm. This evident displacement is accompanied by a marked reduction of the band's intensity as well as a widening of such. The Q band located at 502nm is not observed in any of the spectra, while the band at 630nm remains for all proteins except mMb, which shows a band at 582nm. A Q band near this wavelength (580nm) is characteristic of Mb in its carboxy state. Figure 6.4 illustrates the spectra of metaquo, deoxy, and carboxy mMb in MAA membranes.

Upon reduction to the deoxy state, it can be observed that the Soret bands of none of the proteins encapsulated in the anionic morphology are located at the expected 435nm. The Soret band is blue shifted by an average 16nm. The Q band at 560nm is not observed in any of the spectra. PHb shows a band near 550nm, the closest observed. HMb, bHb, and pHb have a Q band near 630nm, which is a Q band reminiscent of the metaquo state.

Table 6.5 Absorbance parameters of Met, Deoxy, and Carboxy Proteins Encapsulated in the Anionic Morphology
(Position in nm, NV – band not visible)

Proteins	Metaquo		Deoxy		Carboxy	
	Soret	Q	Soret	Q	Soret	Q
mMb	395	582	422	540	406	529 560 623
hMb	396	629	421	518 629	405	522 629
bHb	395	629	416	628	405	522 628
pHb	396	628	419	550 627	406	525 560 627

Finally, ligation of CO to produce a carboxy state produces Soret bands for all proteins at 405 and 406nm, a blue shift of an average 18nm. The Q bands located at 540nm and 579nm are not observed in any of the spectra. All four proteins produce a band near 525nm, as well as another near 630nm, which is a Q band that characterizes the metaquo state of such proteins. MMb and pHb have a conspicuous band near 560nm. Mb and Hb in the deoxy state have a characteristic Q band near this wavelength.

Table 6.6 illustrates the Soret and Q band locations of the metaquo, deoxy, and carboxy states of all four proteins encapsulated in the DMAEM:PEGDMA1000 morphology. The position of the Soret bands is similar to those for the proteins encapsulated in the anionic morphology in this state in that the Soret bands suffer a blue shift to the 390nm region. The Q band near 630nm remains for all proteins. The UV-vis spectrum of hMb was not visible in the 500-700nm region. Therefore, the Q bands could not be distinguished.

The proteins demonstrated a similar behavior in the DMAEM membranes as the proteins encapsulated in the MAA hydrogel membranes, in the deoxy state. The Soret band did not shift to 435nm, but rather was blue shifted to the 415-420nm region. Only mMb has a Q band near 560nm, which is the distinctive Q band for such state. The other proteins, except hMb, displayed the 630nm Q band, indicative of the metaquo state.

Contact of the encapsulated proteins in DMAEM hydrogels with CO caused a shift of the Soret band from the 415-420nm region to 408nm, except mMb, whose Soret band was located at 409nm. This location is blue shifted, as the native Mb and Hb carboxy Soret band is located at 424nm. The native Q bands are located at 529nm and 570nm. Table 6.7 illustrates that only mMb has a band close to 570nm. The 529nm band

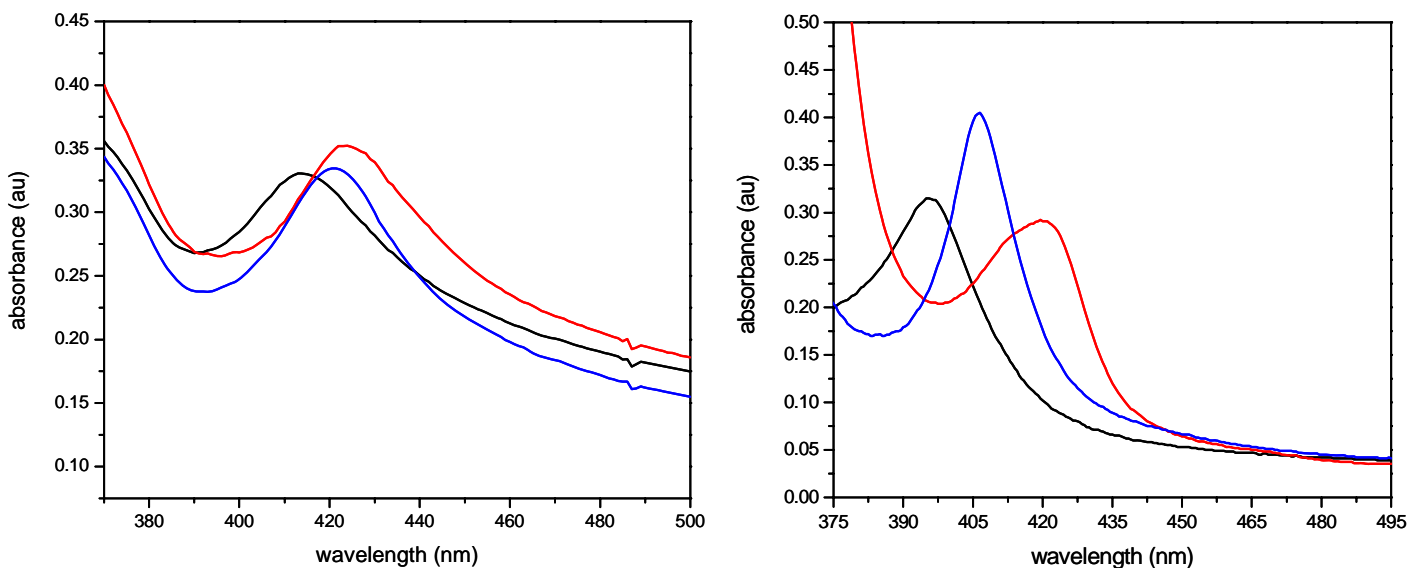


Figure 6.4. Comparison of activity of mMb in (left) PEGMA200:PEGDMA1000 hydrogel membranes and (right) MAA:PEGDMA1000 hydrogel membranes. ■ Metaquo state ($\lambda_{\max} = 413, 395$); ■ Deoxy state ($\lambda_{\max} = 424, 422$); ■ Carboxy state ($\lambda_{\max} = 421, 406$)

Table 6.6 Absorbance parameters of Met, Deoxy, and Carboxy Proteins Encapsulated in the Cationic Morphology
(Position in nm, NV – band not visible)

Proteins	Metaquo		Deoxy		Carboxy	
	Soret	Q	Soret	Q	Soret	Q
mMb	398	629	421	556 630	408	563 625
hMb	397	NV	418	NV	409	NV
bHb	393	628	416	628	409	628
pHb	393	629	417	631	409	628

is not visible in any of the proteins' spectra. The 630nm metaquo Q band was still recognizable.

Finally, Table 6.7 demonstrates the results for all proteins encapsulated in the neutral PEGMA200:PEGDMA1000 membranes. MMb and hMb present metaquo Soret bands at 413 and 411nm, respectively. These locations represent a red shift, on average, of 4nm from the native Soret band location at 408nm. BHb presents a blue shift of 5nm to 403nm, whilst pHb's metaquo Soret band is located at the expected 408nm location. Three of the four proteins present the particular 630nm Q band. The 500-700nm region spectrum for hMb was not clear. Thus, the Q bands could not be correctly and unambiguously identified. Figure 6.4 also depicts the metaquo, deoxy, and carboxy states of all mMb in the PEGMA membranes.

Reduction of the heme groups to the deoxy state, caused a shift of the Soret band to the 420nm region, with an average blue shift of 12nm from the native location at 435nm. MMb did not display a Q band near 560nm, which is the typical location of a deoxy state Q band. PHb did have this band and so did bHb. However, bHb's Q band was blue-shifted by 2nm. HMb presented a band at 555nm, a blue shift of 5nm from the expected 555nm.

Final change of the deoxy to the carboxy state caused a shift to the 420nm region for all proteins. This behavior is unlike that of the protein in the ionic morphologies, which exhibited carboxy Soret bands in the 400nm to 410nm region. MMb, hMb, and pHb presented a blue shift of 4nm from the expected Soret band location at 424nm. BHb presented an unusual wide Soret band with two distinct maxima, one at 406nm and one at 419nm. All proteins showed a band in the 530nm region. However, none of the proteins

Table 6.7 Absorbance parameters of Met, Deoxy, and Carboxy Proteins Encapsulated in the Neutral Morphology
(Position in nm, NV – band not visible)

Proteins	Metaquo		Deoxy		Carboxy	
	Soret	Q	Soret	Q	Soret	Q
mMb	413	630	424	525 628	421	525 559 626
hMb	411	NV	422	526 555 630	418	532
bHb	403	628	421	533 560 628	406 419	534 560 630
pHb	408	635	424	532 558 630	420	535 569 633

display the usual 540nm Q band for the carboxy state. MMb, bHb, and pHb present a small band in the 560nm region, yet do not present the required 579nm Q band. Lastly, all the proteins except hMb present the 630nm Q band reminiscent of the metaquo state.

It can be observed from the previous tables that encapsulation in ionic (both anionic and cationic) morphologies caused a significant blue shift of the Soret band from its normal location ($\lambda = 408\text{nm}, 406\text{nm}$) to the 395 to 400nm region. The Q band expected at 502nm is not visible in any of the spectra obtained; yet, the 630nm is visible for most of the ionic hydrogel systems evaluated. Neutral morphologies for all proteins presented a significantly different behavior upon encapsulation. The Soret bands for mMb and hMb were both red-shifted to the 411-413nm region and their intensity was markedly diminished, as well. BHb presented a blue shift of 5nm while pHb's Soret band was located at the expected wavelength. The Q bands of the proteins encapsulated in the neutral morphology demonstrated a similar behavior to those of proteins encapsulated in the ionic morphologies.

Upon reduction of the heme group with sodium dithionite, a deoxy state was achieved for all proteins. The Soret band of the four proteins presented displacements to the 416 to 424nm region. This is irregular behavior, as the expected wavelength of such state is located in the 430 to 435nm region. All four proteins encapsulated in the neutral PEG membranes maintain their normal Q bands in the 550 to 560nm region. The ionic morphologies seem to have some type of effect on this band as proteins encapsulated in the MAA and DMAEM membranes present an abnormal Q band in diverse wavelengths: the 510's, the 520's, the 530's, and the 540's. Another Q band that is present in the deoxy proteins is the 630nm Q band, typical of a heme group in its metaquo state.

Subsequent ligation of CO to the heme group of the encapsulated proteins shifts the heme groups state from deoxy to carboxy, even though the iron is still in a reduced state (Fe^{2+}). Soret bands of all proteins encapsulated in the ionic (anionic and cationic) and the neutral morphologies presented an average blue shift of 17nm and 4nm, respectively. BHb encapsulated in the neutral membrane presents a maximum with a dual peak. An interesting finding is that the displacement of the Soret band of all proteins encapsulated in the PEG membranes is very short (a few nanometers), compared to the peak's displacement of those proteins encapsulated in the ionic morphologies. None of the expected Q bands at 540 and 579 nm is observed in any of the proteins. However, a small band appears near 535nm and again present are the 560 and 630nm Q bands characteristic of the deoxy state. As observed for all the other states, the Soret bands are reduced in intensity and have a broader shape.

It is not clear what causes the odd location of the metaquo Soret band of the proteins encapsulated in the ionic morphologies. Typically, blue shifts are indicative of protein unfolding at some site within the protein [1, 3-6]. This, in turn, is a sign of loss of biological activity. However, in this case, it is observed that the proteins seem to bind and unbind ligands due to the displacements seen after reduction of the heme group.

The position of mMb's and hMb's Soret band after encapsulation in the neutral morphologies may suggest a coexistence of both reduced and oxidized states of the heme group. A mixture of metaquo and oxy ($\lambda = 416\text{nm}$) states can give rise to a Soret bands which location is between 411 and 413nm. This may be the case of the band obtained after reduction of the heme group to a deoxy state as a band between these two

wavelengths ($\lambda \approx 422\text{nm}$) may imply a mixture of oxy and deoxy states (both reduced states).

The small displacement of the Soret band of the proteins upon equilibration of the neutral PEGMA200 hydrogels with CO gas is yet another result that demands scrutiny. PEG polymers are currently being studied for removal or sequestration of CO and CO₂, due to their affinity for such gases. As both monomer and crosslinker in this morphology are PEG-based, it could be hypothesized that the heme group competes with the polymer for the available CO gas in solution. Thus, a limited amount of CO may be available for binding to the heme groups. Therefore, different species of oxidized heme may coexist as a result. Further experimentation is necessary to better characterize this behavior.

Similar studies of biological activity performed with myoglobin encapsulated in sol-gel systems demonstrate a highly dissimilar behavior. The metaquo, deoxy, and carbonyl (carboxy) Soret bands are located at their expected wavelengths; yet the bands of the encapsulated proteins were less intense and wider than those of the native protein in solution [7]. Edmiston et al. reported that sol-gel entrapped myoglobin presented blue-shifted Soret bands which were also reduced in intensity [2]. These blue shifts were attributed to a variety of Mb structures that were generated by the entrapment. Each of these structures could have varying responses to changes in the sol-gel environment, from native-like to substantially altered.

Friedman and coworkers have also studied the effects of sol-gel encapsulation on the structure and stability of myoglobins [8]. Resonance Raman spectroscopy was utilized to demonstrate that the loss of the iron-histidine bond, vital for the stability of the heme group and which causes severe changes in the Soret band of heme-proteins, is not

immediately broken upon encapsulation in these sol-gels. The group shows that this rupturing process is gradual, due to the diffusional restrictions imposed by the rigidity of the sol-gel structure.

Sol-gel synthesis entails the use of highly acidic or basic solutions. Interestingly enough, this group reported no abrupt response of the proteins to changes in pH and to encapsulation, as reported before [1, 2]. Recently, another group observed that metaquo myoglobin encapsulated in inorganic TMOS gels presented blue shifts similar to those observed for the four proteins encapsulated in the ionic hydrogel membranes [3]. The group reports having made Resonance Raman spectroscopy measurements which were not discussed. The investigators hypothesize, however, that the blue shifts may be due to the restriction of movement that entrapment in these rigid porous networks represent [3].

It is cumbersome to attempt to correlate some of the aforementioned results to the ones reported in this investigation. None of the studies mention if the sol-gel mixtures which were used for encapsulation were a product of an optimization process such as the one exposed in this investigation. The assessment of instability caused by the sol-gel solutions or by the sol-gel encapsulation of myoglobin by diverse spectroscopic techniques is obscure as these groups do not use the same characterization techniques, or do not present the results of such techniques. As the results discussed above are highly controversial, it would have been easier to analyze these results if similar experiments had been carried out.

The results discussed in the previous sections are the foundations of the characterization of several systems that can be applied to diverse applications such as oxygen sequestration for blood substitutes and biosensors for diverse gasses. More

importantly is the fact that these results point out that special care must be taken when encapsulating proteins in systems that utilize organic and polar solvents, as small variations in the system components may cause serious effects on the conformation and activity of these proteins.

6.4 Correlation Length Measurements

Upon successful optimization of the proteins in the three morphologies and characterization of the proteins' behavior after encapsulation, it was necessary to study the structural parameters of the hydrogel membranes. This was achieved by determining the mesh size or average pore diameter of the networks, ξ . Figure 6.5 illustrates the difference in ξ between the three morphologies at two different pH values, acidic and near neutral.

It can be observed that there is a difference of 0.05nm between mesh size measurements of neutral membranes at pH 3 and 7.7. As expected, neutral membranes do not swell or collapse under variant pH conditions. This behavior has been observed in the laboratory for varying molecular weights of the PEG monomers and cross-linkers.

Cationic membranes have a higher ξ at lower pH values. The difference between the ξ values observed is of 0.2nm, which is a significant difference. It must be mentioned that the morphologies utilized for this study are highly cross-linked. This could explain the rigidity of the membrane which translates into a smaller capacity of the membrane to swell.

Podual [9] reported mesh sizes for a dimethyl aminoethyl metacrylate copolymer: P(DMAEM-g-EG). In this investigation, a phosphate buffer was used for pH values between 5 and 8 and dimethyl glutaric acid/NaOH buffer was used for pH values between 3.2 and 5.0. Equilibrium swelling experiments were conducted at pH values of 4.5 and 8.0. At low pH, the mesh size was measured at 45\AA and at high pH, the mesh size was measured at 250\AA . These results were obtained for a cross-linking ratio of 0.02. The increase of cross-linking density caused a significant reduction in the maximum mesh sizes of the membranes, going from 300\AA at $X=0.005$ to 45\AA at $X=0.04$. In our laboratory, we have observed that mesh sizes of DMAEM-PEGDMA ($n=200, 600, 1000$) show no statistical difference. These measurements were determined at pH 7.4 with a phosphate buffer.

Lastly, the anionic membranes evidence the opposite behavior of the cationic membranes. These swell at higher pH values. A large difference of 15nm is observed between the membranes exposed to the varying pH values. MAA-based membranes have a high swelling capacity, which is clearly visible in the figure.

Bell [10] and Kim [11] determined mesh sizes for two methacrylic acid (MAA) copolymers: P(MAA-g-EG) cross-linked with TEGDMA and P(MAA-co-MEG) also cross-linked with TEGDMA. Using a sodium acetate buffer at pH values 4 and 7, Bell observed a range for ξ at pH 4 of 0.3nm to 0.9 nm and a range of 24nm to 35nm at pH 7. Kim performed equilibrium swelling experiments with a phosphate-citrate buffer of pH between 2.2 and 8.0. He observed mesh sizes in the range of 18 to 35\AA at pH of 2.2 and a range of 70 to 111\AA at pH 7.0. Kim pointed out that as the ratio of MAA was increased, the mesh sizes at the collapsed state decreased but they increased for the swollen state.

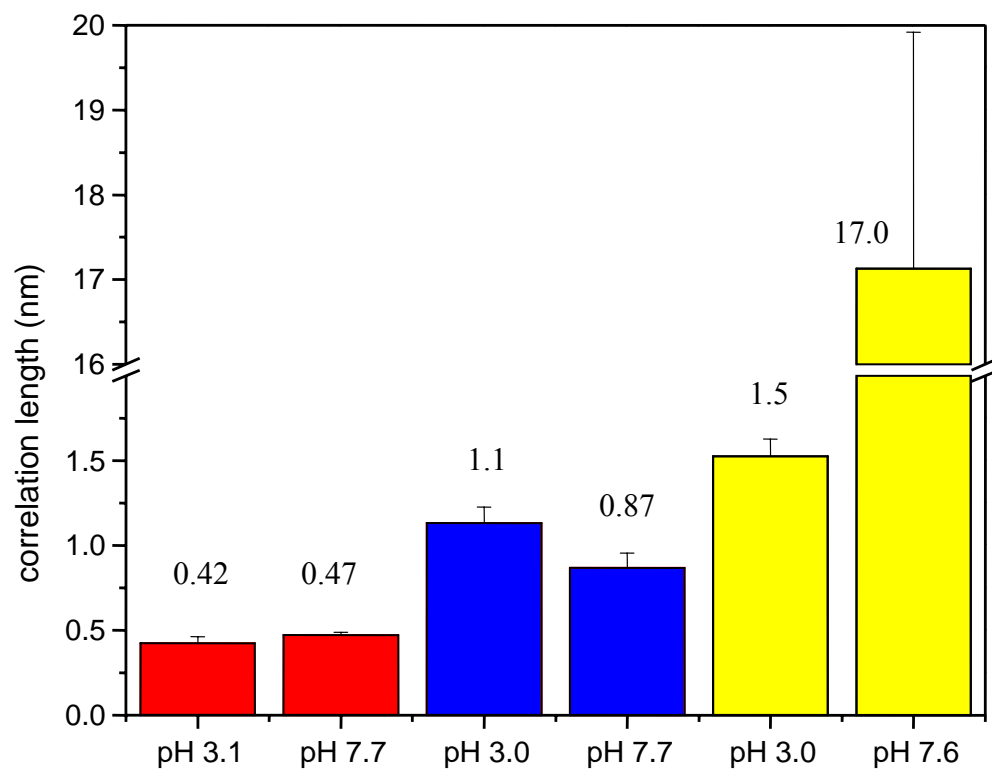


Figure 6.5. Comparison of correlation length (nm) measurements of optimized morphologies. ■ PEGMA200:PEGDMA1000; ■ DMAEM:PEGDMA1000; ■ MAA:PEGDMA1000

This was due to the higher amount of carboxylic acid groups available for ionization. Bell also described this behavior [10]. Their measurements were smaller due to the higher pH (4.0 instead of 2.2) used for experimentation. Hassan and colleagues [12] also conducted investigations on the correlation length of P(MAA-g-EG) membranes. Utilizing dimethyl glutaric acid buffer, they reported mesh sizes of 40Å at pH 4.0 and of 130Å at pH 7.0. These were similar to those reported by Kim and coworkers in 2002 [11].

Cavalieri et al. [12] measured the mesh sizes of PVA-MAA membranes by means of both dynamic mechanical testing and equilibrium swelling studies. Their focus was to simultaneously determine the average molecular weight between cross-links to the Flory interaction parameter, which represent structural and interaction parameters of the hydrogel membranes. The mesh sizes determined by these experiments were in the range of 70Å to 380Å. The correlation lengths increased as the degree of substitution decreased.

6.5 Lysozyme Crystal Stability in Pre-Polymeric Solutions

Protein crystals have proven to be more stable during longer periods of time in organic environments than the soluble protein. Therefore, the stability of HEWL crystals, a well-known crystal system, were exposed to the pre-polymeric solution components of the aforementioned MAA:PEGDMA1000 morphology. HEWL crystals were grown by the hanging-drop method utilizing the following crystallization conditions: a 50:50 solution of 0.1M Sodium Acetate buffer at pH 4.6 and 3.5M NaCl. Crystal stability was evaluated by light microscopy. HEWL crystals were exposed to different concentrations

of EtOH and to pure MAA monomer. The most favorable EtOH concentration was then utilized as a component of the various MAA:PEGDMA1000 pre-polymeric solutions to which the crystals were exposed. Factors taken into consideration were the duration of stability and the condition of the crystal after exposure. Table 6.8 presents duration of exposure of HEWL crystals to several pre-polymeric solution components.

Figure 6.6 depicts a HEWL crystal before and after exposure to a 30% EtOH solution. Fair distortion of the crystal faces can be distinguished in the photograph on the left, which was taken 226min after the crystal came in contact with the solution. It must be mentioned that this is the time at which the crystal started to degrade, not the duration of exposure of the crystal to the solution.

HEWL crystals were also placed in contact with MAA to assess the behavior of the HEWL in an entirely monomeric system. Crystals exposed to 100% MAA can be observed in Figure 6.7. It was curious that crystals in contact with pure MAA can last for considerable amounts of time without suffering any significant degradation. It is also important to comment that the protein crystal lasted almost five hours in the monomeric solution, but the photographic quality worsened as the monomer seemed to commence polymerization due to the light of the bulb

Finally, HEWL crystals were placed in contact with the MAA:PEGDMA1000 morphologies in Table 6.9. It can be observed from Figure 6.8, that the solution started to polymerize, as evidenced by the darker photograph and the distinguishable bubbles. This could be due to the energy supplied by the microscope bulb. However, the HEWL crystal is clearly distinguishable. After 155min, the HEWL crystal maintains its original shape and form and no degradation of the crystalline structure is visible.

Table 6.8. Duration of HEWL Tetragonal Crystals in Pre-Polymeric Solution Components

Pre-polymeric Solution Components	Duration (min)
EtOH 50%	127
EtOH 40%	229
EtOH 30%	226
MeOH 50%	329
MAA 100%	160

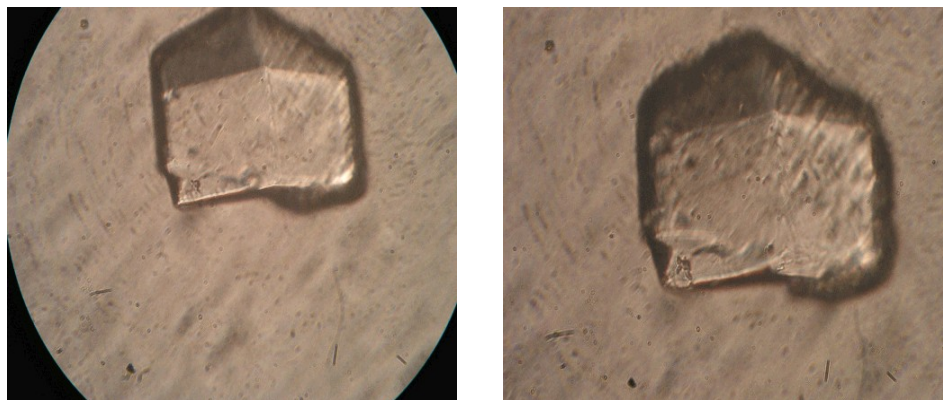


Figure 6.6. Comparison of HEWL Crystal (left) Before and (right) After Exposure to 30% EtOH Solution. Time of Exposure: 226min

Cohen-Nadar and coworkers have successfully encapsulated HEWL crystals in acrylamide hydrogels [13]. These crystals have been cross-linked with glutaraldehyde prior to encapsulation. These investigators claim that this cross-linking, which is utilized to stabilize drugs for the gastrointestinal tract [14, 15], provides the crystals with stability in aqueous solutions for up to 20 hours. More importantly, this group claims that the voids or channels of the protein crystal have been successfully filled with the hydrogel. Also, the methods by which the group assessed the filling of these channels are highly obscure.

The results presented above are preliminary results, yet are highly promising, as HEWL crystals embedded in MAA:PEGDMA1000 hydrogel membranes have already been viewed by microscopy in our laboratory. However, these protocols are still being revised and it is hoped that, in the near future, more decisive results will be obtained that will allow for a better assessment of the feasibility of the encapsulation of protein crystals in hydrogel membranes. Investigators observe the same degradation effect in un-cross-linked crystals detected in the above photographs. However, no time scale for the degradation process is mentioned.

The ability to encapsulate functional proteins in hydrogel systems is highly relevant to multiple fields of science such as catalysis, drug delivery, and other medical applications. The characterization of such systems is of imminent importance as investigators are turning to proteins for answers to many unsolvable conundrums of the past and present. The fact that not only solubilized proteins can be encapsulated within such materials is also of scientific interest as protein crystallization has become a vital element of the fields in which hydrogel systems could be utilized. The results presented

above are only the beginning of a series of test that must be undertaken to completely prove the efficacy of these systems above others mentioned such as sol-gels. It is hoped that in the near future a more complete panorama of the behavior of proteins in hydrogel systems will be achieved.

Table 6.9. Duration of HEWL Tetragonal Crystals Exposed to Various MAA:PEGDMA1000 Morphologies

MAA:PEGDMA1000 Ratio (molar)	Dilution %	Duration (min)
88:12	60	156
		95
	40	335
		51
		151
70:30	60	172
	40	198
		127
60:40	60	26

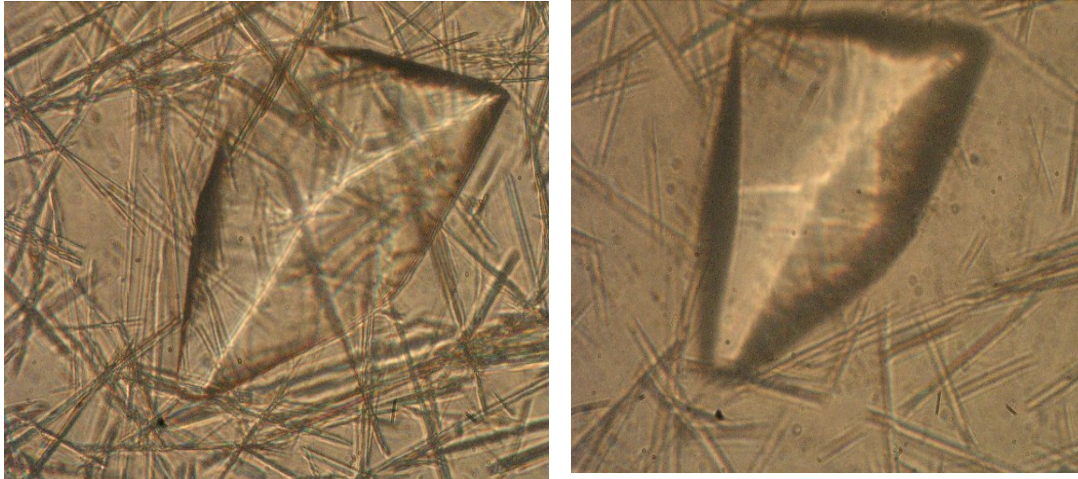


Figure 6.7 Comparison of HEWL crystals before and after exposure 100% MAA
Time of exposure: MAA – 2h 45min

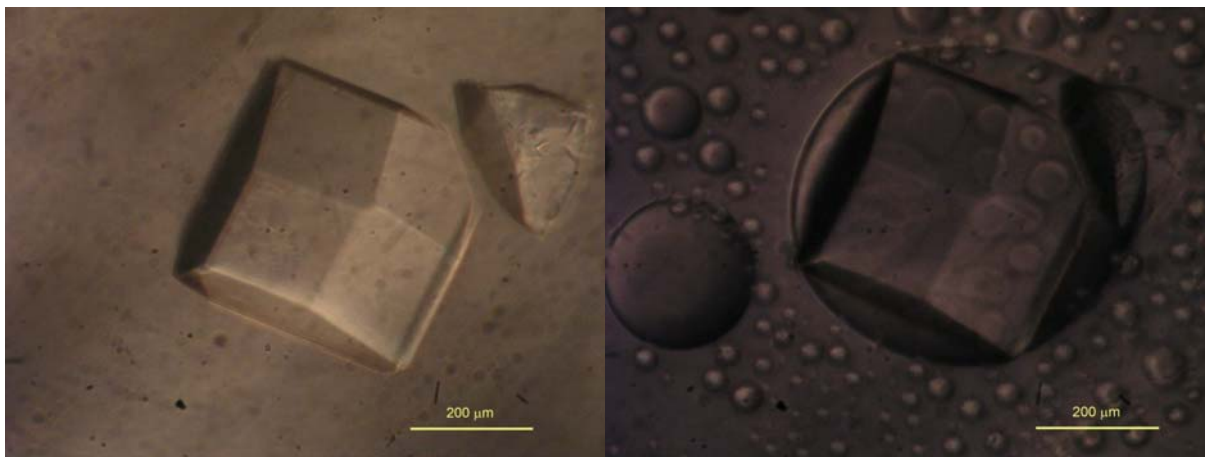


Figure 6.8. Comparison of HEWL crystal (left) before and (right) after exposure to
MAA:PEGDMA1000 pre-polymeric solution. Time of exposure: 155min.

6.5 References

- [1] J. T. Sage, D. Morikis, and P. M. Champion, "Spectroscopic Studies of Myoglobin at Low pH: Heme Structure and Ligation," *Biochemistry*, vol. 30, pp. 1227-1237, 1991.
- [2] P. L. Edmiston, C. L. Wambolt, M. K. Smith, and S. S. Saavedra, "Spectroscopic Characterization of Albumin and Myoglobin Entrapped in Bulk Sol-Gel Glasses," *Journal of Colloid and Interface Science*, vol. 163, pp. 395-406, 1994.
- [3] M. Bottini, A. Di Venere, and P. R. Lugli, N., "Conformation and stability of myoglobin in dilute and crowded organically modified media," *Journal of Non-Crystalline Solids*, vol. 343, pp. 101-108, 2004.
- [4] C. L. Stevenson, "Characterization of protein and peptide stability and solubility in non-aqueous solvents," *Current Pharmaceutical Biotechnology*, vol. 1, pp. 165-82, Sep 2000.
- [5] T. T. Herskovits, B. Gadegbeku, and H. Jaillet, "On the structural stability and solvent denaturation of proteins. I. Denaturation by the alcohols and glycols," *The Journal of Biological Chemistry*, vol. 245, pp. 2588-98, May 25 1970.
- [6] J. Miksovská, J. Yom, B. Diamond, and R. Larsen, "Spectroscopic and photothermal study of myoglobin conformational changes in the presence of sodium dodecyl sulfate," *Biomacromolecules*, vol. 7, pp. 476-482, FEB 2006.
- [7] L. M. Ellerby, C. R. Nishida, F. Nishida, S. A. Yamanaka, B. Dunn, J. Selverstone-Valentine, and J. I. Zink, "Encapsulation of Proteins in Transparent Porous Silicate Glasses Prepared by the Sol-Gel Method," *Science*, vol. 255, pp. 1113-1115, 1992.
- [8] T. K. Das, I. Khan, D. L. Rousseau, and J. M. Friedman, "Preservation of the Native Structure in Myoglobin at Low pH by Sol-Gel Encapsulation," *J. Am. Chem. Soc.*, vol. 19987, pp. 10268-10269, 1998.
- [9] K. Podual, F. Doyle, and N. Peppas, "Preparation and dynamic response of cationic copolymer hydrogels containing glucose oxidase," *Polymer*, vol. 41, pp. 3975-3983, MAY 2000.
- [10] C. Bell and N. Peppas, "Water, solute and protein diffusion in physiologically responsive hydrogels of poly(methacrylic acid-g-ethylene glycol)," *Biomaterials*, vol. 17, pp. 1203-1218, JUN 1996.

- [11] B. Kim and N. Peppas, "Synthesis and characterization of pH-sensitive glycopolymers for oral drug delivery systems," *Journal of Biomaterial Science - Polymer Edition*, vol. 13, pp. 1271-1281, 2002.
- [12] F. Cavalieri, F. Miano, P. D'Antona, and G. Paradossi, "Study of gelling behavior of poly(vinyl alcohol)-methacrylate for potential utilizations in tissue replacement and drug delivery," *Biomacromolecules*, vol. 5, pp. 2439-2446, NOV-DEC 2004.
- [13] N. Cohen-Hadar, Y. Wine, E. Nachliel, D. Huppert, M. Gutman, F. Frolow, and A. Freeman, "Monitoring the Stability of Crosslinked Protein Crystals Biotemplates: A Feasibility Study," *Biotechnology and Bioengineering*, vol. 94, pp. 1005-1011, 2006.
- [14] N. Clair, B. Shenoy, L. Jacob, and A. Margolin, "Cross-linked protein crystals for vaccine delivery," *Proceedings of the National Academy of the Sciences of the United States of America*, vol. 96, pp. 9469-9474, AUG 17 1999.
- [15] D. Haring and P. Schreier, "Cross-linked enzyme crystals," *Current Opinion in Chemical Biology*, vol. 3, pp. 35-38, FEB 1999.

7 Conclusions

The stability, biological activity and subsequent immobilization of heme proteins have been addressed for a limited number of systems. The behavior of such proteins is highly ambiguous as various groups claim differing results, specifically in sol-gel systems. Due to such discrepancies in literature, the study of the stability and activity of four heme-proteins in solution - mMb, hMb, bHb, and pHb- in hydrogel membranes was undertaken. These proteins were chosen due to their commercial availability and to the structural similarities. As protein crystals are appealing due to their stability and duration in aqueous and organic environments, the stability of such were also studied. Three monomers were utilized for these studies: MAA (ionic), DMAEM (cationic), and PEGMA200 (neutral).

Stability experiments showed that heme-proteins with similar structural and molecular characteristics such as pI, molecular weight, and chain length can be stabilized in the same anionic, cationic, and neutral morphologies. This stabilization does, however, affect these proteins, as reduction and broadening of the Soret bands indicates possible denaturation and unfolding of the proteins at some site, possibly far away from the heme prosthetic group. More thorough experimentation is necessary to assess if the red shifts of the Soret bands of pHb in contact with the neutral morphology are a product of a coexistence of multiple oxidative states of the Fe ion of the heme group.

Biological activity of the heme-proteins upon encapsulation in the various hydrogel morphologies is not fully affected. Redox reactions of the heme group demonstrate the ability of the proteins to bind and unbind multiple ligands such as H₂O

and CO. However, the effect of the polymerization on the proteins per se is still vague due to the blue shifts in the Soret bands that are observed specifically for the proteins encapsulated in the metaquo state in the ionic morphologies, upon reduction of the heme group to the deoxy state, and upon the addition of CO, these last two for all three morphologies

Red shifts of the metaquo Soret bands from 408nm to 413nm of bHb and pHb upon encapsulation in neutral membranes may indicate an unknown interaction of the heme group with the polymer that may result in a creation of multiple oxidative states of the proteins, as observed in the neutral PEG based pre-polymeric solutions with pHb. This could also be the case for the unusual Soret bands ($\lambda = 418$ to 422nm) observed for all proteins in the carboxy state encapsulated in this morphology. Additional experimentation is necessary to confirm this hypothesis.

The small displacements of the Soret bands of the four proteins when changed from the deoxy state to the carboxy state within the neutral PEG based membranes may be due to a higher affinity of the CO for the polymer than for the heme group. Affinity experiments of CO to the PEG based membranes alone must be undertaken to further prove this hypothesis.

Exposure of the solubilized proteins to the UV light source utilized for the hydrogel polymerization has a detrimental effect upon the proteins as indicated by the reduction in absorbance and broadening of the Soret bands of all proteins. This effect is more evident when the proteins have been exposed to the light source for longer periods of time, as during the polymerization of the ionic hydrogel membranes. This could

provide a possible explanation for the unusual locations of the Soret bands of the proteins upon encapsulation in MAA and DMAEM based hydrogels.

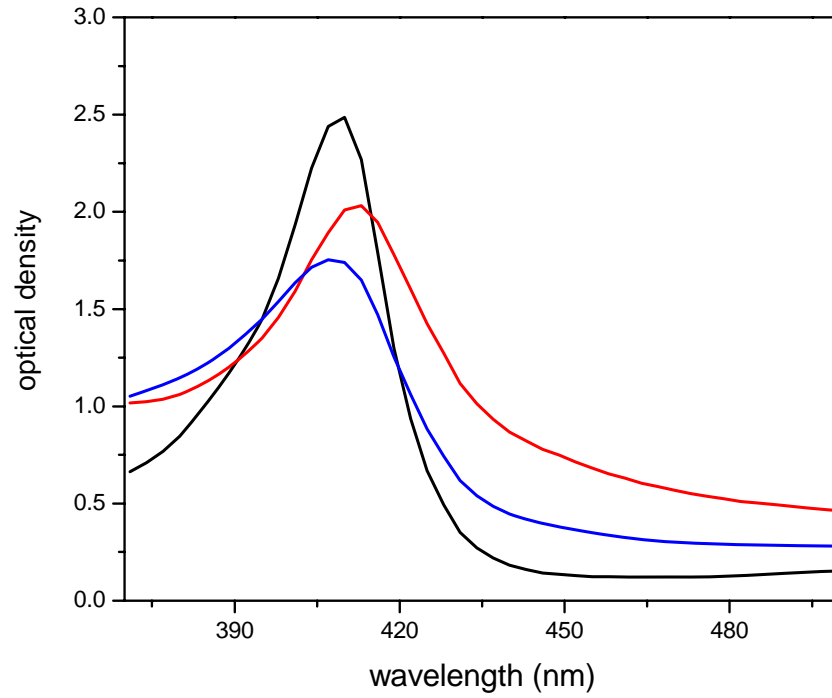
Examination of the pore sizes of the different morphologies reveal highly cross-linked and rigid membranes, which is advantageous for the applications for which these systems could be utilized. Varying the pH of the media from acidic to neutral had no significant effect upon the mesh size of the neutral PEG based membranes. DMAEM based hydrogel membranes collapsed upon contact with neutral media, while swelling was observed when exposed to acidic media. MAA based hydrogels presented the opposite behavior: swelling in neutral media and collapsing in acidic media. The behavior of these three morphologies is consistent with what has been observed and documented in the literature.

Preliminary stability experiments of lysozyme crystals in MAA based pre-polymeric solutions demonstrate that crystals may be stable, in their shape and form, for periods of more than two hours. Whole lysozyme crystals encapsulated in this morphology have also been observed.

Although structural confirmation of the conformational changes, if any, suffered by the heme-proteins is vital, the results obtained in this investigation show these proteins can be successfully encapsulated in these membranes and that these retain some indication of biological activity. More importantly, these results show that the whole protein does not need to be structurally sound if the active site of the protein is intact. In the near future, it is hoped these results stimulate the creation of drug delivery, biosensor and other therapeutic systems.

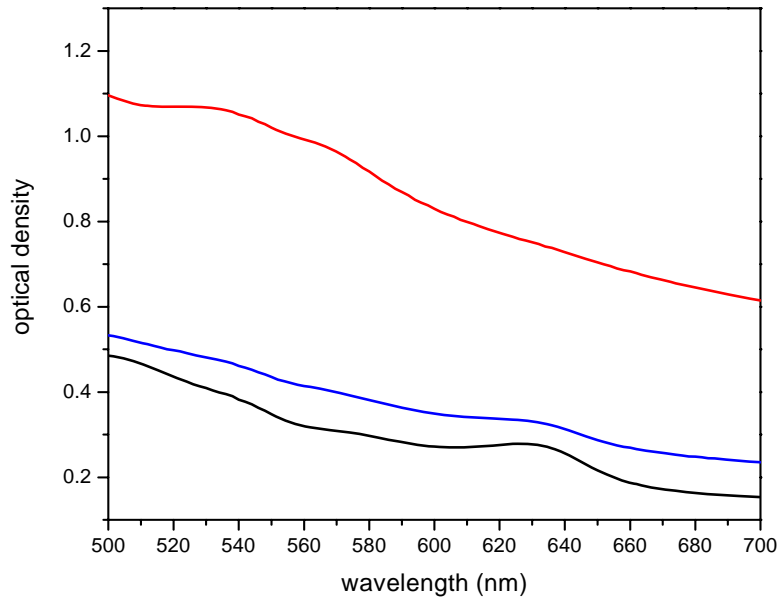
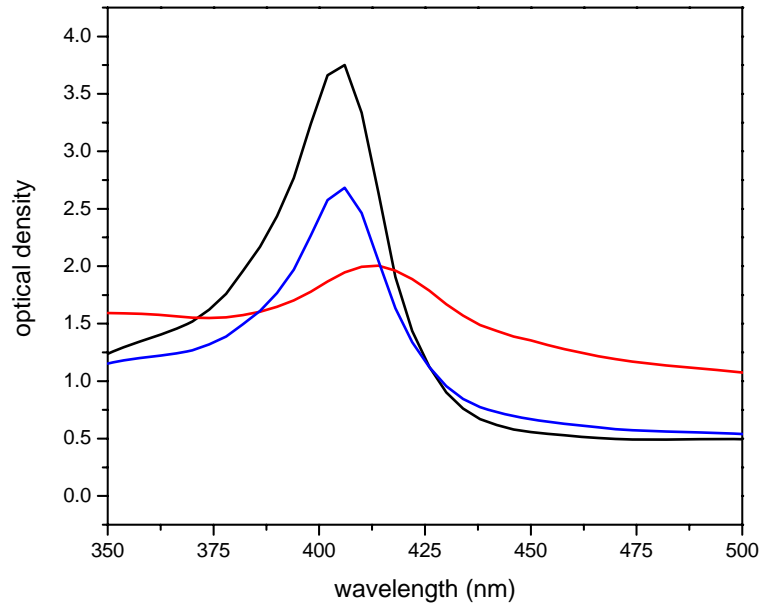
APPENDIX 1.1

Soret Band of hMb in MAA:PEGDMA1000 Pre-Polymeric Solution Components. ■ hMb+MAA+NaOH 5M ($\lambda_{\max} = 410\text{nm}$); ■ hMb+PEGDMA1000+EtOH ($\lambda_{\max} = 413\text{nm}$); ■ hMb+Pre-Polymeric Solution ($\lambda_{\max} = 407\text{nm}$)



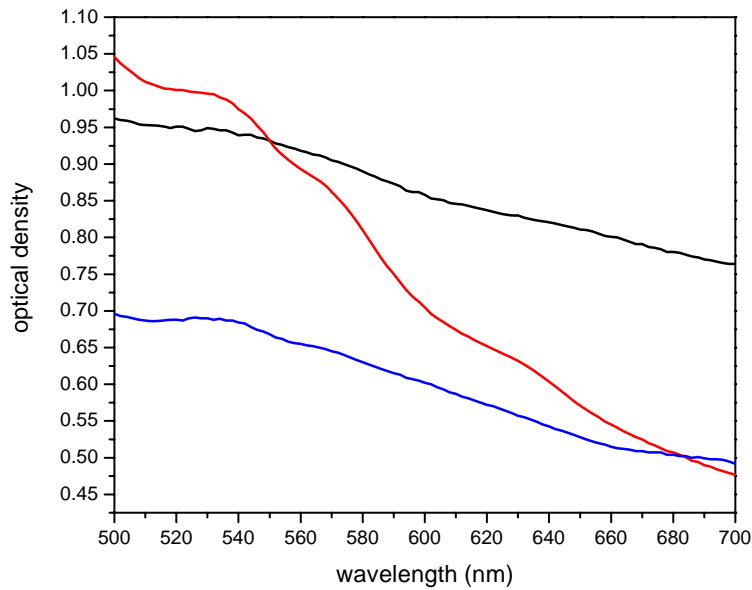
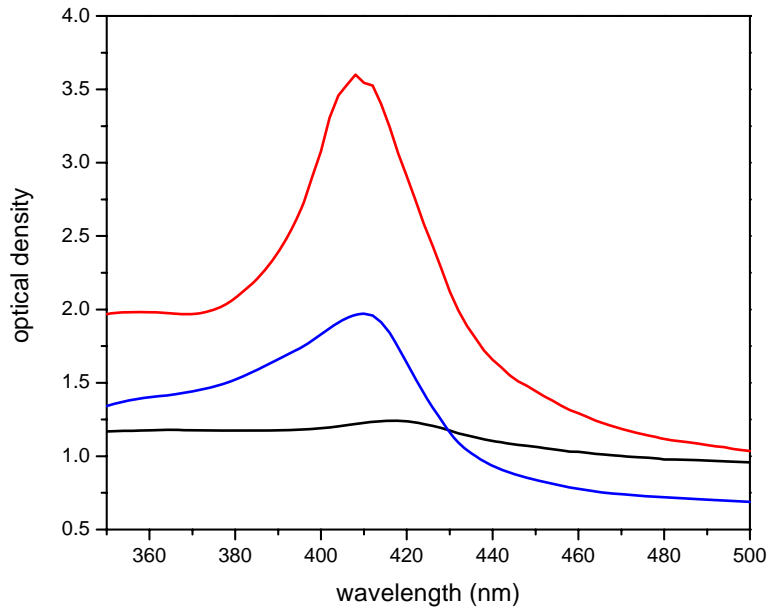
APPENDIX 1.2

Soret and Q Bands of bHb in MAA:PEGDMA1000
Pre-Polymeric Solution Components. ■
bHb+MAA+NaOH 5M (Soret λ_{\max} = 406nm; Q λ_{\max} = 628nm); ■ bHb+PEGDMA1000+EtOH (Soret λ_{\max} = 414nm; Q λ_{\max} = 524nm); ■ bHb+Pre-Polymeric Solution (Soret λ_{\max} = 406nm; Q λ_{\max} = NV). NV = not visible



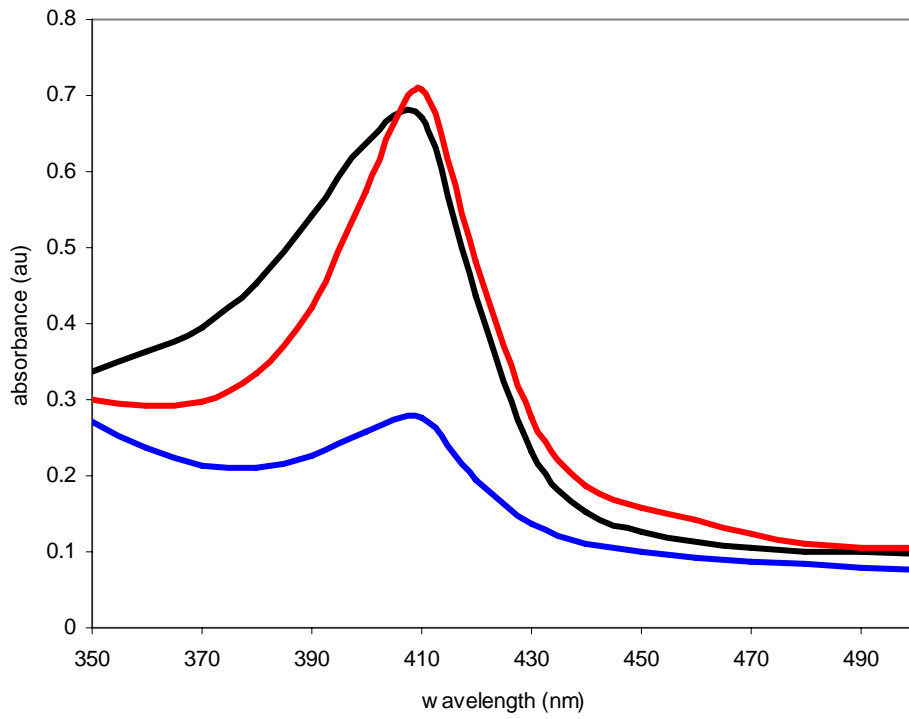
APPENDIX 1.3

Soret and Q Bands of pHb in MAA:PEGDMA1000 Pre-Polymeric Solution Components. ■ pHb+MAA+NaOH 5M (Soret λ_{\max} = 416nm; Q λ_{\max} = NV); ■ pHb+PEGDMA1000+EtOH (Soret λ_{\max} = 408nm; Q λ_{\max} = NV); ■ pHb+Pre-Polymeric Solution (Soret λ_{\max} = 410nm; Q λ_{\max} = NV)



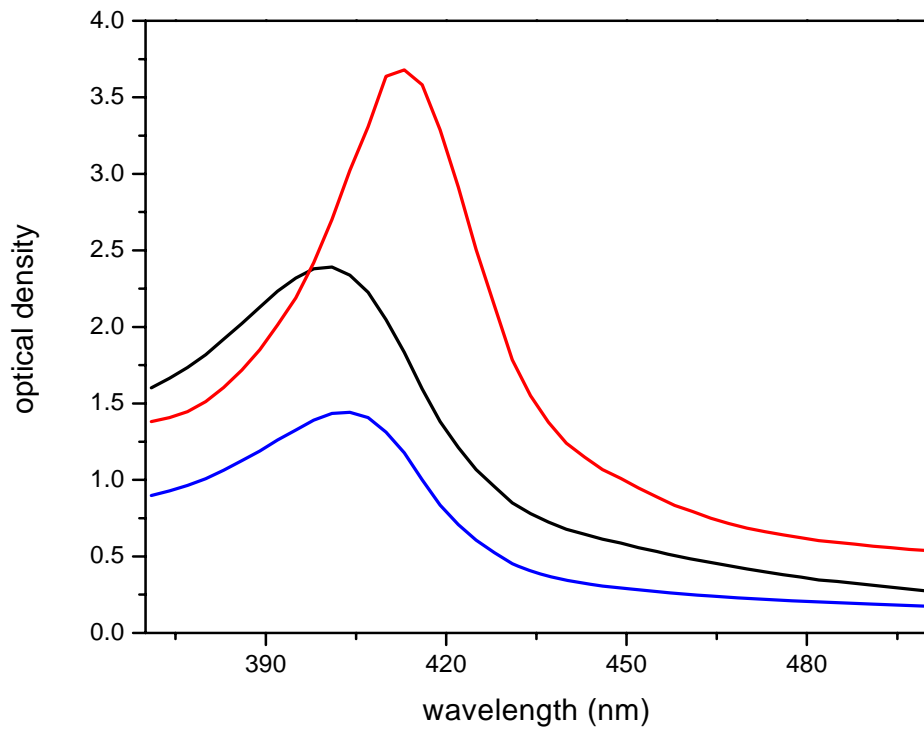
APPENDIX 1.4

Soret Band of mMb in DMAEM:PEGDMA1000
Pre-Polymeric Solution. ■ mMb+DMAEM+HCl 6N
($\lambda_{\max} = 410\text{nm}$); ■ mMb+PEGDMA1000+EtOH
($\lambda_{\max} = 410\text{nm}$); ■ mMb+Pre-Polymeric Solution
($\lambda_{\max} = 410\text{nm}$)



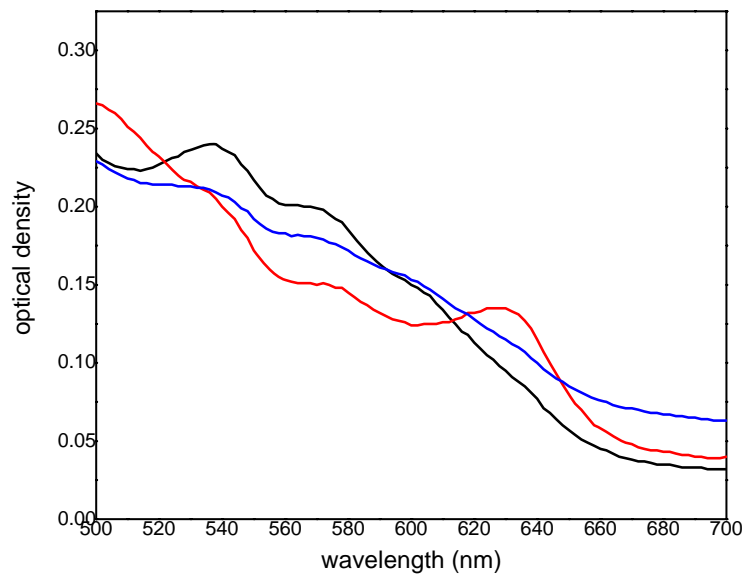
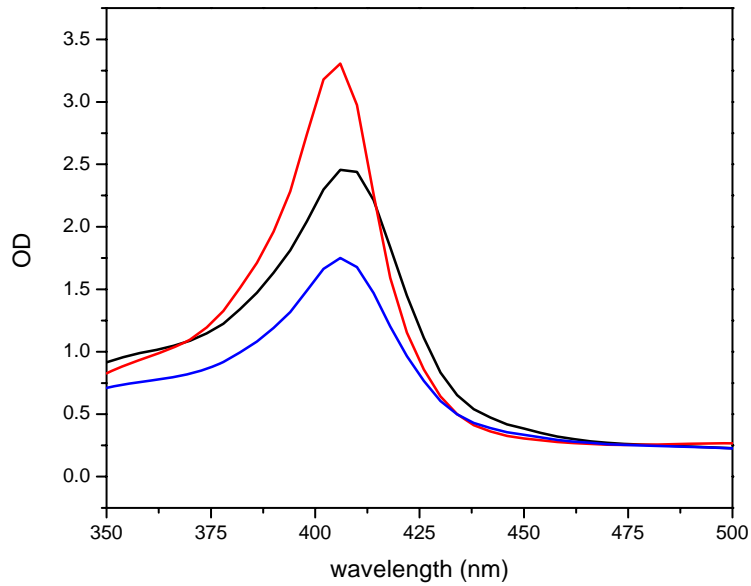
APPENDIX 1.5

Soret band of hMb in DMAEM:PEGDMA1000 Pre-polymeric Solution Components. ■ hMb+DMAEM+HCl 6N ($\lambda_{\max} = 401\text{nm}$); ■ hMb+PEGDMA1000+EtOH ($\lambda_{\max} = 413\text{nm}$); ■ hMb+Pre-Polymeric Solution ($\lambda_{\max} = 404\text{nm}$)



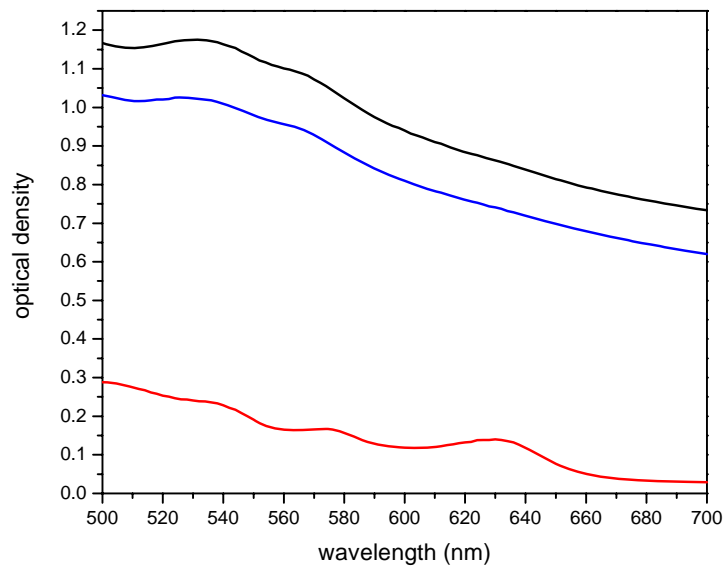
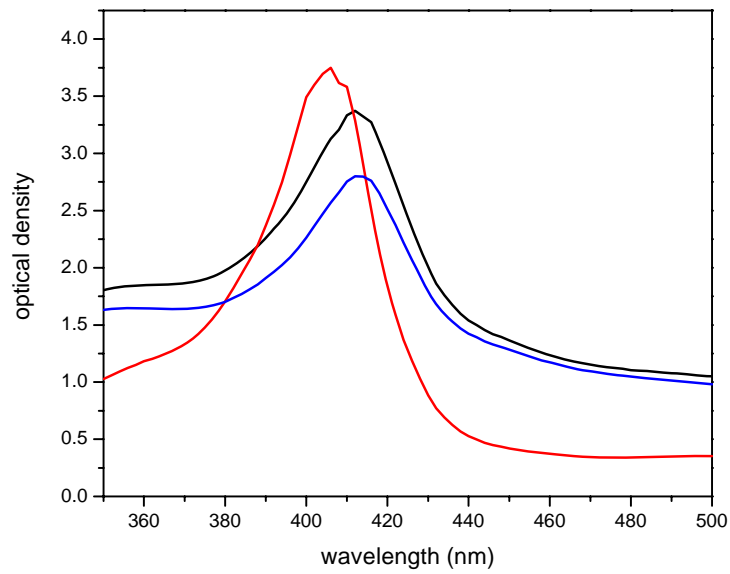
APPENDIX 1.6

Soret and Q Bands of bHb in DMAEM:PEGDMA1000
Pre-Polymeric Solution Components. ■
bHb+DMAEM+HCl 6N (Soret λ_{\max} = 406nm; Q λ_{\max} =
538nm); ■ bHb+PEGDMA1000+EtOH (Soret λ_{\max} =
406nm; Q λ_{\max} = 630nm); ■ bHb+Pre-Polymeric
Solution (Soret λ_{\max} = 406nm; Q λ_{\max} = NV). NV = not
visible



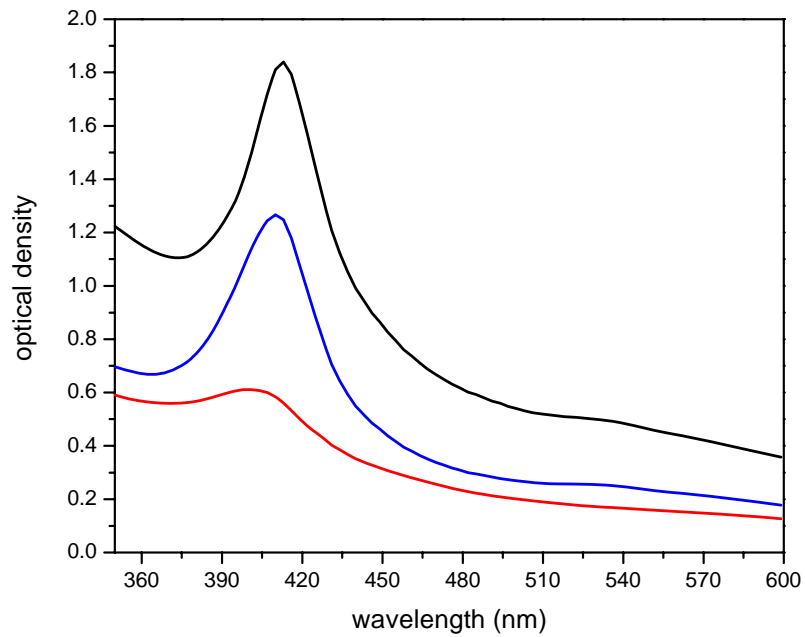
APPENDIX 1.7

Soret and Q bands of pHb in DMAEM:PEGDMA1000 Pre-polymeric Solution Components. ■ pHb+DMAEM+HCl 6N (Soret λ_{\max} = 412nm; Q λ_{\max} = 521nm); ■ pHb+PEGDMA1000+EtOH (Soret λ_{\max} = 410nm; Q λ_{\max} = 573nm, 630nm); ■ pHb+Pre-Polymeric Solution (Soret λ_{\max} = 412nm; Q λ_{\max} = 531nm)



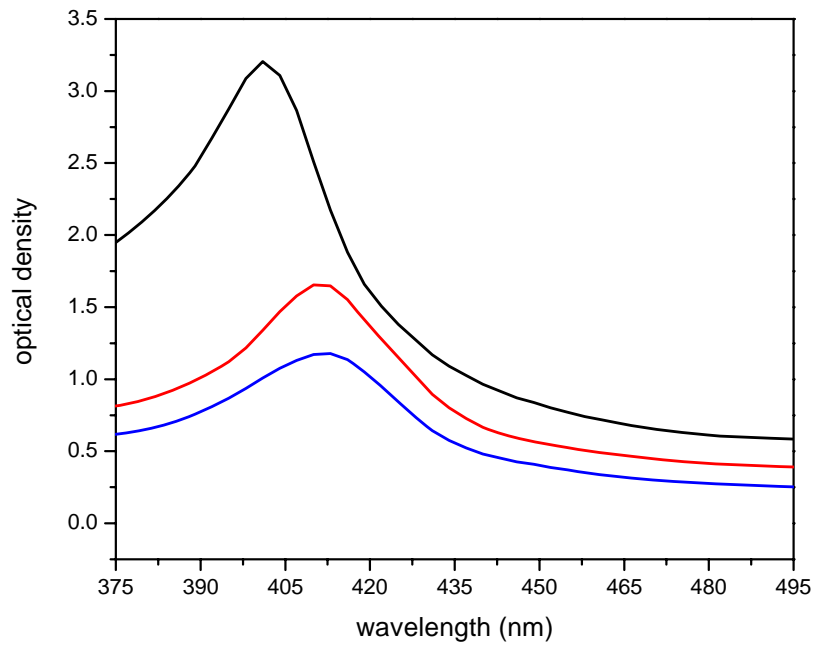
APPENDIX 1.8

Soret Bands of mMb in PEGMA200:PEGDMA1000 Pre-polymeric Solution Components. ■
mMb+PEGDMA1000+EtOH ($\lambda_{\max} = 413\text{nm}$); ■
mMb+PEGMA200+EtOH ($\lambda_{\max} = 401\text{nm}$); ■ mMb+Pre-Polymeric Solution ($\lambda_{\max} = 410\text{nm}$)



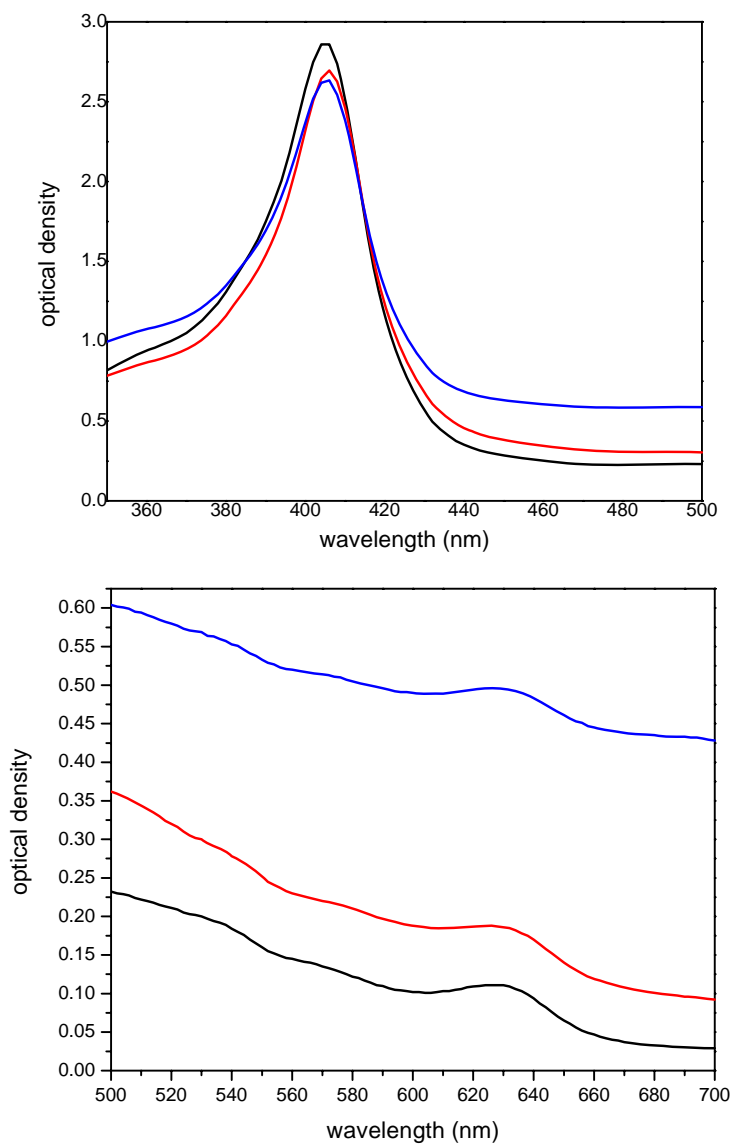
APPENDIX 1.9

Soret Band of hMb in PEGMA200:PEGDMA1000 Pre-polymeric Solution Components. ■ hMb+PEGMA200 ($\lambda_{\max} = 401\text{nm}$); ■ hMb+PEGDMA1000+EtOH ($\lambda_{\max} = 410\text{nm}$); ■ hMb+Pre-Polymeric Solution ($\lambda_{\max} = 413\text{nm}$)



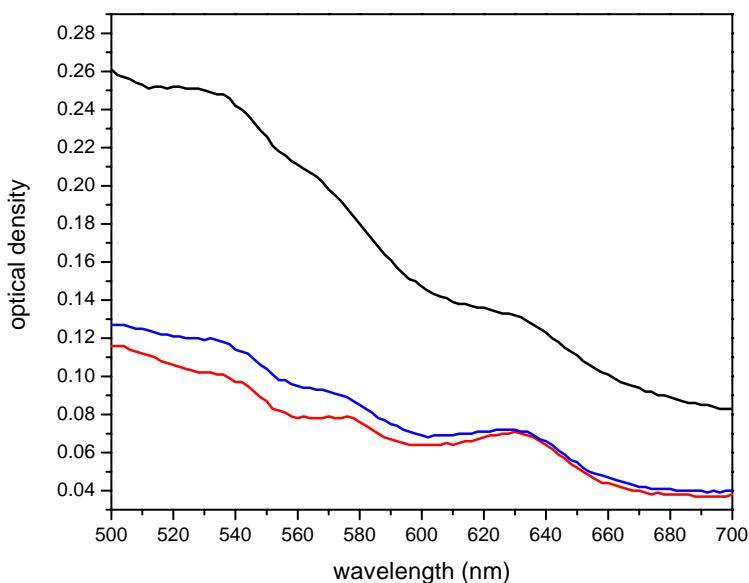
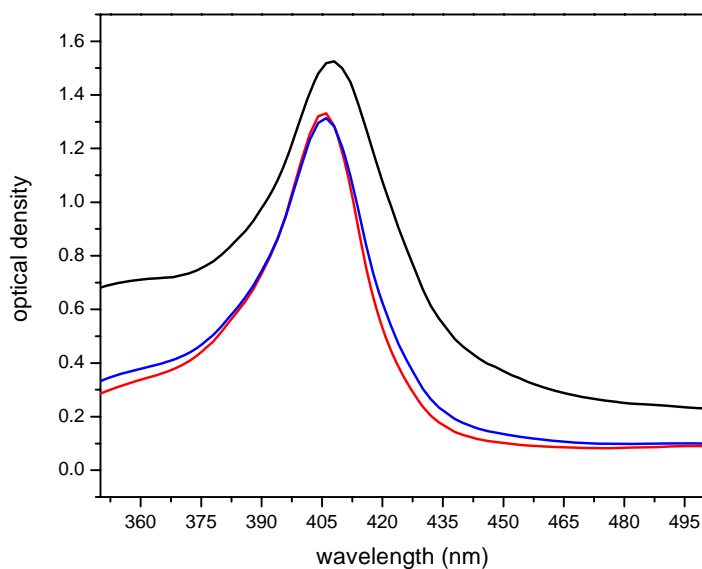
APPENDIX 1.10

Soret and Q bands of bHb in PEGMA200:PEGDMA1000
Pre-polymeric Solution Components. ■
bHb+PEGMA200+EtOH (Soret λ_{\max} = 406nm; Q λ_{\max} = 630nm); ■ bHb+PEGDMA1000+EtOH (Soret λ_{\max} = 406nm; Q λ_{\max} = 626nm); ■ bHb+Pre-Polymeric Solution (Soret λ_{\max} = 406nm; Q λ_{\max} = 628nm)



APPENDIX 1.11

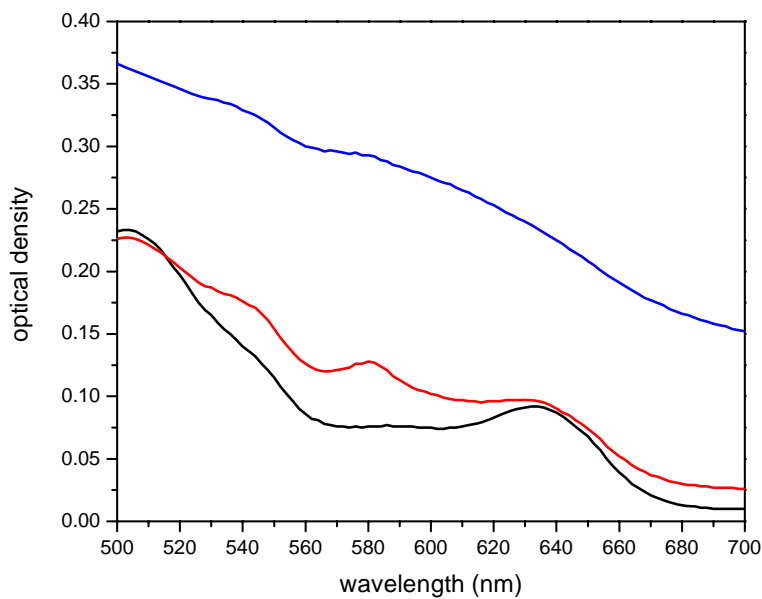
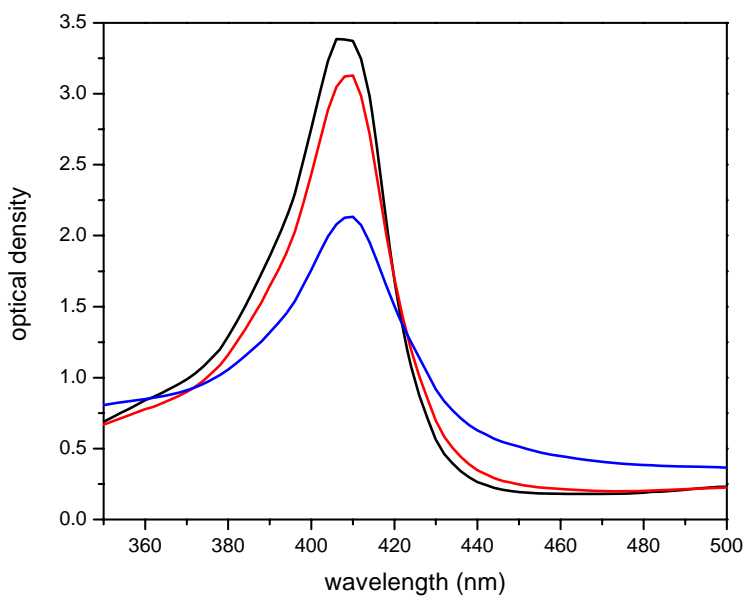
Soret and Q bands of pHb in PEGMA200:PEGDMA1000 Pre-polymeric Solution Components. ■ pHb+PEGMA200+EtOH (Soret λ_{\max} = 408; Q λ_{\max} = 630nm); ■ pHb+PEGDMA1000+EtOH (Soret λ_{\max} = 404; Q λ_{\max} = 636nm); ■ pHb+Pre-Polymeric Solution (Soret λ_{\max} = 406; Q λ_{\max} = 628nm)



APPENDIX 1.12

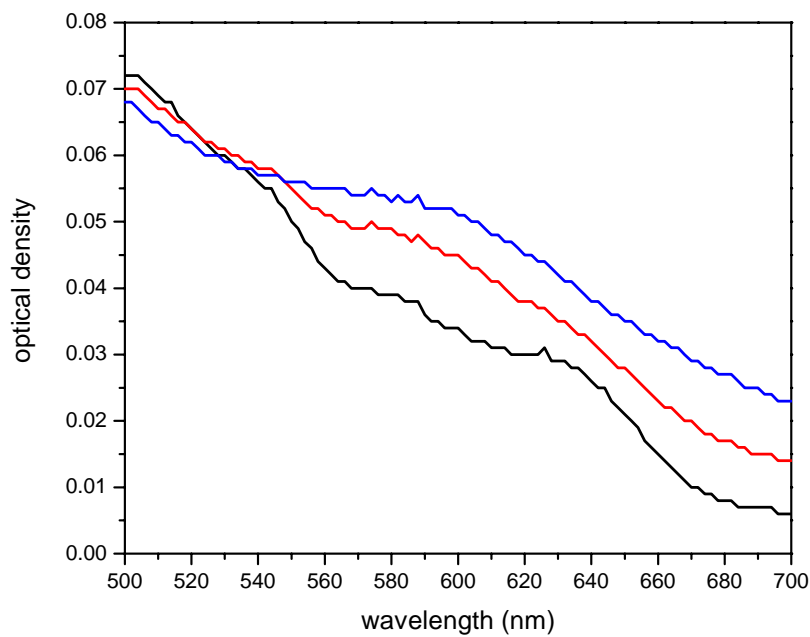
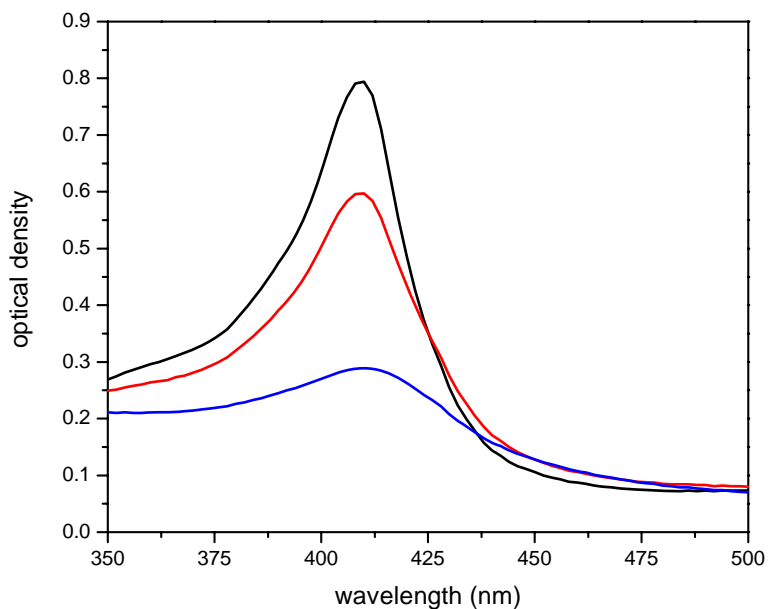
Soret and Q bands of mMb After Exposure to UV light.

■ native mMb (Soret $\lambda_{\max} = 406\text{nm}$; Q $\lambda_{\max} = 634\text{nm}$);
■ mMb after 300s (Soret $\lambda_{\max} = 410\text{nm}$; Q $\lambda_{\max} = 580\text{nm}$); ■ mMb after 1200s (Soret $\lambda_{\max} = 410\text{nm}$; Q $\lambda_{\max} = \text{NV}$). NV = not visible



APPENDIX 1.13

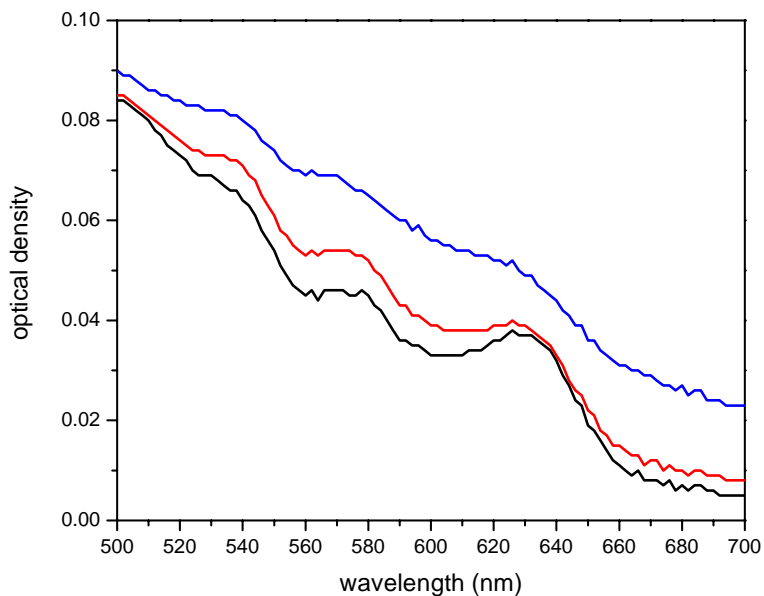
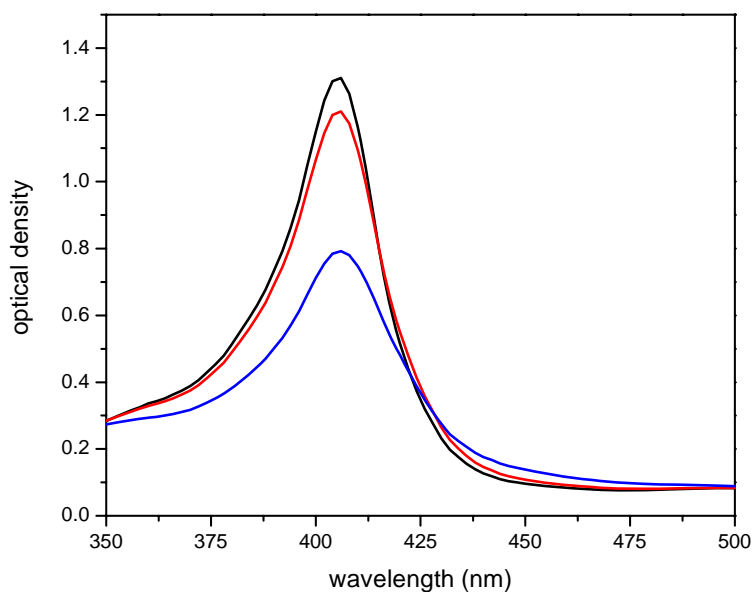
Soret and Q bands of hMb After Exposure to UV light. ■ native hMb (Soret λ_{\max} = 410nm; Q λ_{\max} = NV); ■ hMb after 300s (Soret λ_{\max} = 410nm; Q λ_{\max} = NV); ■ hMb after 1200s (Soret λ_{\max} = 410nm; Q λ_{\max} = NV). NV = not visible



APPENDIX 1.14

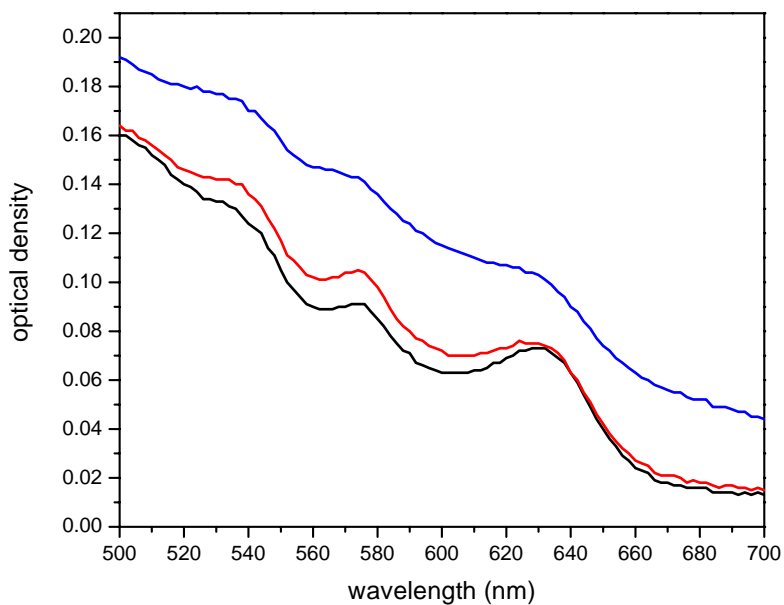
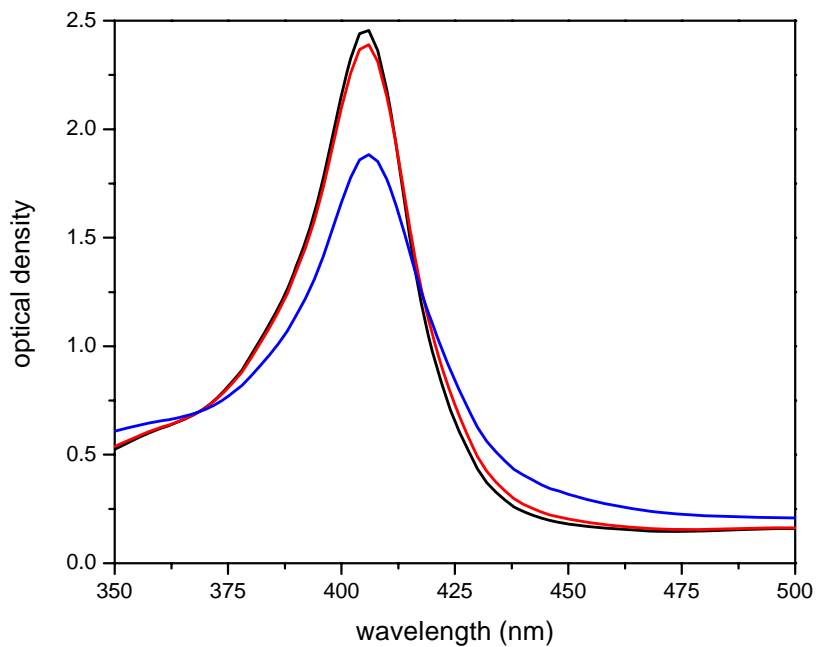
Soret and Q bands of bHb After Exposure to UV light.

■ native bHb (Soret λ_{\max} = 406nm; Q λ_{\max} = 536nm, 578nm, 626nm); ■ bHb after 300s (Soret λ_{\max} = 406nm; Q λ_{\max} = 536nm, 578nm, 626nm); ■ bHb after 1200s (Soret λ_{\max} = 406nm; Q λ_{\max} = NV). NV = not visible



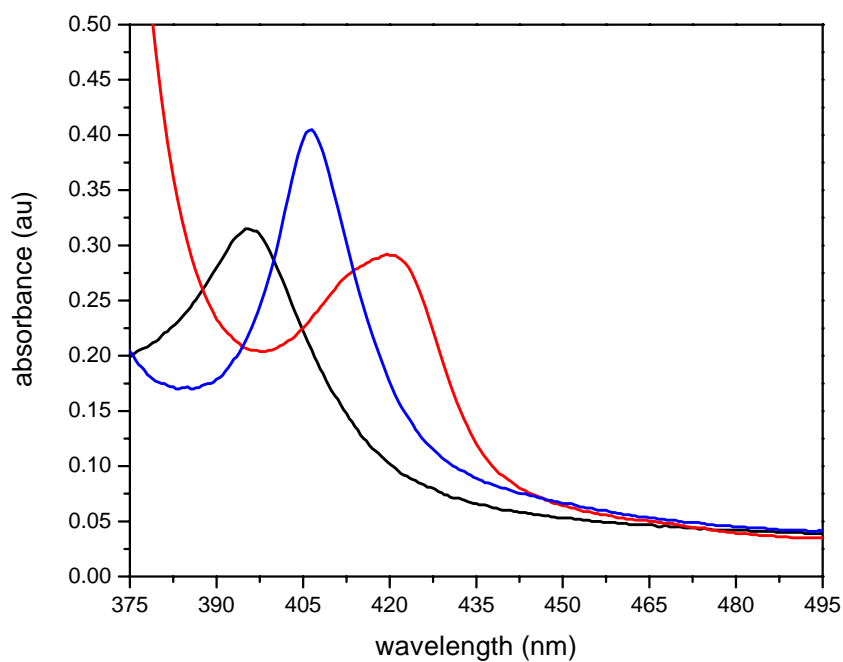
APPENDIX 1.15

Soret and Q bands of pHb After Exposure to UV light. ■ native pHb (Soret λ_{\max} = 406nm; Q λ_{\max} = 536nm, 630nm); ■ pHb after 300s (Soret λ_{\max} = 406nm; Q λ_{\max} = 536nm, 630nm); ■ pHb after 1200s (Soret λ_{\max} = 406nm; Q λ_{\max} = 536nm, 630nm)



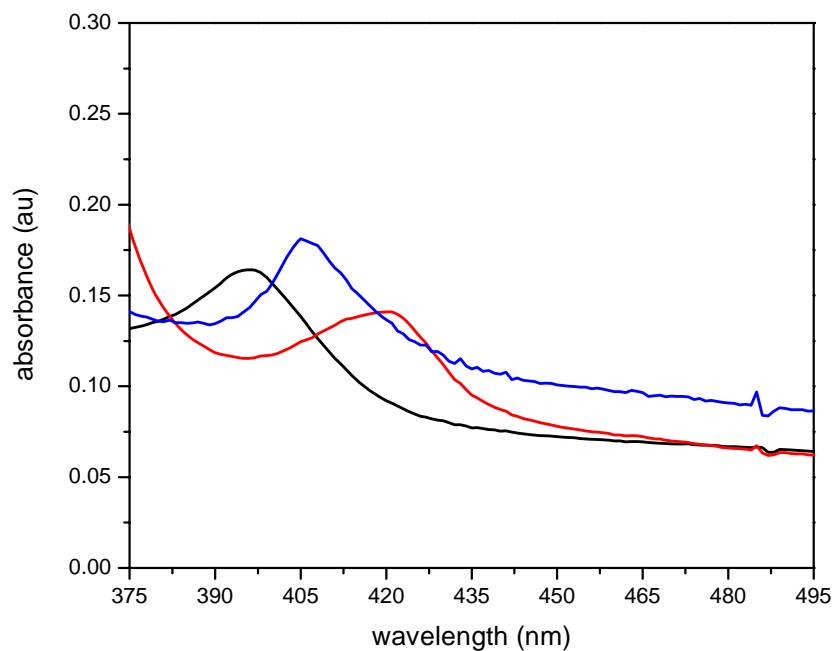
APPENDIX 1.16

Biological Activity of mMb in MAA:PEGDMA1000 Membranes.
■ metaquo ($\lambda_{\max} = 395\text{nm}$); ■ deoxy ($\lambda_{\max} = 422\text{nm}$); ■ carboxy ($\lambda_{\max} = 406\text{nm}$)



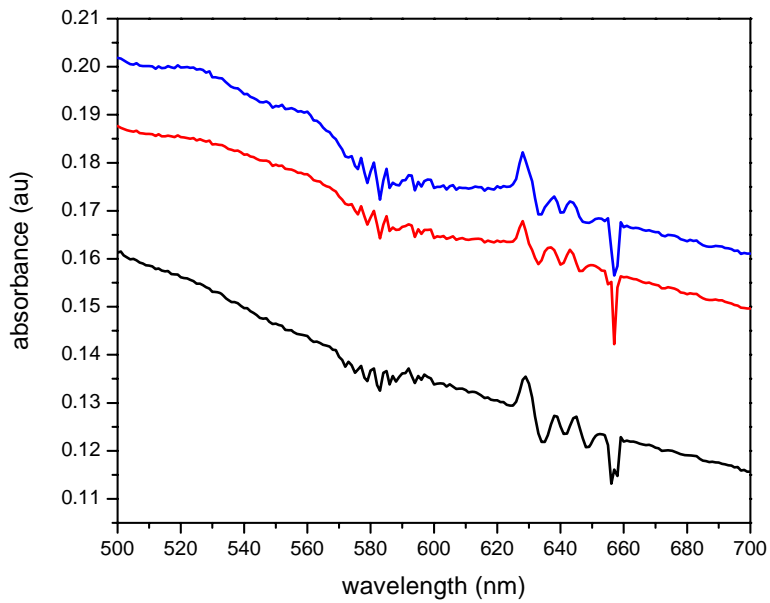
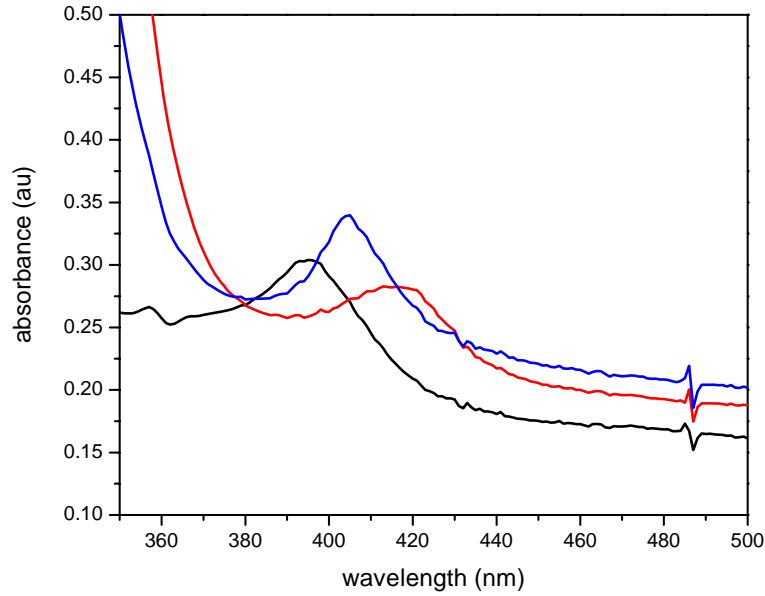
APPENDIX 1.17

Biological Activity of hMb in MAA:PEGDMA1000 Membranes.
■ metaquo ($\lambda_{\max} = 396\text{nm}$); ■ deoxy ($\lambda_{\max} = 421\text{nm}$); ■ carboxy ($\lambda_{\max} = 405\text{nm}$)



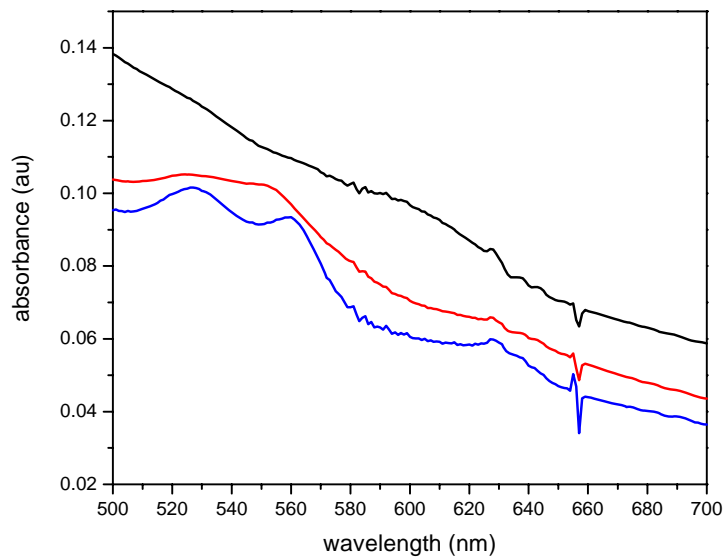
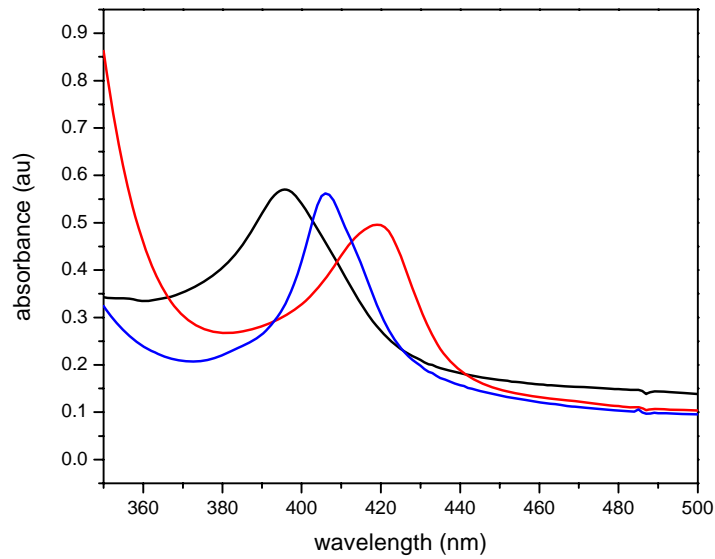
APPENDIX 1.18

Biological Activity of bHb in MAA:PEGDMA1000 Membranes. ■ metaquo (Soret λ_{\max} = 396nm; Q λ_{\max} = 629nm); ■ deoxy (Soret λ_{\max} = 416nm; Q λ_{\max} = 628nm); ■ carboxy (Soret λ_{\max} = 405nm; Q λ_{\max} = 522nm, 628nm)



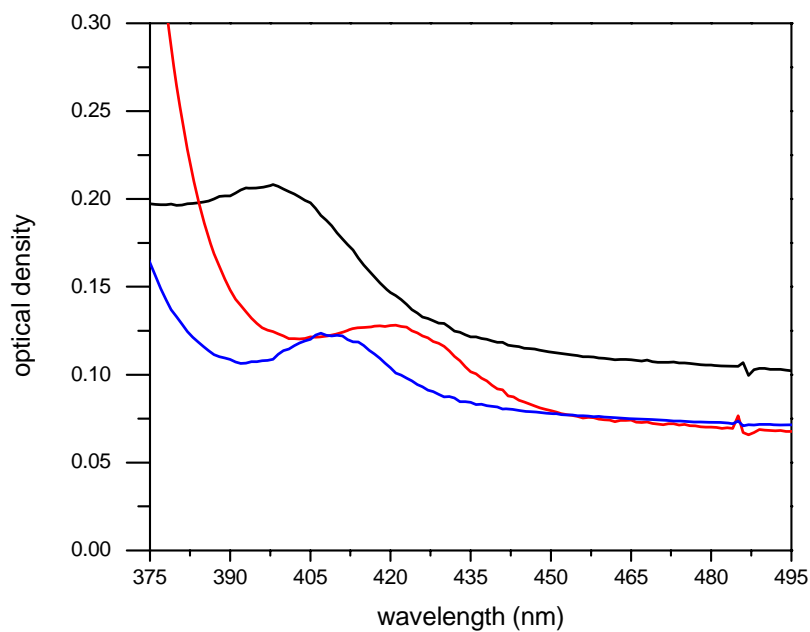
APPENDIX 1.19

Biological Activity of bHb in MAA:PEGDMA1000 Membranes. ■ metaquo (Soret λ_{\max} = 396nm; Q λ_{\max} = NV); ■ deoxy (Soret λ_{\max} = 419nm; Q λ_{\max} = NV); ■ carboxy (Soret λ_{\max} = 406nm; Q λ_{\max} = 525nm, 560nm). NV = not visible



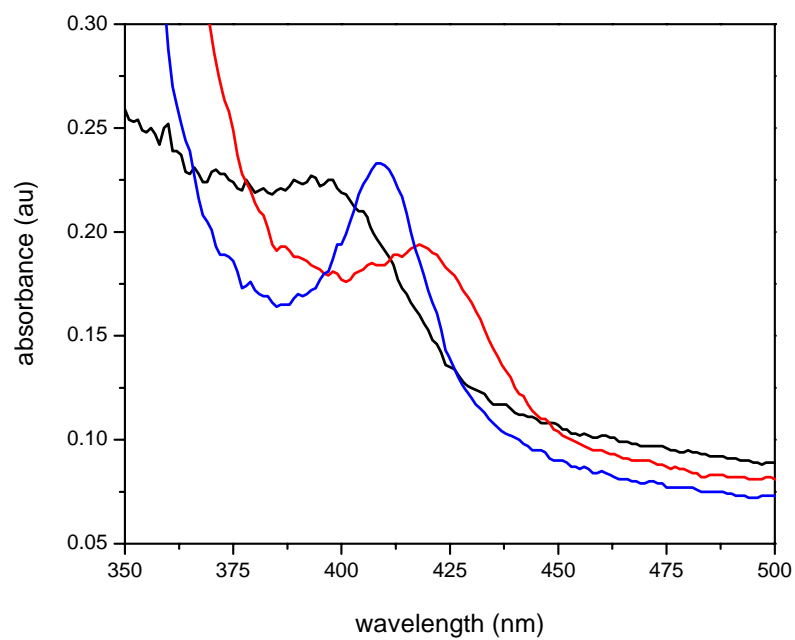
APPENDIX 1.20

Biological Activity of mMb in DMAEM:PEGDMA1000 Membranes. ■ metaquo (λ_{\max} = 398nm); ■ deoxy (λ_{\max} = 421nm); ■ carboxy (λ_{\max} = 421nm)



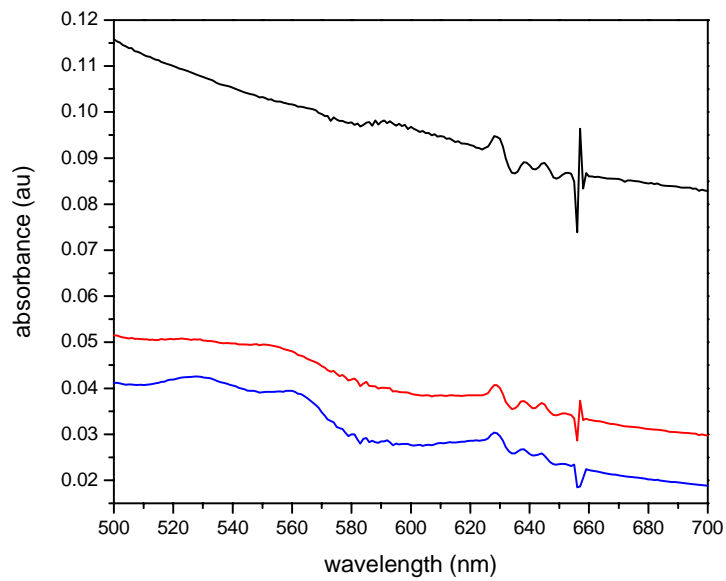
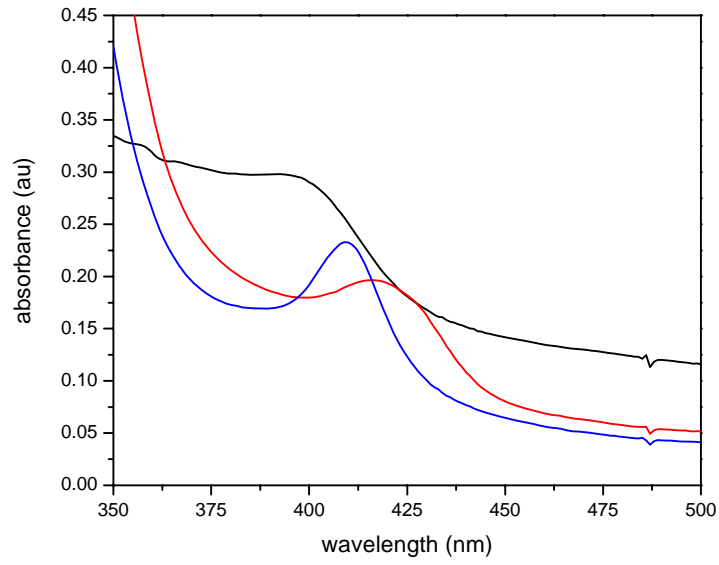
APPENDIX 1.21

Biological Activity of hMb in DMAEM:PEGDMA1000 Membranes. ■ metaquo ($\lambda_{\max} = 397\text{nm}$); ■ deoxy ($\lambda_{\max} = 418\text{nm}$); ■ carboxy ($\lambda_{\max} = 409\text{nm}$)



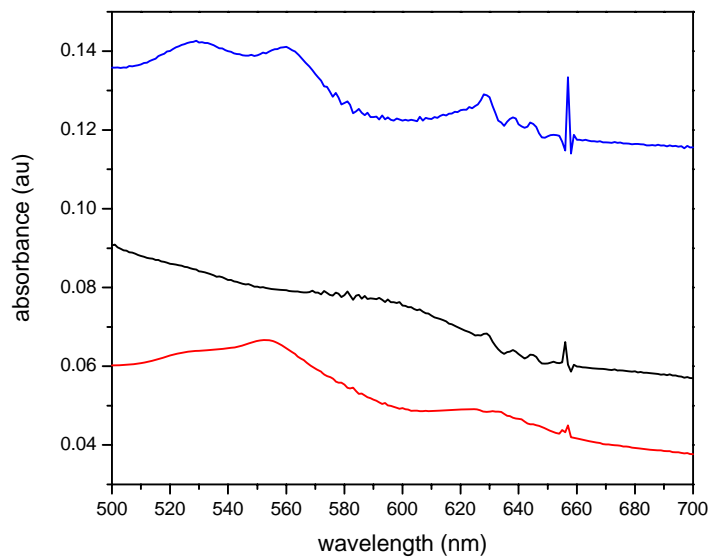
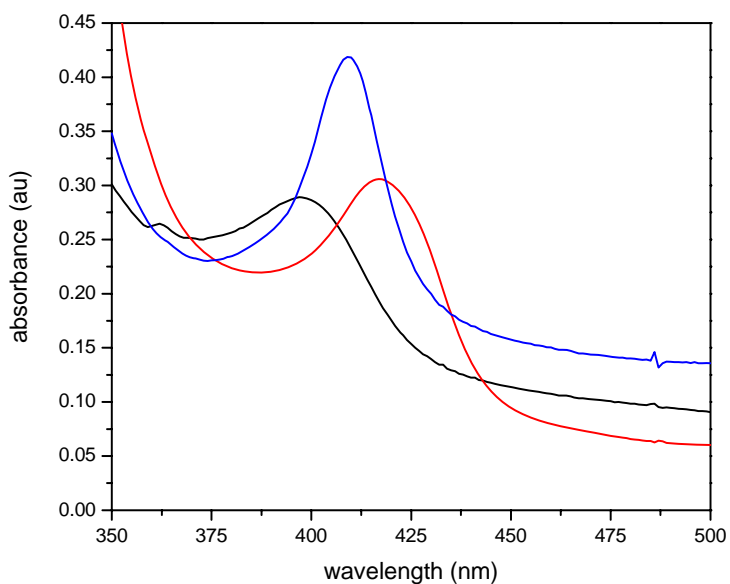
APPENDIX 1.22

Biological Activity of bHb in DMAEM:PEGDMA1000 Membranes. ■ metaquo (Soret λ_{\max} = 393nm; Q λ_{\max} = 628nm); ■ deoxy (Soret λ_{\max} = 416nm; Q λ_{\max} = 628nm); ■ carboxy (Soret λ_{\max} = 409nm; Q λ_{\max} = 628nm)



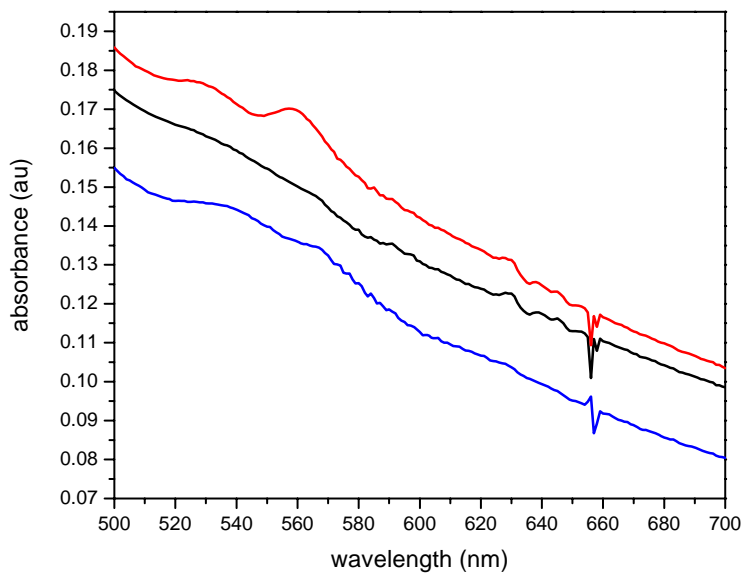
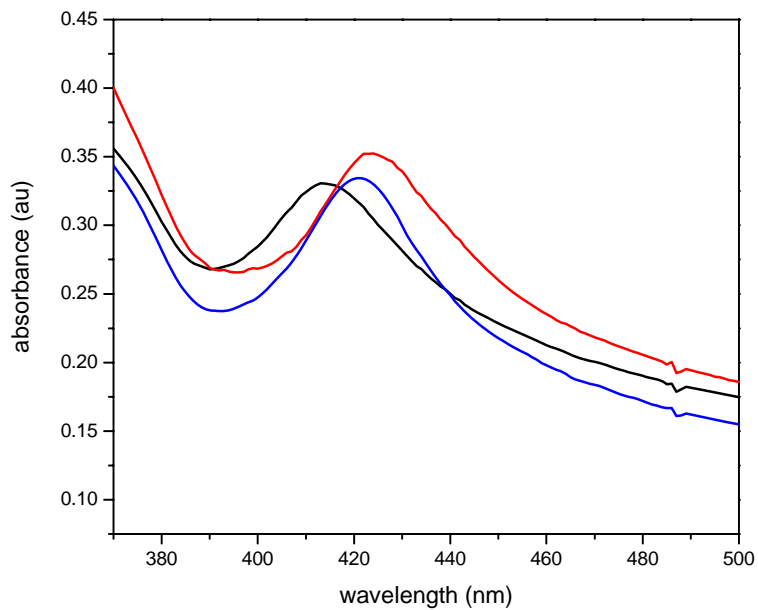
APPENDIX 1.23

Biological Activity of pHb in DMAEM:PEGDMA1000 Membranes. ■ metaquo (Soret λ_{\max} = 397nm; Q λ_{\max} = 577nm, 628nm); ■ deoxy (Soret λ_{\max} = 417nm; Q λ_{\max} = 553nm); ■ carboxy (Soret λ_{\max} = 409nm; Q λ_{\max} = 548nm, 560nm, 628nm)



APPENDIX 1.24

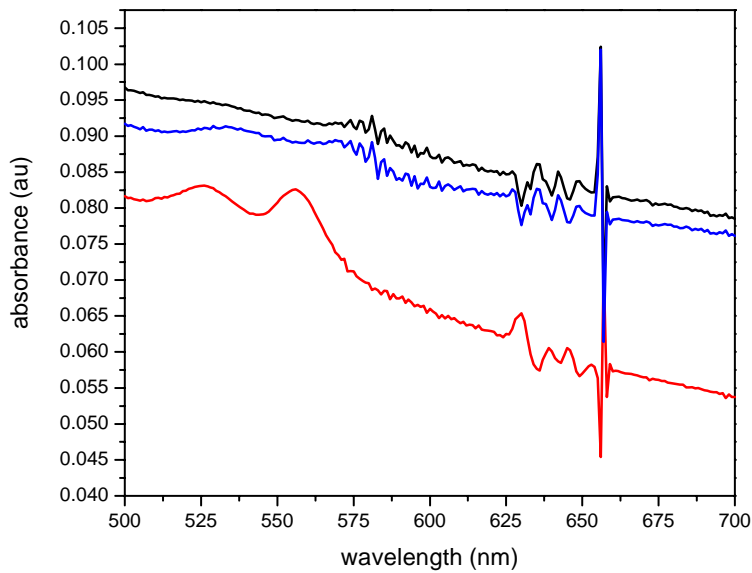
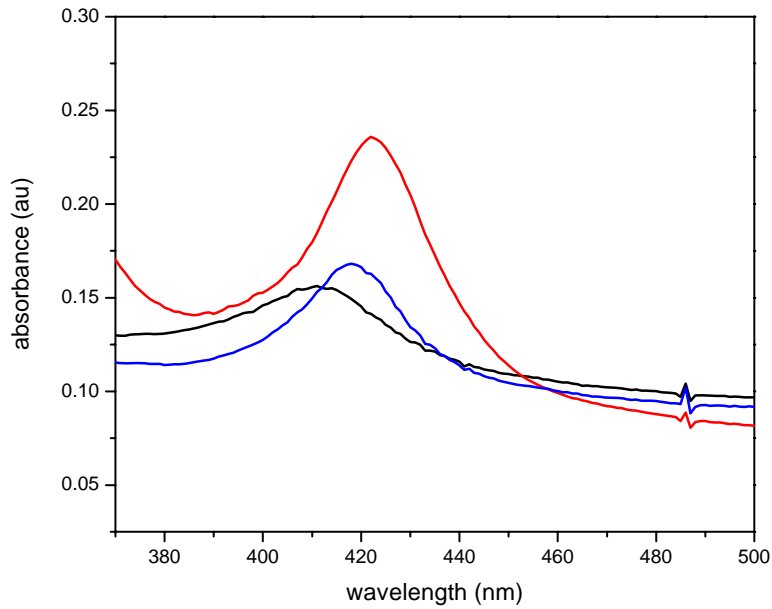
Biological Activity of mMb in PEGMA200:PEGDMA1000 Membranes. ■ metaquo ($\lambda_{\max} = 413\text{nm}$); ■ deoxy ($\lambda_{\max} = 424\text{nm}$); ■ carboxy ($\lambda_{\max} = 421\text{nm}$)



APPENDIX 1.25

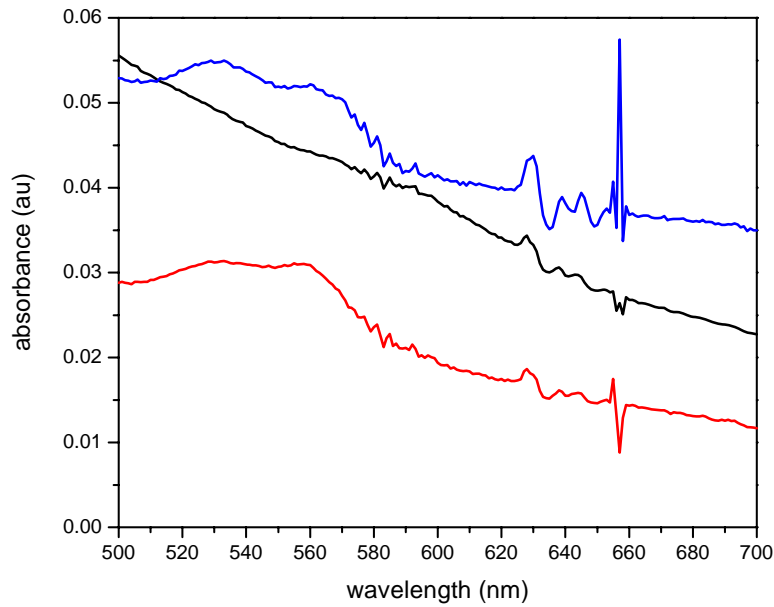
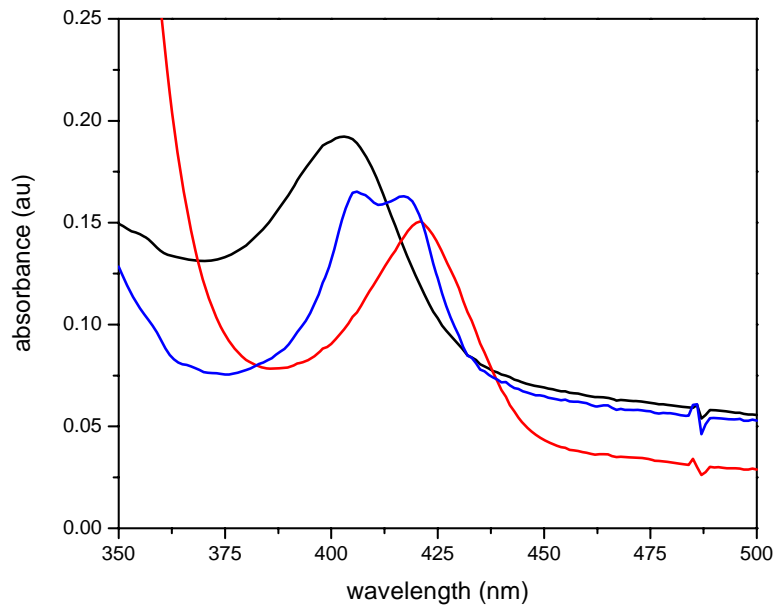
Biological Activity of hMb in PEGMA200:PEGDMA1000

Membranes. ■ metaquo ($\lambda_{\max} = 411\text{nm}$); ■ deoxy ($\lambda_{\max} = 422\text{nm}$); ■ carboxy ($\lambda_{\max} = 418\text{nm}$)



APPENDIX 1.26

Biological Activity of bHb in PEGMA200:PEGDMA1000 Membranes. ■ metaquo (Soret λ_{\max} = 403nm); Q λ_{\max} = 628nm); ■ deoxy (Soret λ_{\max} = 406nm, 419nm); Q λ_{\max} = 533nm, 560nm, 628nm); ■ carboxy (Soret λ_{\max} = 421nm; Q λ_{\max} = 534nm, 560nm, 630nm)



APPENDIX 1.27

Biological Activity of pHb in PEGMA200:PEGDMA1000 Membranes. ■ metaquo (Soret λ_{\max} = 408nm; Q λ_{\max} = 635nm); ■ deoxy (Soret λ_{\max} = 424nm; Q λ_{\max} = 532nm, 558nm, 630nm); ■ carboxy (Soret λ_{\max} = 420nm; Q λ_{\max} = 535nm, 569nm, 633nm)

